NGU Report 2008.029

# Structural and ore geological studies in the northwestern part of the Repparfjord Window, Kvalsund, Finnmark, Norway.

NGU
Norges geologiske undersøkelse
Geological Survey of Norway

Geological Survey of Norway
NO-7441 Trondheim, Norway
Tel.: 47 73 90 40 00
Telefax 47 73 92 16 20

# REPORT

| Report no.: 2008.029 | ISSN 0800-3416 | Grading: Confidential until 01.04.2010 |
|---|---|---|

Title:
Structural and ore geological studies in the northwestern part of the Repparfjord Window, Kvalsund, Finnmark, Norway.

Authors:
Giulio Viola, Jan S. Sandstad, Lars Petter Nilsson and Bjørn Heincke

Client:
Nussir AS

County:
Finnmark

Commune:
Kvalsund

Map-sheet name (M=1:250.000)
Hammerfest & Honningsvåg

Map-sheet no. and -name (M=1:50.000)
Vargsund, Repparfjorden

Deposit name and grid-reference:

Number of pages: 93 Price (NOK):
Map enclosures:

| Fieldwork carried out: | Date of report: | Project no.: | Person responsible: |
|---|---|---|---|
| 1.-14.08 2007 | 01.04.2008 | 320600 | Jan S Sandstad |

Summary:
NGU has completed reconnaissance structural mapping and an ore geological investigation on selected targets in the northwestern part of the Repparfjord Tectonic Window, Finnmark, northern Norway, as part of a consulting job for Nussir AS. The goals of the study were to shed light on several critical aspects of the structural framework of the Paleoproterozoic rocks of the Repparfjord Window within the Nussir West area. Unravelling of the structural set up is crucial for the understanding of the economic Nussir I copper mineralisation and for a possible existence of a Nussir II mineralisation, described so far only as part of a conceptual model, but poorly tested against real geological or geophysical constraints. Another goal was to investigate the characteristics and the structural setting of a number of abandoned copper operations (Porsa, Bachke and Vesterdalen plus several minor prospects), with the aim of adding constraints to the understanding of mineralised systems within the Paleoproterozoic rocks.
Field structural analysis and qualitative interpretation of a new airborne geophysical survey of the area suggest a revised structural scheme for this part of the window and for the genesis of the copper mineralisations studied. It is proposed that the structural framework of the area is largely controlled by thrusts with top-to-the-SE transport direction (of unknown age) and a set of NE-SW striking ductile and brittle-ductile shear zones that bound a broad, copper-mineralised shear corridor. It is suggested that the Nussir I copper deposit may continue westward, although more information is needed in order to verify the validity of this model. A top-to-the-SE thrust is inferred at the base of the Nussir Group, thus forming a tectonic contact between the Nussir greenstones and the overridden Saltvatn Group, which contains the Nussir I deposit. No convincing evidence was found of top-to-the-NW thrusting, as proposed by Pharaoh et al. (1983).
The Porsa, Bachke and Skifergangen copper deposits are all genetically linked to transpressive dextral shear zones and a link between shearing and mineralisation is proposed. Our structural model is also relevant to an alternative interpretation for the formation of Nussir I; textures of the copper mineralisation observed in drill cores in fact suggest that an epigenetic mode of formation might be a valid alternative to the existing syngenetic model.
Recommendations for future work are given, including detailed structural mapping, core logging and geophysical modelling as well as geophysical ground measurement with follow-up drilling.

| Keywords: Structural geology | Ore geology | Copper |
|---|---|---|
| Geophysics | | |
| | | |

# Table of Contents

## 1. Introduction and aims of the study

As part of a consulting job for Nussir AS, NGU completed reconnaissance structural mapping and ore geological investigations on selected targets in the northwestern part of the Repparfjord Window, Finnmark, northern Norway (Figure 1). Fieldwork was carried out in the period 1.-14. August 2007 by geologists Giulio Viola, Lars Petter Nilsson and Jan Sverre Sandstad from the Geological Survey of Norway (NGU).

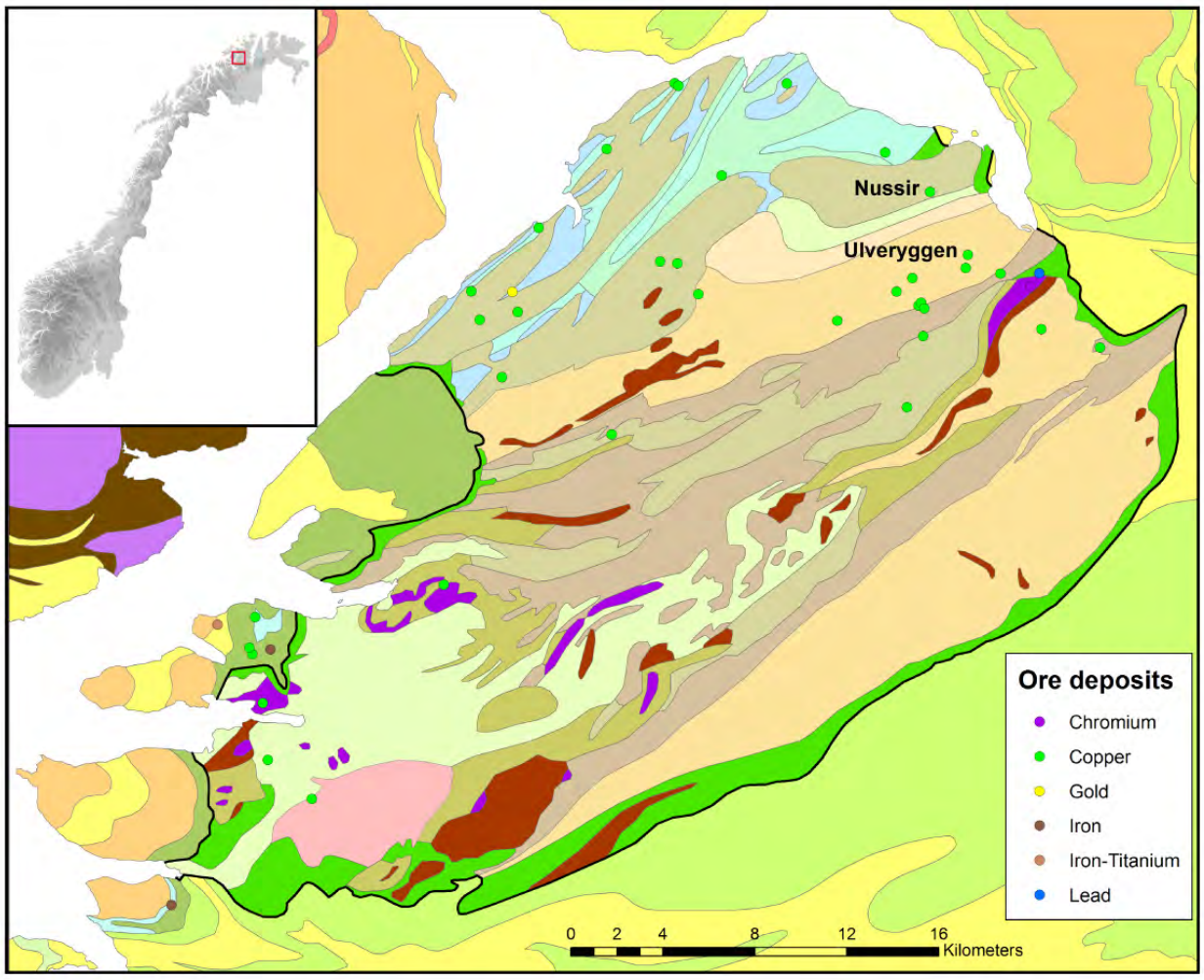


*Figure 1: Location of the Repparfjord Window (red square in the inset) and of known commodities deposits in its Paleoproterozoic rocks. The thin black line represents the boundaries of the window, corresponding to the Caledonian front.*

The goals of the study were:

1) To shed light on several critical aspects of the structural framework of the Paleoproterozoic rocks of the Repparfjord Window within the Nussir West area, which are in turn crucial for the understanding of the economic Nussir I copper

mineralisation. Structural constraints from this area are also pivotal in order to test the possible existence of a Nussir II mineralisation, described so far only as part of a conceptual model, but poorly tested against real geological or geophysical observations.

2) To investigate the characteristics and the structural setting of a number of abandoned Cu operations within the Repparfjord Window (Porsa, Bachke and Vesterdalen), with the goal of adding robust constraints to the understanding of mineralised systems within the Paleoproterozoic rocks of the tectonic window. Results from these investigations may help understand better the mineral potential of other parts of the window or neighbouring areas.
3) To establish better constraints on the lithotectonic architecture of the northern part of the window and to investigate further the relationships between Svecokarelian and Caledonian deformational episodes in the area, and their temporal relationships to known mineralisations.

In the late summer 2007 NGU acquired an airborne magnetic, radiometric and electromagnetic geophysical survey of the study area, also on contract for Nussir AS (Heincke et al., 2008). It was decided that our report would also propose an interpretation of the results of the geophysical dataset and would incorporate them into a comprehensive scheme. It has to be stressed that our interpretation of the geophysical data is largely qualitative, based solely on visual examination of images of the data. Obviously, any interpretation of airborne geophysical data should be anchored to a ground truth. Our ground truth is the detailed geological observation sites within the geographic extent of the new airborne geophysical surveys.

This study represents only a first step towards a better understanding of the complex geology of the Repparfjord Tectonic Window. A much more detailed study is needed to unravel the many unsolved issues that remain after only a few days fieldwork.

## 2. Geological background

The Komagfjord (Reitan 1963) or Repparfjord-Komagfjord (Pharaoh et al. 1983) Tectonic Window forms a large basement culmination within the Caledonides of west Finnmark. The investigations for this report concentrated on the northwestern part of the window, and the term Repparfjord Window is subsequently used. The first detailed bedrock mapping of the region was carried out by Reitan (1963). Revised mapping of the northern part was done in the 1970's by Pharaoh et al (1983). Later on, more detailed mapping of the area was conducted by Nilsen & Nilsson (1996). Geochemical studies of the metavolcanites were performed by Jensen (1996).

The bedrock of the window consists predominantly of metavolcanic and metasedimentary rocks. They are intruded by mafic, ultramafic and felsic intrusive rocks. Although geochronological constraints are generally scarce, the metasupracrustals are assumed to be primarily of Early Proterozoic age, even though the lowermost stratigraphic sequences might represent Archaean rocks, as suggested by the comparison to correlative sequences in inner Finnmark. The oldest metavolcanic unit within the Kautokeino greenstone belt, the Gåldenvarri Formation, has revealed an Archaean age (~2780 Ma, A. Solli pers. comm. 2008). The Paleoproterozoic rocks are overlain by thin sequences of Neoproterozoic sediments. The basement rocks are overthrust by allochtonous rocks of the Caledonian Nappe Complex and have undergone multiphase deformation during the Svecokarelian and Caledonian orogenies.

Reitan (1963) informally subdivided the Paleoproterozoic metasupracrustals into two groups, the Repparfjord and Saltvann Groups (Figure 2). The Repparfjord Group contains greenstones and metasediments (Holmvann Formation) and is unconformably overlain by quartzites of the Doggeelv Formation. Slates and sandstones of the Lomvann Formation overlie the Doggeelv Formation. The black slates and phyllites of the Kvalsund Formation, which directly overlie the Holmvann Formation in the north, are correlated by Reitan (1963) with the Lomvann Formation. The Saltvann Group is assumed to be equivalent to or younger than the upper formations of the Repparfjord Group (Reitan 1963). The Repparfjord Group is thrust upon the Saltvann Group in the northwest. The lower Saltvann Group contains the arkosic sandstones and conglomerates of the Steinfjell Formation, overlain by greenstone conglomerates of the Djupelv Formation and conglomeratic arkosic sandstones with purple coloured microporphyry pebbles of the Fiskvann Formation on the top.

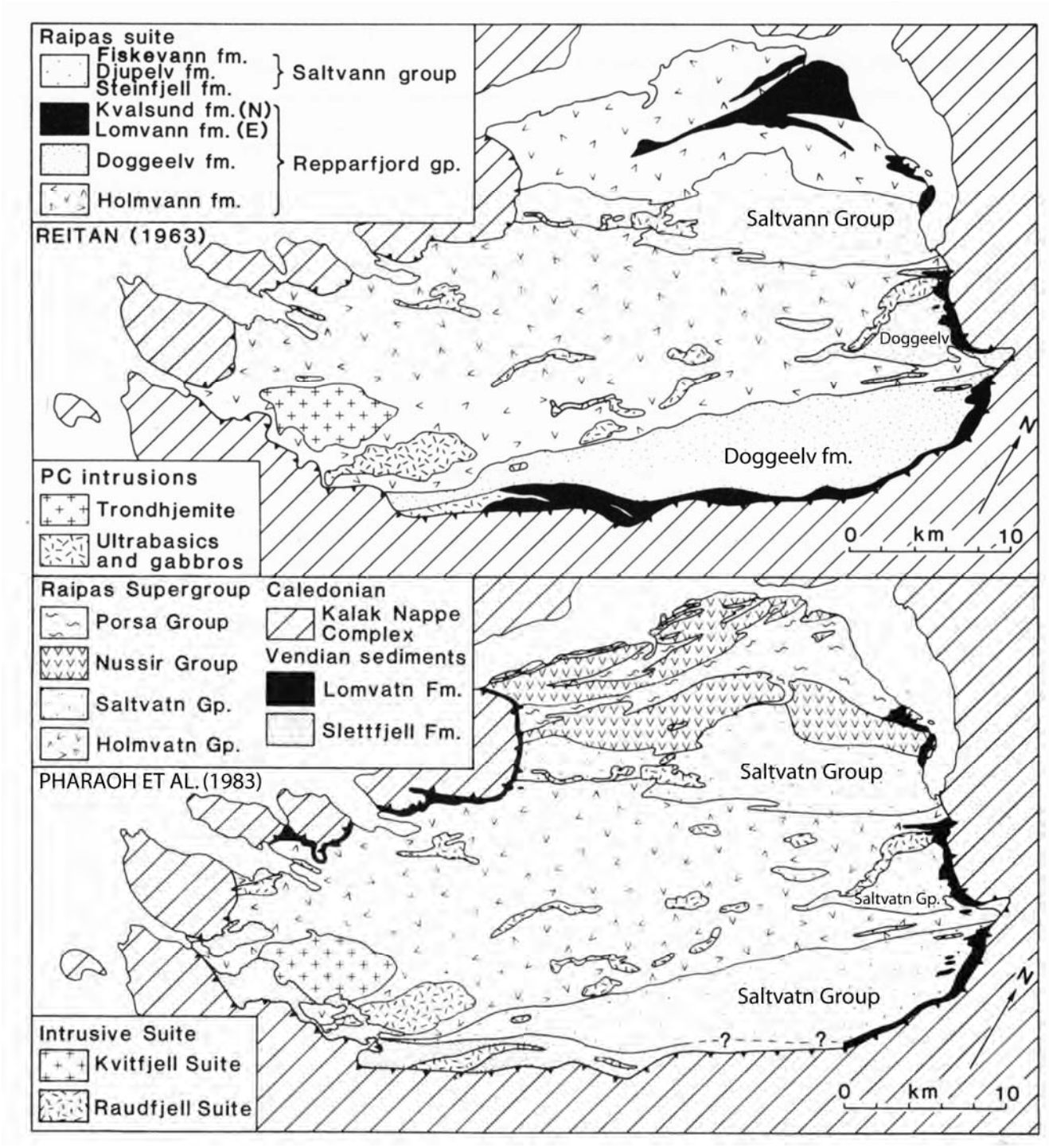


*Figure 2: Simplified geological maps of the Repparfjord Window illustrating the different lithostratigraphic interpretations proposed by Reitan (1963, above) and Pharaoh et al. (1983, below).*

Pharaoh et al. (1983) subdivided the metavolcanites and metasediments of the Holmvann Group of Reitan (1963) into two groups, the Holmvatn Group in the southeast and the Nussir Grup in the northwest (Figure 2). The Holmvatn Group is assumed to be the lowermost stratigrahic unit (Pharaoh et al. 1983) in the window. It comprises an at least 3 km-thick sequence of immature metasediments interbedded with metavolcanic horizons of basic and

intermediate composition. Structurally it cores a major open antiform and is unconformably overlain by the c. 3 km thick metasedimentary Saltvatn Group, which is in turn subdivided into three formations, as per the interpretation of Reitan (1963). The lowermost formation, the Ulveryggen Formation, consists of meta-arenites with interbedded conglomeratic layers. It is overlain by the Djupelv and Stangvatn Formations, made up by greenstone conglomerate and porphyrite conglomerate, respectively. Conformably above the porphyrite conglomerate are situated the copper mineralised dolomite and schistose siltstones that host the Nussir deposit. They are, in turn, conformably overlain by the metavolcanic Nussir Group (> 1,7 km thick), which is dominated by metabasalts and metatuffites. The metasedimentary Porsa Group is assumed to unconformably overlie the Nussir metavolcanites (Pharaoh et al. 1983). It is subdivided into three formations, the Vargsund Formation, comprising dolomites, quartzites and conglomerates, the Kvalsund Formation, containing graphitic schists, and the Bierajav'ri Formation, which consists of carbonates, tuffs, sandstones and schists. If not otherwise stated, the naming of the units in this report follows Pharaoh et al. (1983).

The subdivision of the metavolcanites into two groups, the Holmvatn and Nussir Group, is substantiated by the interpretation of the geochemical signatures of the rocks. The lower Holmvatn Group has calc-alkaline affinity, indicative of subduction-type magmatism (Pharoh & Pearce 1984, Pharaoh & Brewer 1990). The upper Holmvatn Group is composed of tholeiitic pillow lavas and tuffs and shows a within-plate signature. It also shows enrichment of LIL and Ce, similarly to the lower Holmvatn Group (Pharoh & Brewer 1990). An arc-related magmatism for the Holmvatn Group is also suggested by the study of Jensen (1996). The Nussir Group, instead, consists of tholeiitic metavolcanites and their trace element geochemistry suggests deposition within a submarine rift within continental crust (Pharoh & Pearce 1984, Pharaoh 1985, Pharoh & Brewer 1990).

A major discrepancy, therefore, exists in the interpretation of the tectonic evolution in the Nussir area of Reitan (1963) and Pharaoh et al. (1983). Reitan (1963) suggested a major NW-dipping thrust with overthrusting towards the southeast along the contact between the Saltvatn and Nussir Groups. Pharaoh et al. (1983), instead, proposed overthrusting towards the northwest, with a thrust plane intersecting the Nussir Group (Figure 4). The Stangvatn Group is thrust upon the Nussir Group in the southwest, and the Nussir Group is thrust upon the Porsa Group in the northeast.

The age of the Porsa Group is also discussed in the literature. Pharaoh et al. (1983) have included the unit as part of the Paleproterozoic sequence, while Reitan (1963) correlated part

of the group with the Lomvatn Formation of assumed Neoproterozoic age. Nilsen & Nilsson (1996) interpret the Porsa Group as part of the Paleoproterozoic sequence on the bedrock map sheet Vargsund, but in a preliminary version of the map sheet Repparfjord suggest later that the unit is Neoproterozoic. Carbonate dating by Sr and C isotope models of sea water evolution could shed light on this issue.

## 3. Structural analysis

During the limited time spent in the field, structural investigations were conducted in a number of key areas, with the goal of maximising the amount of information gathered from the study. In the structural scheme adopted here, deformational events are termed “Dn”, “Dn+1,” “Dn+2” with a chronological connotation, whereby Dn represents the oldest recognised event and Dn+1, 2 etc are subsequent episodes. A deformational episode Dn leads to the generation of folds Fn, planar fabrics Sn and so on.

Figure 3 plots the localities that were investigated. These have been subdivided in a set of sub-areas on the basis of the specific structural aspects that were under study. The orange shaded areas in Figure 3 show these sub-areas and in the following we will presents our results according to their numbering, before elaborating a summary and an interpretation of the field results at the end of the report, based also on the information gathered from the analysis of the new geophysical survey. Observation points not covered by the orange shading refer to the copper mineralisations described in chapter 4. These also provided useful information to the understanding of the geological evolution of the area.

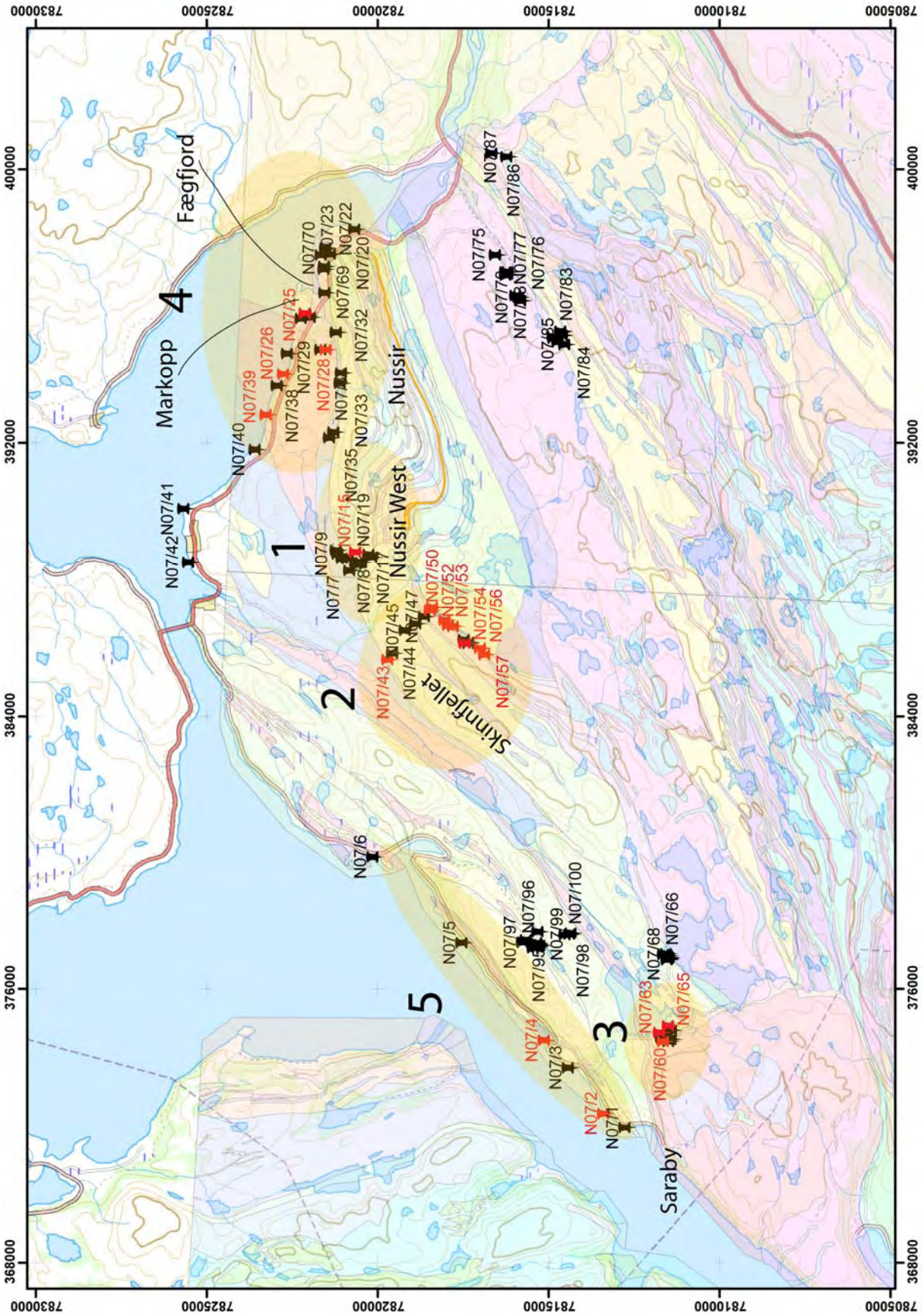


*Figure 3: Localities investigated during this study reported on a topographic/geological base. See Figure 4 for the legend to the geological map. Specific localities described and discussed in the text are drawn in red.*

### 3.1 Area 1: Nussir West area

As obvious from the geological map of the region (Figure 4), the Nussir West area of the Repparfjord Window is characterized by the abrupt westward termination of the Nussir volcano-magmatic-sedimentary and Saltvatn Groups against a sharp geological discontinuity; this geological relationship is indeed of great interest in that the Saltvatn group contains the mineralised and highly economic Nussir I ore dolomite (Figure 4). The discontinuity that apparently bounds the mineralisation to the west has been interpreted in the past as a major Svecokarelian structure, characterised by thrust kinematics with an overall top-to-the-NW transport direction (e.g. Pharaoh et al., 1983). The trend of the thrust proposed by Pharaoh et al. (op.cit.) is highlighted by a thin red line in Figure 4. No detailed structural and kinematic characterization, however, was provided, which in turn made it difficult to fully understand the geology of the area and to draw any satisfactory conclusion. Open questions remain therefore as to the discontinuity character, its real kinematics and geometry, as well as its age and lateral extent.

As mentioned in the introduction, one of the main aims of the study is to improve the understanding of the apparent western termination of the Nussir and Saltvatn Groups. Obviously, this impacts directly on the possibility of establishing whether there is any potential for a westward continuation of the mineralised Nussir I unit into a postulated Nussir II ore body, an issue with great economical implications. Great attention was paid therefore in our study to the geometry and kinematics of several outcrops located along this reported discontinuity, as modern kinematic analyses were never carried out before in the region.

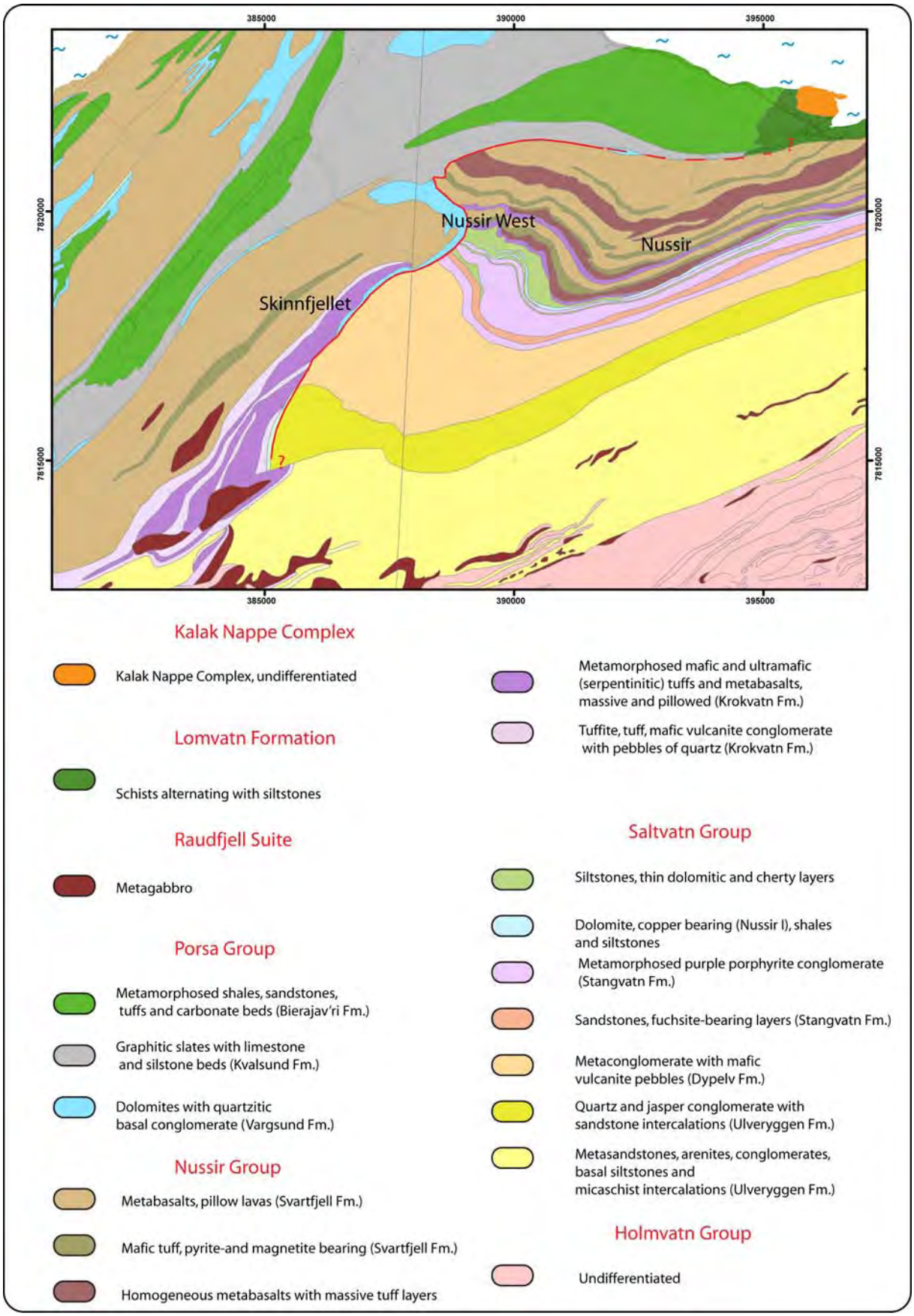


*Figure 4: Detailed geological map of the central-eastern part of the Repparfjord Window. The trend of the thrust proposed by Pharaoh et al. (1983.) is highlighted by a thin red line.*

Figure 5 shows the structures observed at outcrop N 07/15 (UTM 35N, 388492 7820491, Figure 3). NW-dipping, strongly sheared Nussir greenstones contain evidence of pervasive top-to-the-E-ESE shearing. As illustrated in the photos of Figure 5a, b, and c (all taken with view to the northeast), individual shear bands and localised extensional crenulation cleavage planes indicate a consistent shear direction, which, at the present orientation of the foliation, corresponds to thrusting, with the hanging wall transport direction shown by the yellow arrow in the stereonet of Figure 5d. The intersection between the average orientation of the shear bands and of the foliation planes defines a line that is perpendicular (within the foliation plane) to the overall transport direction. The white dot in the stereonet that lies along the average foliation orientation great circle, plots the only stretching lineation observed and measured; this is indeed perpendicular to the intersection, thus confirming the overall top-to-the-E-ESE transport.

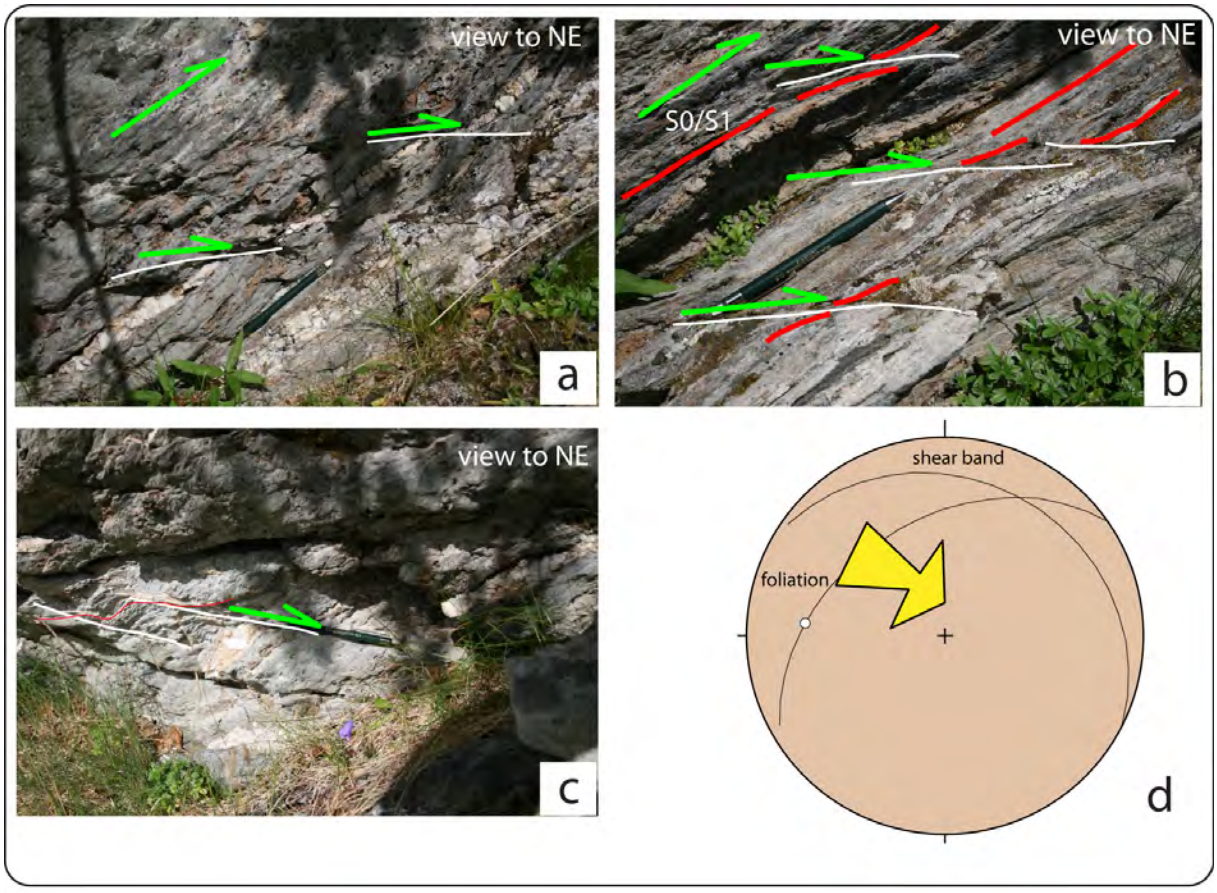


*Figure 5: Structural features of outcrop N 07/15. a), b) and c) show individual shear bands or extensional crenulation cleavages that deform strongly foliated Nussir greenstones. The direction of transport (shown by the yellow arrow in the stereonet of d)) is determined by the asymmetric bending of the foliation (S planes) into the shear planes of the shear bands (C planes). All stereonets in this report utilize a lower-hemisphere, equal-area Schmidt projection.*

We could not document any other kinematic indicators in the area. Dolomites (probably belonging to the Porsa Group) are exposed immediately to the south of the sheared contact of Pharaoh et al. (1983). They show sign of pervasive deformation, with tight folding and fracturing/jointing.

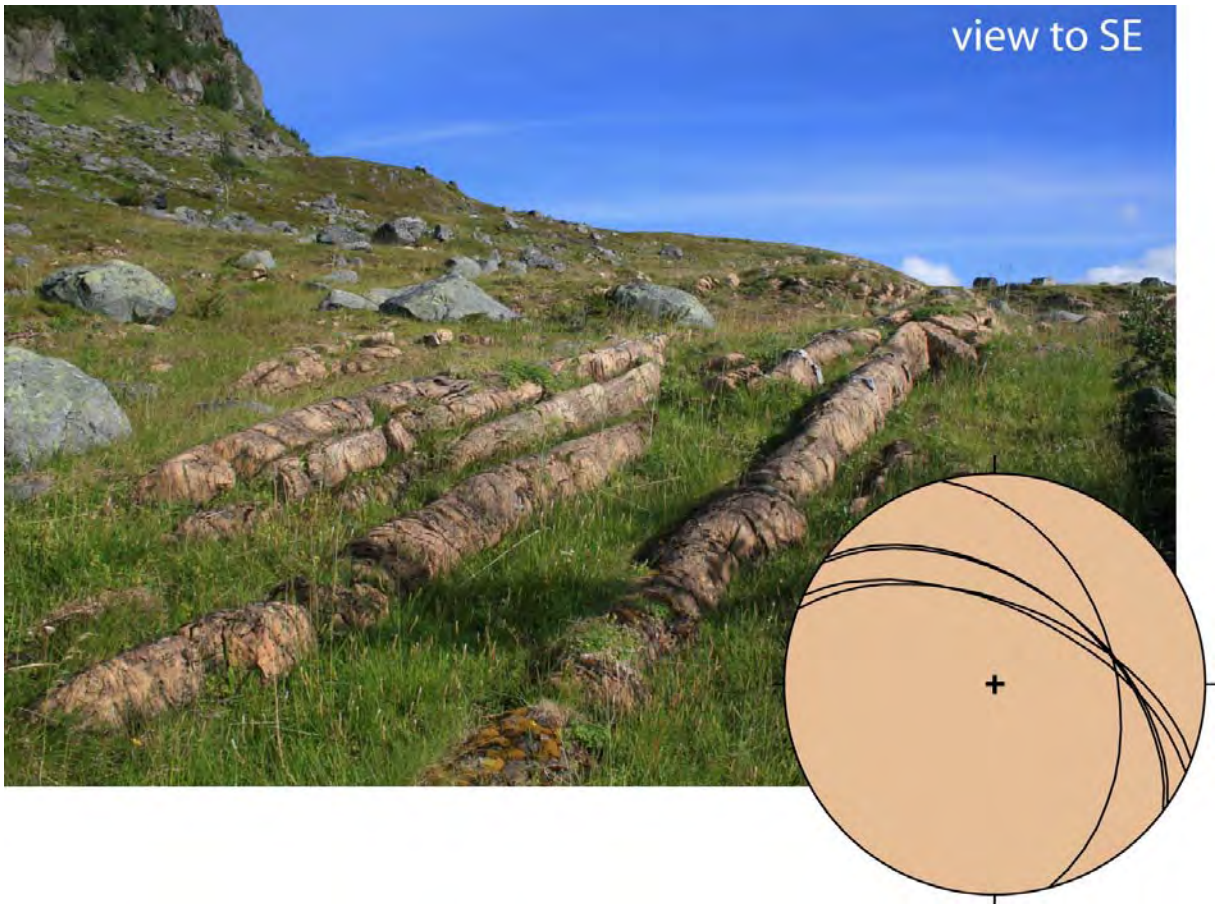


*Figure 6: Field view of the dolomites in the Nussir West area and stereonet projection of their bedding orientation.*

Although only a few readings of the dolomite bedding orientation were taken, these confirm the overall folded pattern of the dolomites (as also visible from the geological map of Figure 4) around a moderately E-ENE-plunging axis. This is interpreted as a Fn+1 fold. The dolomites rest conformably on a quartz- and greenstone-pebble conglomerate on top of the greenstones exposed to the southwest of the discontinuity of Pharaoh et al. (1983).

### 3.2 Area 2: Skinnfjellet

The structural set-up of the Nussir greenstones to the west of the discontinuity and their relationships to the Saltvatn conglomerate (Dypelv Formation) exposed to the east were

investigated along a field traverse that crossed first the greenstones of Skinnfjellet along a NW-SE direction (outcrops N 07/43 to N 07/49) and then followed the strike of the contact to the conglomerate to the southwest (N 07/50 to 07/53; Figure 3 and Figure 4).

The greenstone body is bound to the northwest and southeast by a thin dolomitic layer, seemingly resting on the greenstones. A similar dolomite bed is found on the southeasterm flank of Skinnfjellet, and marks the boundary between the greenstones and the Dypelv formation conglomerates (Figure 8a). As shown in Figure 4, dolomites to the southeast of the Skinnfjellet greenstones are connected to the dolomites described in the previous section, forming part of the same unit.

The dolomite bedding orientation is plotted in Figure 7a by red great circles; the sequence is folded about a Fn+1 NE-plunging fold axis in a slightly asymmetric antiform cored by the greenstones, with the northwestern limb dipping steeply to the NW and the southeastern limb subvertically to the SE. Black great circles plot cleavage planes within the greenstones.

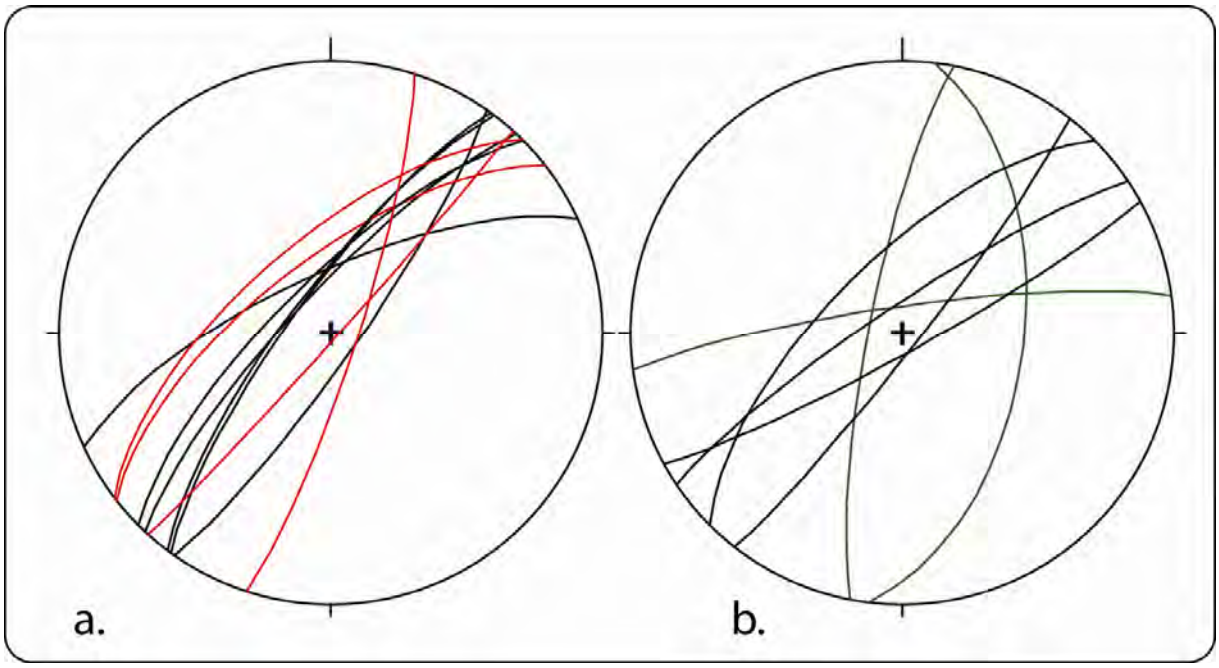


*Figure 7: Lower hemisphere projection of structural readings along the Skinnfjellet section. a): Red great circles plot the orientation of bedding in the dolomite, which underlies the Nussir greenstones. Dolomites are folded around a Fn+1 NE-plunging fold axis. The fold is upright and slightly asymmetric, with the northwestern limb dipping less steeply than the southeastern limb. Cleavage orientation in the greenstones is plotted by black great circles. b): Green great circles plot bedding orientation of the Dypelv Formation conglomerates and conglomeratic sandstones, whereas black great circles show cleavage orientation.*

The generally upright geometry of the fold is confirmed by subvertical cleavage planes. Recognition of minor, second-order folds within the greenstones at the core of the fold proved

very challenging due to the homogeneous lithology and the lack of obvious visual structural markers. The contact between the greenstones and the Dypelv Formation in this area was the key element in Pharaoh et al.'s interpretation of a Svecokarelian top-to-the-NW thrust. We observed no shear indicators along the contact marked by the dolomites. A proto- to mylonitic sequence was, however, observed and studied in detail in the gorge shown in Figure 8a. The dashed red line traces the contact between dolomites and greenstones to the northwest and Dypelv Formation conglomerates to the southeast. As demonstrated by outcrop N 07/54 (UTM 35N, 610292 7817086; Figure 3) the contact is tectonic. The outcrop is formed by lower greenschist-facies mylonites. Foliation planes dip very steeply to subvertically to the southeast (Figure 8b and c). Asymmetric clasts and a pervasive extensional crenulation cleavage indicate reverse kinematics, with an overall top-to-the-NW transport direction (Figure 8d and e). The mylonitic fabric is locally overprinted by brittle deformational features. Down-dip striations are commonly found on foliation planes and slickensides indicate top-to-the-NW brittle faulting, thus with identical kinematics to the ductile deformational episode (Figure 8f). Rocks record therefore a shearing history with an overall reverse kinematics characterized by transport to the NW evolving along a retrograde path from ductile to brittle conditions. Previously formed mylonitic foliation planes were thus reactivated as fault surfaces during the later brittle overprint.

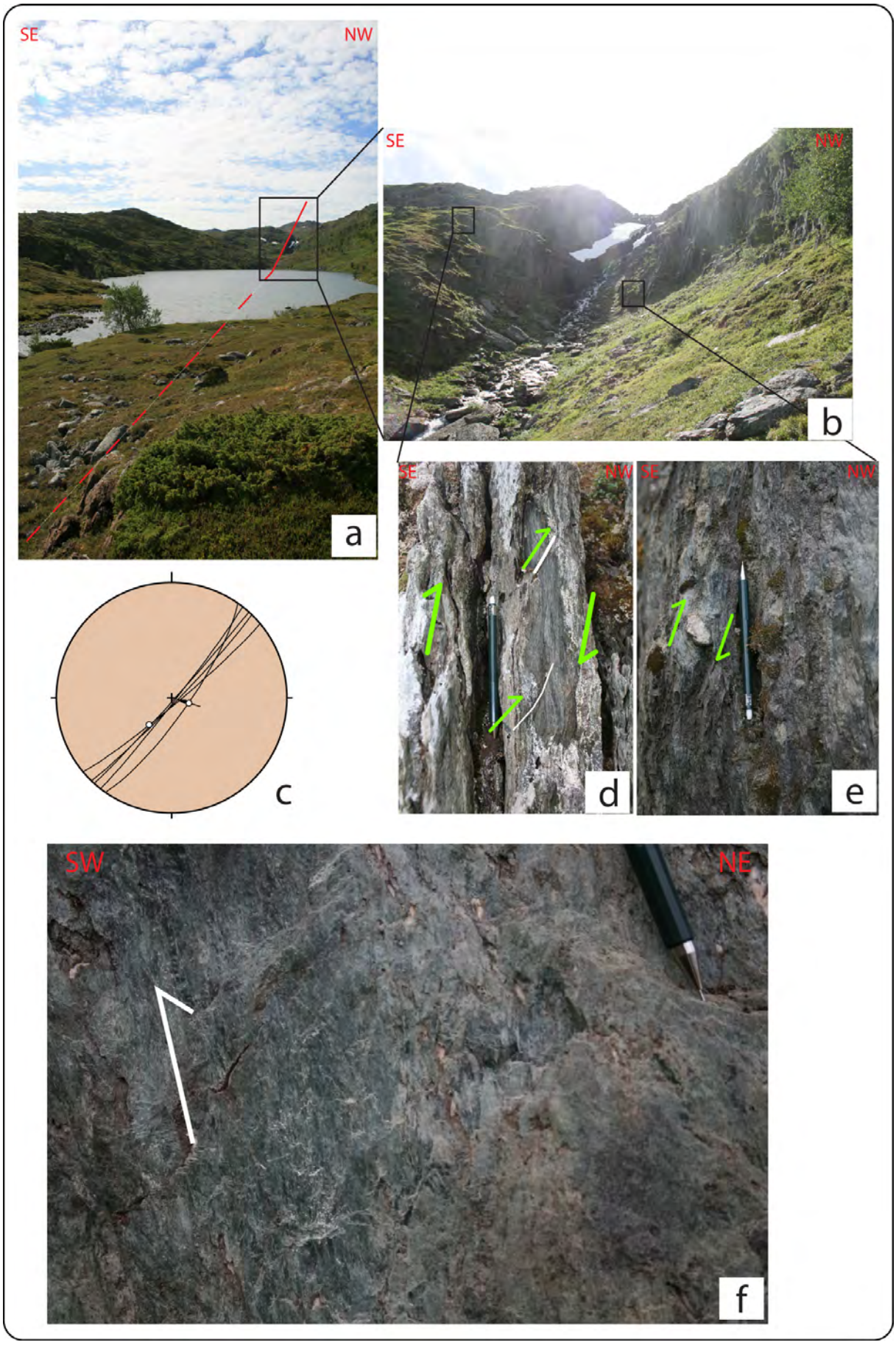
SE
NW
a
SE
NW
b
c
SE
NW
d
SE
NW
e
SW
NE
f

*Figure 8: a): view to the southwest of the tectonic contact between the Dypelv Formation conglomerates to the southeast and dolomites and greenstones to the northwest. b): Detail of the gorge hosting the penetratively mylonitic contact. Here the dolomites are not exposed and strongly sheared greenstones are juxtaposed directly against the conglomerates. Two black squares indicate the location of the kinematic indicators shown in d) and e). c): Orientation of the mylonitic foliation, of one W-WSW-plunging stretching lineation (white dot) and of a W-WNW-plunging striation (white dot with arrow, the latter indicating the hanging wall movement direction). The arrow head indicates a reverse top-to-the-W-WNW shear direction as shown by the stepped slickensides of f). d): top-to-the-W-WNW extensional crenulation cleavage. e): Asymmetric σ clast showing top-to-the-W-WNW transport.*

The mylonitic foliation is gently crenulated (Figure 9) by Fn+2 open folds that are coaxial with the orientation of the overall Fn+1 Skinnfjellet antiform and the folds documented in the previous section.

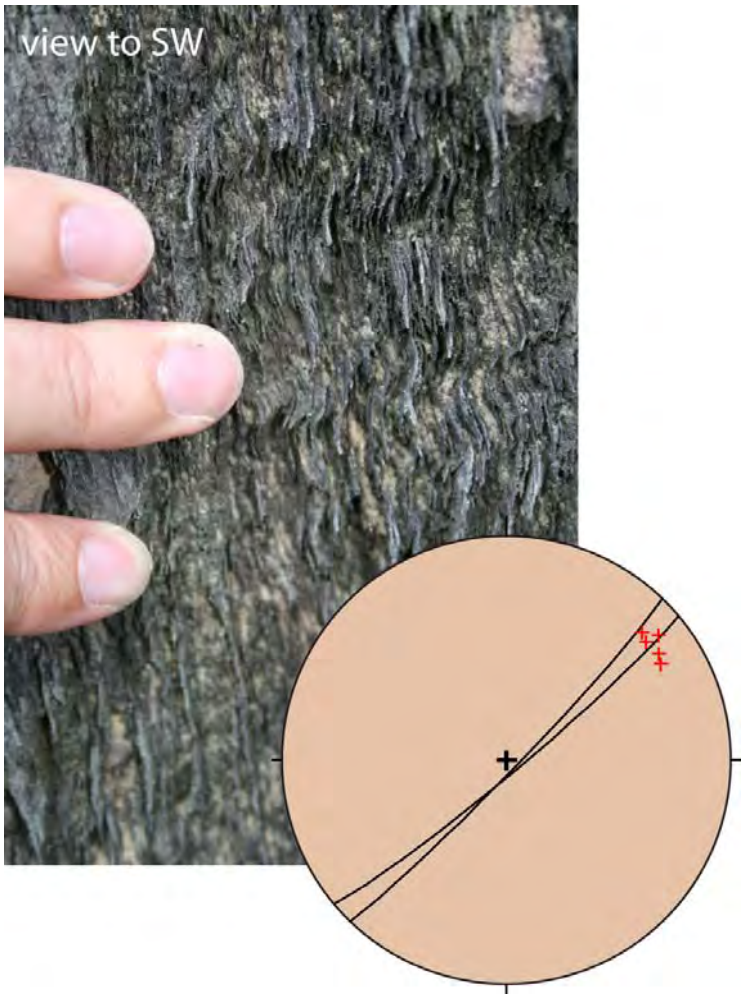


*Figure 9: Sn+2 crenulated mylonitic foliation of outcrop N 07/54 shown in Figure 8. Axes plunge shallowly northeast.*

The stereonet of Figure 7b plots bedding and cleavage orientations of the Dypelv Formation conglomerates. Presumably Fn folding is locally very intense and with tight to isoclinal

geometry (Figure 10a). The axial planar cleavage can be very penetrative at the outcrop scale and is generally defined by newly-grown chlorite. Both bedding and cleavage orientation change significantly over short distance, and depending on the outcrop considered, they can be at very different orientation to the strike of the tectonic contact (see end member situations shown in Figure 10a and b, where they are orthogonal and parallel to the contact, respectively).

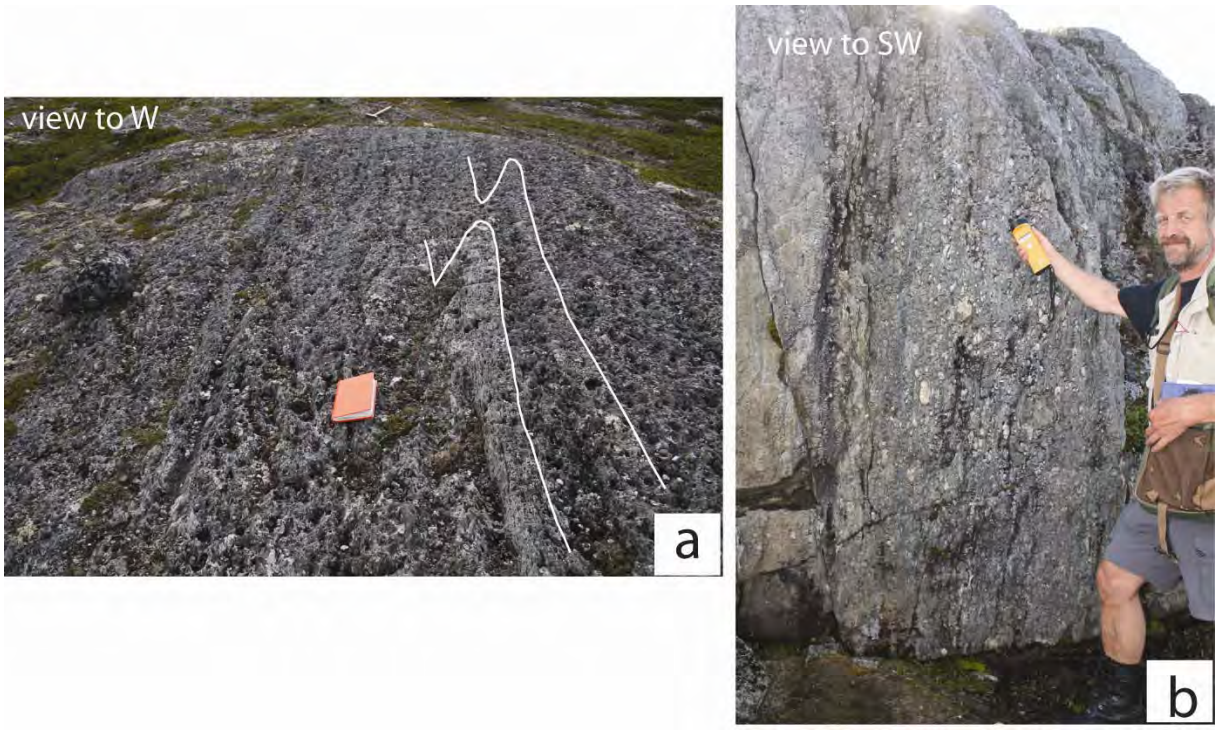


*Figure 10: a): Isoclinally folded bedding (Fn folds outlined by the white lines) in the Dypelv Formation conglomerates. Both bedding and cleavage are at high angle to the trend of the tectonic contact to the greenstones (N 07/56, UTM 34N, 610188, 7816734). b): Steeply SE-dipping cleavage in the conglomerates, here parallel to the contact (N 07/57, UTM 34N, 610017, 7816587)*

### 3.3 Area 3: Western Caledonian front along the Saraby section

One of the challenges that became obvious during this study is the determination of the age of the various deformational events affecting the rocks investigated. The lack of direct chronological constraints makes it difficult to assign structures and fabrics to the different orogenic episodes that acted in the region and one can therefore rely only on relative geochronological evidence to unravel the observed evolution. In order to add relative time constraints to our structural observations, it was decided to inspect two key areas (subarea 3 and 4, described here and in the next section, respectively; Figure 3), where the presence of units belonging to the Caledonian Kalak Nappe Complex should be of great help in

discriminating pre-Caledonian fabrics (likely the result of the Svecokarelian orogeny) from Caledonian and younger structures.

The reported occurrence at the base of the overriding nappes of a poorly deformed parautochtonous unit, the Lomvatn Formation of Neoproterozoic age, would represent a useful tool to separate the effects of pre- and post-Neoproterozoic deformation. The map by Pharaoh et al. (1983) shows the Lomvatn Formation as a thin, very continuous unit that is preserved almost ubiquitously at the base of the Kalak Nappe Complex around the Repparfjord Window. Cross sections drawn by the same authors (one of them runs right through the section that is discussed below) illustrate explicitly the geometric relationships between a pre-Neoproterozoic basement and the Lomvatn Formation, which rests nonconformably over the strongly deformed Paleoproterozoic rocks. Detailed inspection of the same area illustrated by the section of Pharaoh et al. (op. cit.), however, disclosed a significantly different situation.

Figure 11 shows a number of selected photographs from the Saraby section, illustrating structural relationships from the western shore of Storvatnet (Figure 3). The most significant observation is the lack of a clearly visible nonconformity: metavolcanites of the Kalak Nappe Complex rest directly on strongly Fn+1 folded and cleaved rocks that can be possibly ascribed to the Porsa Group, without any obvious intervening Lomvatn Formation (Figure 11a and b). The orientation of the axial planes of the Fn+1 tight to isoclinal folds immediately below the floor thrust of the Caledonian nappe complex is plotted by the red great circles in the stereonet of Figure 12, whereas black great circles plot all foliation measurements derived from the section inspected. It is clear that the local foliation is axial planar to these folds, whose axes plunge gently to the southwest, only a few degrees across the horizontal from the plunge of the folds described in the Nussir West area. Observations from within the footwall to the Caledonian front (e.g. Figure 11c) confirm that fabrics and structures with the exact same orientations deform rocks belonging to the Porsa Group. In summary, the section studied does not contain Lomvatn Formation, which in turn hampers the establishment of a relative geochronology of the observed structures.

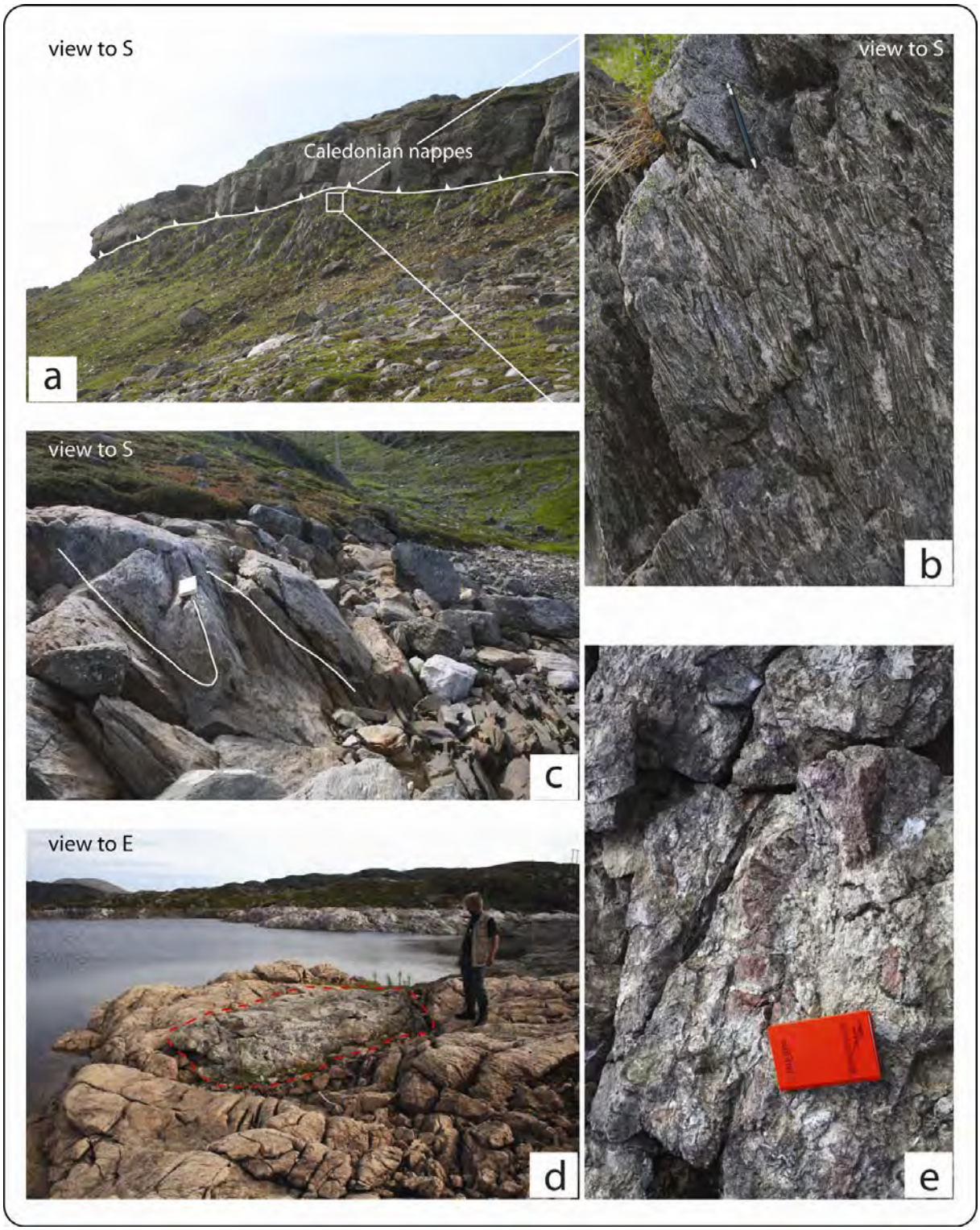


*Figure 11: a): View of the lowermost part of the Kalak Nappe Complex to the west of Porsavatnet, truncating the strongly Fn+1 folded and cleaved schists of (b). No Lomvatn Formation and nonconformity are seen at this locality (outcrop N 07/60, UTM 34N, 599334 7810054). c): Inclined Fn+1 isoclinal folds within the Porsa Group lithologies c. 200 m below the Caledonian front (N 07/63, UTM 34N, 599425 7810178). These folds have the same orientation of the folds truncated by the floor thrust of the nappe complex. d): Small patches of coarse conglomerate are found resting nonconformably on the Porsa group dolomites (N 07/65, UTM 34N, 599657 7810055). e): Large, irregular clasts of jasper occur in the conglomerates.*

Small patches of a coarse-grained, jasper-clast-containing conglomerate were actually found resting nonconformably on Porsa dolomites along the shore of Storvatnet (Figure 11d and e). These pockets are preserved locally and fill in small depressions on top of the dolomites. Their stratigraphic relationships to the cleaved schists truncated by the Caledonian front are however unclear and therefore they cannot be used to discriminate deformational episodes of different ages.

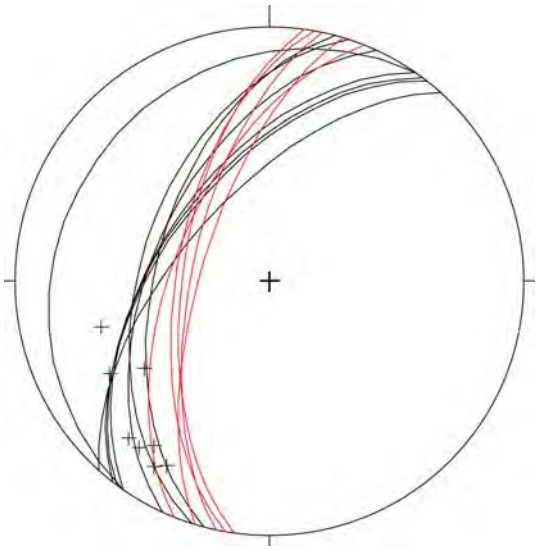

*Figure 12: Orientation of axial planes of the folds shown in Figure 11 (red great circles) and of the foliation measured in the area. Fold axes plunge moderately southwest (black crosses).*

### 3.4 Area 4: Eastern Caledonian front along the Markopp-Fægfjord section

The Lomvatn Formation is also reported from along the easternmost edge of the Repparfjord Window (e.g. Figure 3 and Figure 4; Pharaoh et al., 1983; Reitan, 1963). Nevertheless, our mapping confirms the observations made and conclusions drawn from the Saraby section, that is, we did not observe any nonconformable contact below the Kalak Nappe Complex. Instead, structural observations made in sub-area 4 (Figure 3) confirm that the floor thrust of the Caledonides truncates sharply strongly folded and cleaved rocks that do not correlate to the Lomvatn Formation.

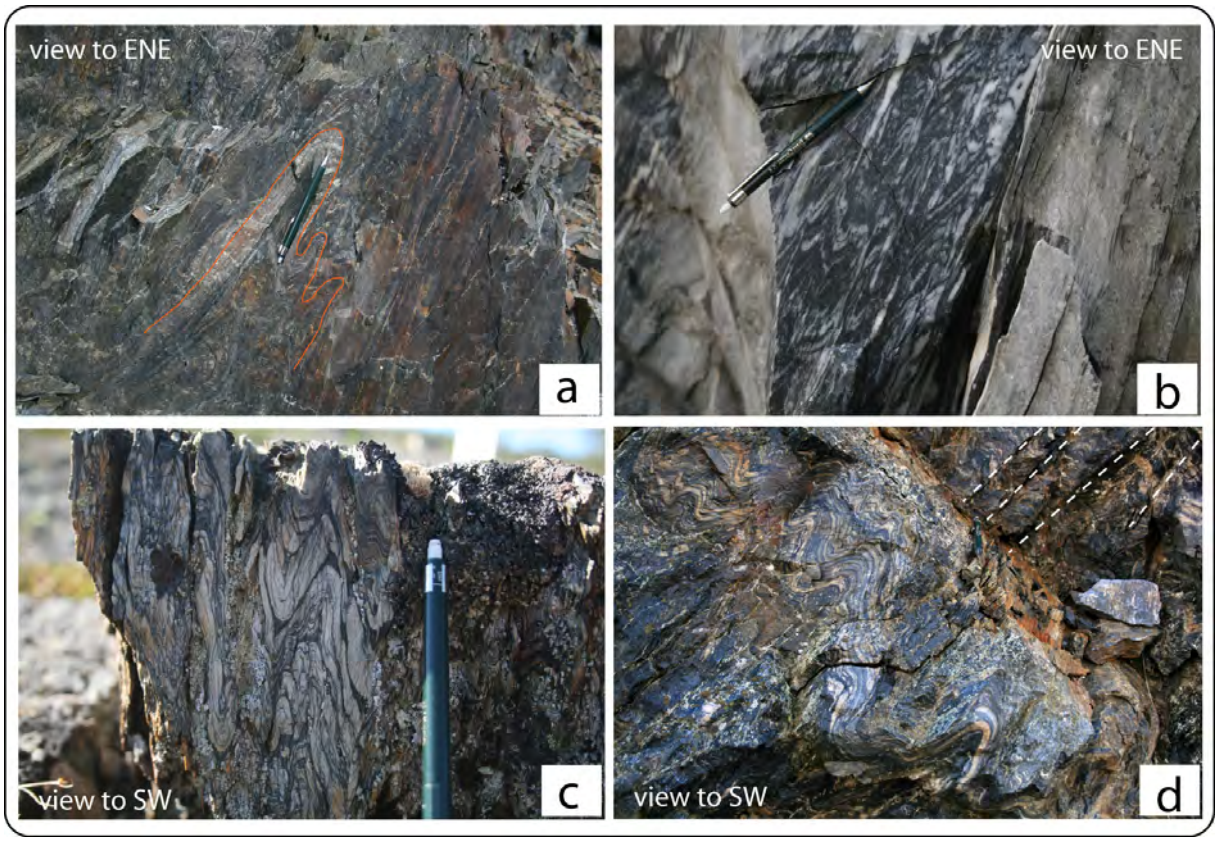


*Figure 13: a): Quartzitic schists with Fn+1 tight to isoclinal folds and pervasive NW-dipping axial plane cleavage (N 07/25, UTM 35N, 395670 7821899). b): Porsa Group limestones/marbles, strongly folded by Fn+1 folds and cleaved. Axial planes and axial plane cleavage dip to the northwest (N 07/26, UTM 35N, 394608 7822561). c): Tightly-folded, thinly-laminated schists. It is unclear to which formation they belong (N 07/28, UTM 35N, 395228 7821134). d): Strongly folded Quartzitic schists/shales of the Porsa group. Axial planes dip to the southeast (N 07/39, UTM 35N, 392813 7823182).*

Figure 13a shows selected structures from the immediate footwall to the Kalak Nappe Complex. Strongly folded and cleaved schists have a very pervasive NW-dipping axial planar foliation. The Porsa Group is also affected by the same deformational episode, as shown by the identically oriented axial planar cleavage that deforms the marbles and limestones of Figure 13b. This cleavage is itself affected by a later folding episode. SE-dipping axial planes and cleavage surfaces are observed in the entire subarea 4 (Figure 14b). Poles to foliation planes spread along a well-defined great circle (Figure 14a), which constraints a fold axis oriented 048/21 (black triangle in Figure 14a). This calculated axis is coaxial with a large set of crenulation and fold axes measured directly in the field (red crosses), and also corresponds to the orientation of many more fold axes measured throughout the field area of this study. These observations establish that NE-plunging folds postdate and overprint earlier roughly coaxial folds.

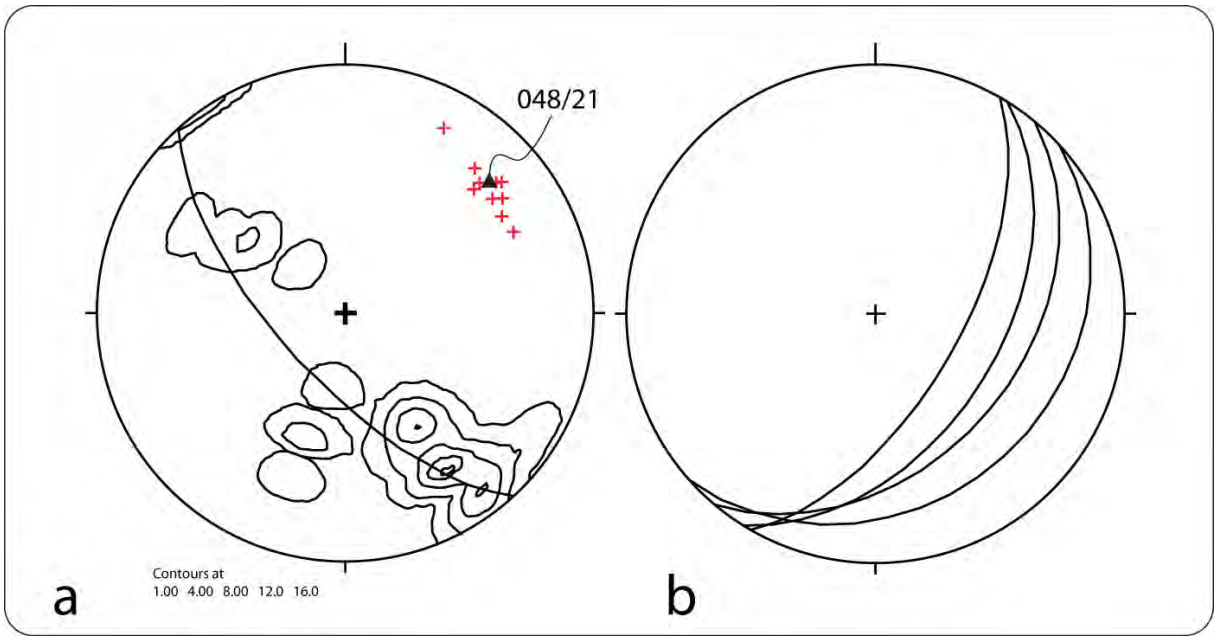


*Figure 14: a): Poles to foliation planes in sub-area 4. They spread along a well-defined great circle, which produces a calculated Fn+2 axis oriented 048/21-black triangle. Red crosses plot measured fold and crenulation axes. b): Fn+2 SE-dipping axial planes to the folds shown in Figure 13d.*

Another, separate fabric was recognised in this subarea (Figure 15). Very shallow, open Fn+3 folds were observed in the easternmost part of the section, in the immediate footwall to the Caledonian front. These folds refold the earlier fabrics shown in Figure 13 and plotted in Figure 14 and are therefore the product of the last of a long series of deformational episodes. Fold axes plunge shallowly E-ENE (crosses in Figure 15). Subhorizontal axial planes require a component of vertical shortening. A plausible explanation, given the only local occurrence of these folds and their proximity to the floor Caledonian thrust, is that they formed in response to a subvertical shortening stress due to loading from the Kalak Nappe Complex. Rice (1998) reports similarly oriented foliation planes from within the nappes of two small klippen at Fægfjord (Figure 3).

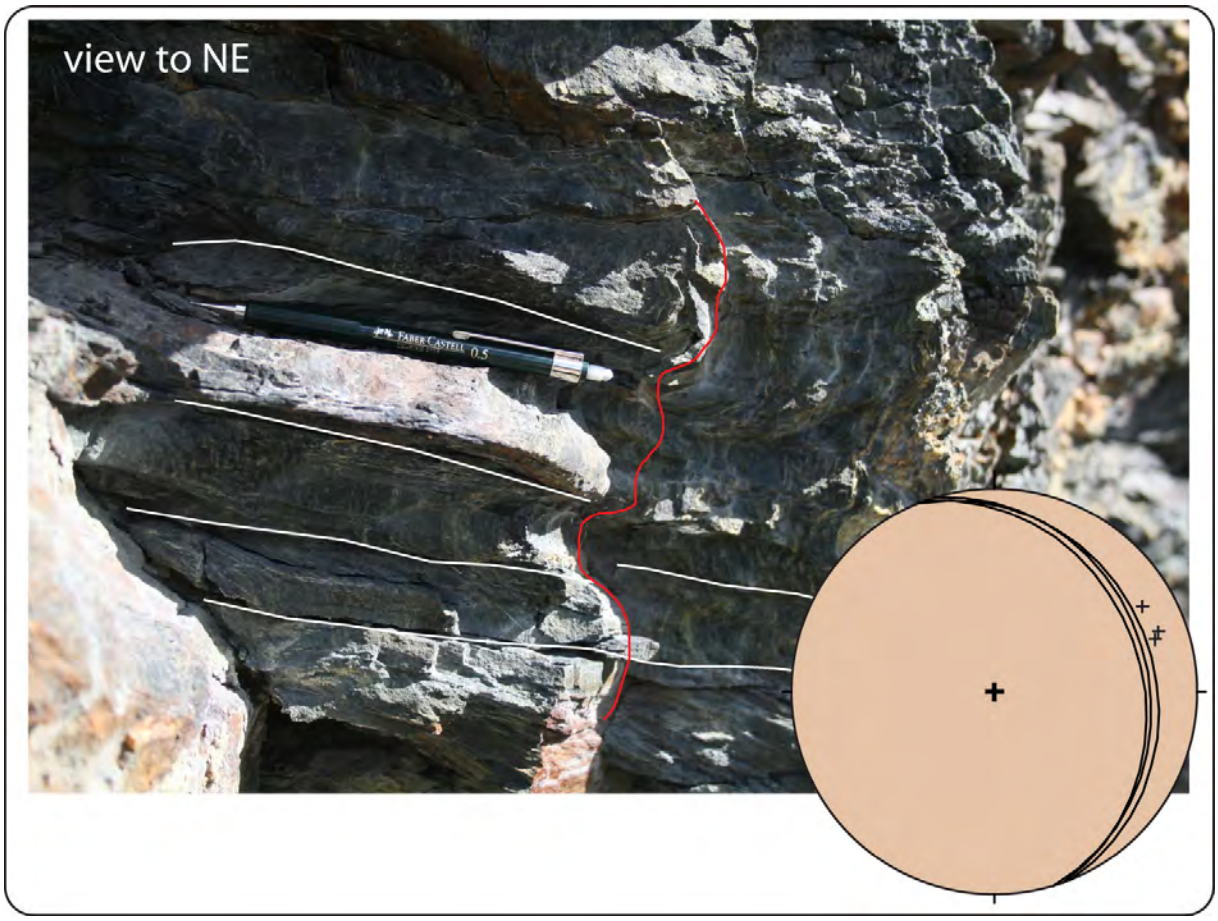


*Figure 15: E-ENE-dipping subhorizontal cleavage, axial planar to open, shallow Fn+3 folds (N 07/24, UTM 35N, 396385 7821475). This planar fabric overprints the fabrics described above.*

The absence of a clearly identifiable Lomvatn Formation prevents from assigning all these structures and fabrics to specific events and only speculations can be made.

### 3.5 Area 5: Porsa thrusts

The dominant structural feature of the Porsa/Saraby area is an array of thrust faults of inferred Caledonian age (although no direct age constraints exist) that cause significant repetition of the local stratigraphy. Some of the thrusts were only briefly investigated in subarea 5 (Figure 3), but their areal distribution covers a much larger portion of the Repparfjord Window and their importance should not be overlooked. The lithologies affected and repeated by the thrusts are the Nussir greenstones and the Bierajav'ri, Kvalsund and Vargsund Formations of the Porsa Group (Figure 3 and Figure 4).

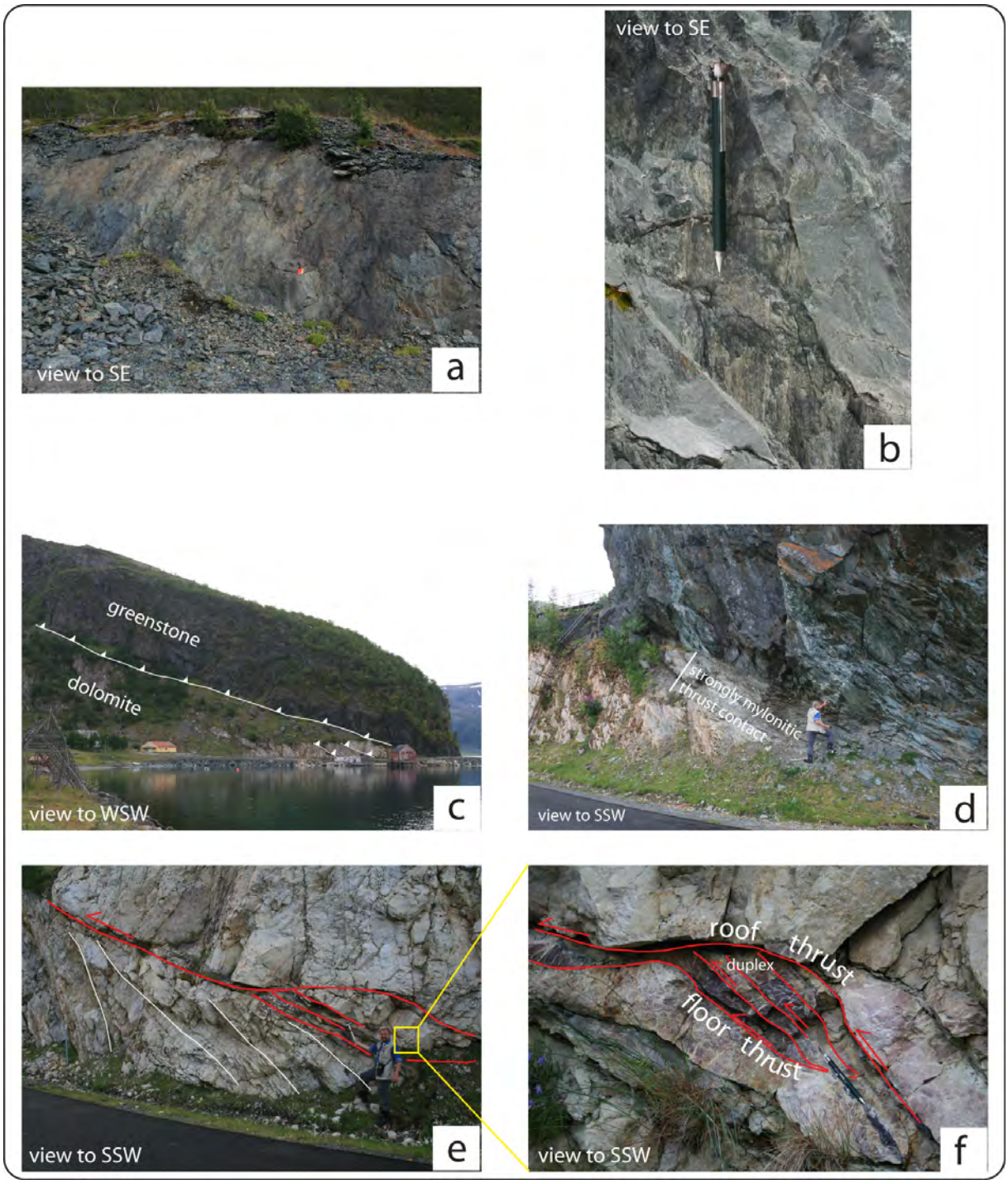


*Figure 16: Field photographs of deformational features linked to the Porsa thrusts in subarea 5. a): Striated fault plane in foliated greenstones and b) detail of the slickensided surface used to constrain the kinematics of the fault (N 07/2, UTN 34N, 596989 7811802). See Figure 17 for fault-slip data from the area. c): View of an easily accessible thrust along the coastal road to Porsa and Saraby (N 07/4, UTM 34N, 598940 7813746). d): Detailed view of the thrust contact with Nussir greenstones in the hanging wall and Porsa dolomites in the footwall. e) and f): Imbricates and small-scale duplex along an intraformational thrust within the Porsa dolomites at the footwall of the thrust of c).*

The deformation style associated with these structures covers the entire spectrum of brittle/ductile conditions, as illustrated by the few selected examples shown in Figure 16.

Striated fault planes, for example, are easily observed within the greenstones of the Nussir Group (Figure 16a and b) and the identification of slickensides on a number of slip planes has led to the establishment of an overall top-to-the-ESE/SE transport direction (Figure 17).

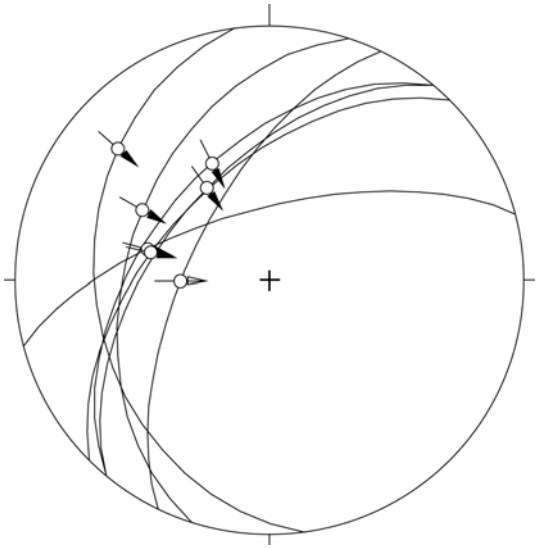

*Figure 17: Fault-slip data constrain an overall top-to-the-ESE/SE transport direction for brittle fault planes within the Nussir greenstones.*

Outcrop N 07/4 (Figure 3) preserves an outstanding exposure of ductile thrusting, where Nussir greenstones override Porsa dolomites along an about NW-dipping thrust fault plane (Figure 16c, and d and stereonet in Figure 18). The thrust contact can be readily followed along the mountain side. The contact itself is defined by a c. 2 m thick ultra-mylonitic/mylonitic level formed predominantly at the expense of the footwall dolomites (Figure 18a). NW-plunging stretching lineations (crosses in the stereonet of Figure 18), combined with consistent NW-side up kinematic indicators (asymmetric deflection of foliation planes into the thrust glide surface, imbricates and duplexes), confirm the overall top-to-the-SE transport direction of the ductile thrust, thus in agreement with the brittle kinematics established from other outcrops in subarea 5. The lowermost part of the greenstone hanging wall is intensely sheared and strongly crenulated, with small-scale chevron folds (Figure 18b). Fold axes, although scattered, plunge generally south, southwest and are thus perpendicular to the reconstructed transport direction.

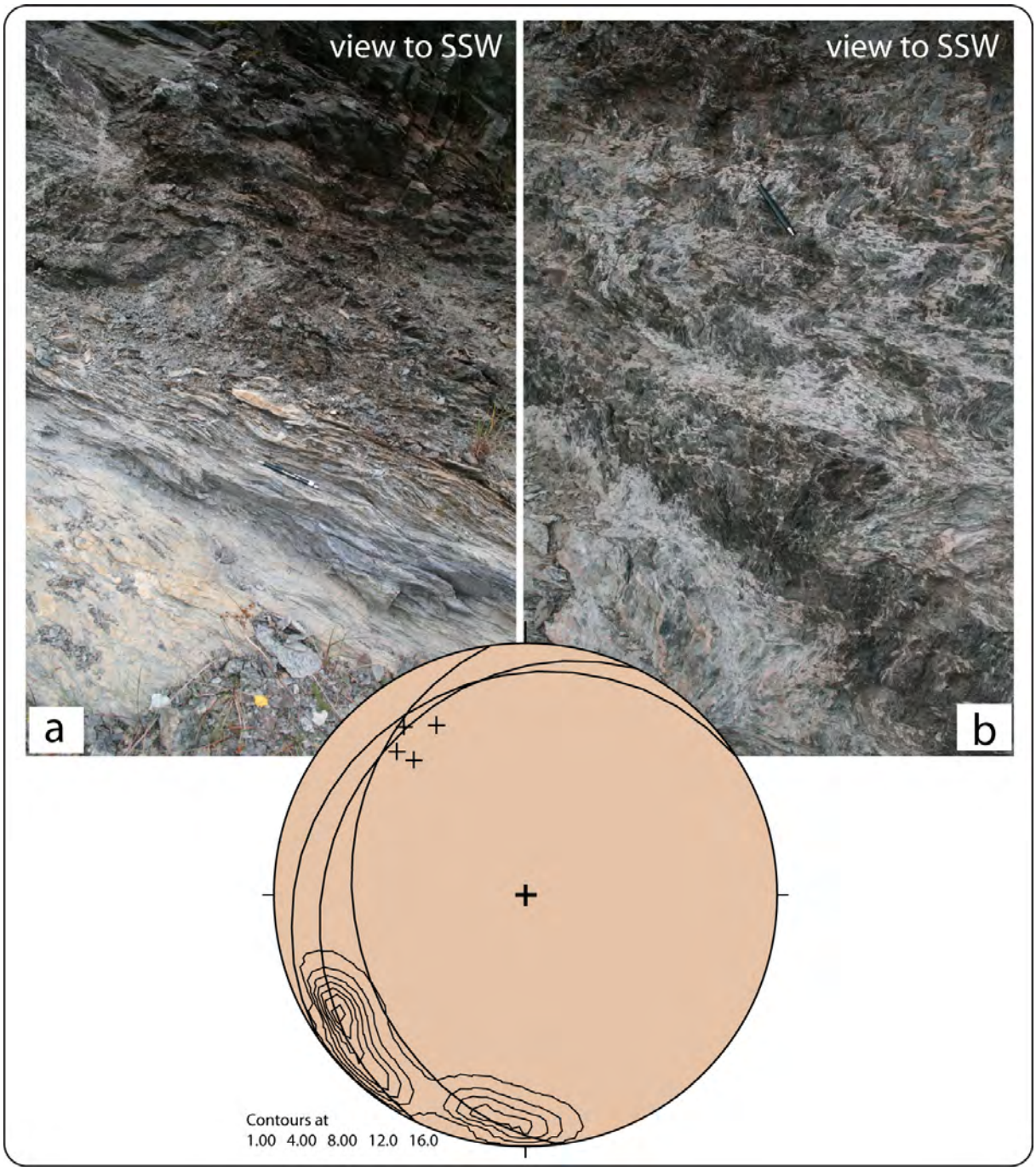


*Figure 18: a): Ultra-mylonites are developed in the uppermost part of the sheared Porsa dolomites (green pencil for scale). b): Nussir greenstones are intensively crenulated in the lowermost section of the hanging wall (green pencil for scale). The stereonet plots the orientation of the thrust fault plane (great circles), of stretching lineations within the dolomite ultra-mylonites (black crosses) and the contoured orientation of nine fold axes from the crenulated greenstones. Note how the fold axes lie at right angle to the transport direction indicated by the observed stretching lineation.*

Thrusts are also developed within the footwall, where they affect only Porsa dolomites. The kinematics of these intraformational faults (shown in Figure 16c) are constrained by small-scale duplexes and imbricates (Figure 16e and f). Jasper lenses are common in the fault zones and are themselves imbricated.

## 3.6 Summary

### 3.6.1 Folding history

The structural grain of the area is the result of the complex superposition of several shortening events that were accommodated by faulting and folding. Reitan (1963) and Pharaoh et al. (1983) produced detailed fold and fault maps of the window, and our work integrates their study by proposing a modified evolutionary scheme for the observed deformation episodes.

The large-scale structure of the Repparfjord Window is characterised by regional E/ENE-W/WSW trending folds, which can be recognised on any geological map of the window. In this structural frame, for example, the Holmvatn Group (the oldest stratigraphic unit in the legend of Figure 4) cores an antiform, which is transitional to a northern synform containing large part of the Saltvatn Group. The responsible folding episode is here referred to as **Fn**, as it encompasses the oldest recognised structures and folds. The suffix "n", on the other side, does not preclude the existence of a still unrecognised older deformational/folding event. Evidence for Dn is found throughout the southern part of the study area, especially in the Saltvatn Group lithologies (Figure 10a). Sandstad et al. (2007), for example, have described Fn folds affecting the sandstones of the Ulveryggen Formation. Folds are generally upright and open to tight.

**Fn+1** folds are common in the study area. They trend generally SW-NE, plunge moderately northeast or southwest and are upright to inclined with axial planes dipping generally to the northwest. They vary in style from tight to isoclinal. They are only slightly misoriented to Fn folds and are thus not easily distinguishable from the earlier folds. Penetrative axial plane cleavage is generally associated with these folds and locally Sn+1 is the regionally dominant fabric (e.g. Figure 11 and Figure 13). The large-scale fold affecting the greenstones of Skinnfjellet (subarea 2) is interpreted as a Fn+1 structure.

**Fn+2** folds are developed only very locally, but in our model they are of great importance. They trend SSW-NNE and plunge moderately northeast, thus only slightly misaligned to Fn+1 folds. Their wavelength is kilometric. The large folds that affect the Saltvatn and Nussir Groups in the Nussir West area (subarea 1) are interpreted as Fn+2 folds that refold an earlier Fn+1 fold (see the final discussion for more details on the model). Fn+2 folds are interpreted

as result of the progressive evolution and reorientation of the shortening field that formed Fn+1 folds. Figure 14a shows the effect of Fn+2 folding on earlier Sn+1 cleavage/foliation planes. No significant Sn+2 axial planar cleavage is pervasively developed.

**Fn+3** folds are observed only in the easternmost part of subarea 4. They refold all earlier fabrics and, as discussed above, are interpreted as being due to vertical shortening (hence their subhorizontal axial planes) derived from the load of the Caledonian nappes.

### 3.6.2 The thrust of Pharaoh et al. (1983)

Our structural analysis of the Nussir West area does not provide conclusive evidence in favour of a major top-to-the-NW thrust (of inferred Svecokarelian age by Pharaoh et al., 1983). Outcrops N 07/15 and N 07/54 have documented top to-the-SE and top-to-the-NW shearing, respectively. The two sites are located on the opposite limbs of the large Skinnfjellet Fn+1 antiform. Our observations show that the folding process that affected the Skinnfjellet antiform, accommodated by flexural flow/slip type mechanisms, is likely the responsible for localised shearing along the limbs, with opposing kinematics (Figure 19). Our view is that shearing is therefore primarily due to strain accommodation along the limbs of the large-scale fold. Furthermore, whereas top-to-the-SE kinematic indicators are common in the entire study area and are related to the Porsa thrust shortening episode, no other evidence of top-to-the-NW shearing was observed, strengthening the idea that top-to-the-NW deformation along the southeastern limb of the Skinnfjellet antiform is only reflecting local conditions and not a shearing event of regional importance.

We question therefore the existence of Pharaoh et al's major discontinuity. In chapter 5 we present other evidence in favour of our model and against the existence of a significant discontinuity.

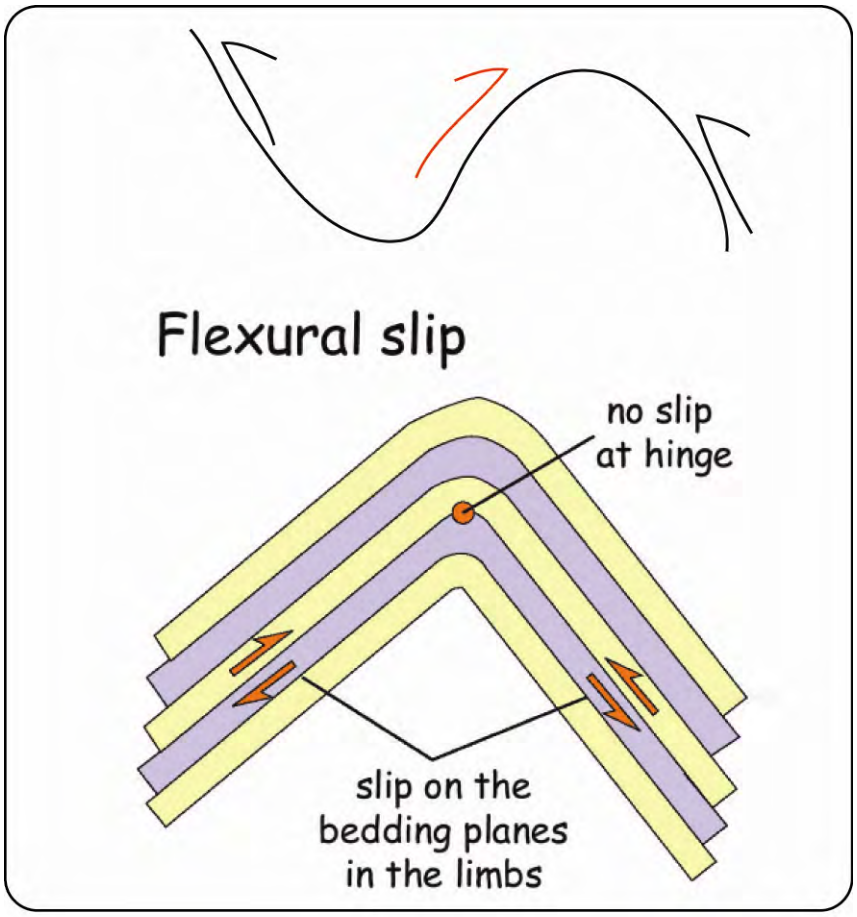


*Figure 19: Proposed model for the occurrence of opposite kinematics on the northwestern and southeastern limbs of Skinnfjellet antiform. Flexural slip is invoked as a viable mechanism.*

# 4. Investigations of selected copper mineralisations in the Repparfjord Window

During the study we have also investigated the structural characteristics and the ore deposit aspects of the Porsa and Bachke copper mineralisations that were exploited in the past but are now abandoned. In addition, we also have briefly investigated the Vesterdalen copper prospect, which locally has yielded high gold values (up to 10 g/t Au). Minor copper occurrences in the area around these deposits were also inspected. The mined areas are generally well exposed, although outcropping remnants of the ore itself are rarely well preserved with the exception of the Porsa mine.

Representative samples of the mineralisations were collected and analysed by NGU in the past, and the data can be found in the Ore Database at NGU. Sampling conducted during this field season was aimed to give a better interpretation of the ore genesis, and focussed on samples of the shear zone rocks, ore types and zones of alteration. Due to excellent outcrop conditions, abundant and detailed sampling was concentrated at the abandoned Porsa mine. Ore samples were analysed by ACME Analytical Laboratories, Vancouver, Canada by ICP-ES after aqua regia digestion for 23 elements and fire assay for the precious metals (Au, Pt and Pd). XRF-analyses of fresh and altered greenstones were conducted by NGU.

## 4.1 Porsa mine

### 4.1.1 Background information

Porsa mine is located at Gruvvatnet (Øvre Porsavatn), 4 km to the south-southeast of the Porsa village (Figure 20). The mine, situated close to a dam built for electrical power-supply purposes, is easily accessible via a well-maintained, toll road.

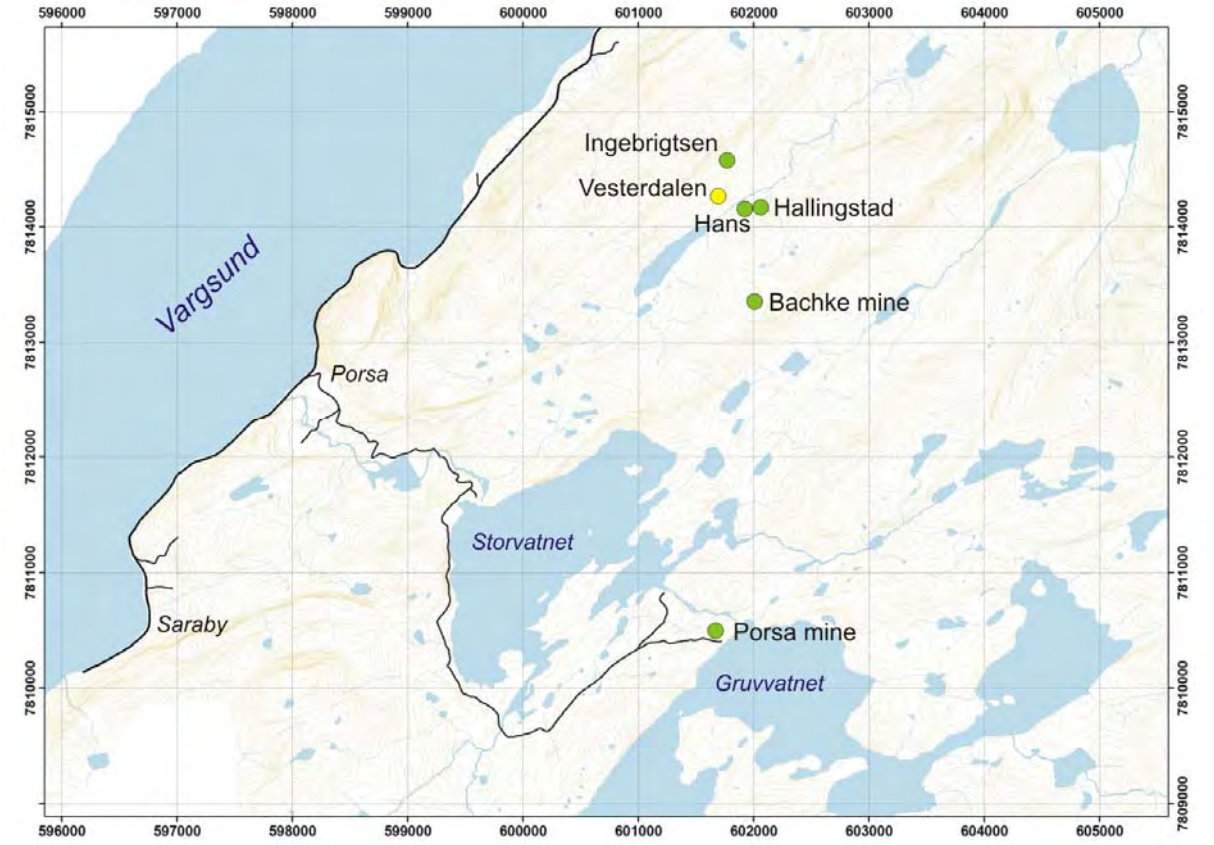


*Figure 20: Location of Porsa Mine along the northwestern shore of Gruvvatnet. Bachke mine and Vesterdalen, Ingebrigtsen, Hans and Hallingstad prospects are also shown on the map. Green dots are copper deposits, the yellow Vesterdalen prospect is gold-copper.*

Mining in the Porsa area started already in 1900 with the opening of the Bachke mine, nearly 3 km north of the Porsa mine. The company A/S Vesterdalen Kobbergruver carried out investigations in Porsa in 1905, although Porsa Copper Mines Ltd, a company based on English investments and directed by Louis Greville, had by then already conducted minor prospecting in the area. Mining right disputes between the two companies were never settled. A/S Vesterdalen Kobbergruver went however bankrupt by the end of 1905, and its properties were taken over by the Swedish company Skandia. Skandia conducted only very limited investigations in the period 1906-07, and sold eventually the rights to Porsa Copper Mines Ltd. Test mining was carried out in Porsa in 1905 and 1906 and full scale production started soon after. Ca. 600-700 t of ore were sold to Alten Kobberverk in Kåfjord and partly shipped to a smelter in Swansea in England. Porsa Copper Mines Ltd continued the mining activity and the annual ore production was 3-4000 t in the period 1909-1911. In 1911 the mine was closed down for reasons that remain unknown. In 1918 the mine was reopened by A/S Porsa Kobbergruver, which actively mined it until 1931.

### 4.1.2 Geological framework and ore geology

The mined Porsa copper deposit consists of two parallel, nearly east-west orientated carbonate+quartz veins (Figure 21). The ore-bearing veins are about 100 m long, 3 to 10 m thick and are located about 150 m apart. They were named “Greville” (the one to the south) and “Parallel” (also named Chr. Michelsen in some reports). Other minor subparallel veins are also present but were not mined. The two main shafts at the Greville and Parallel veins were mined down to a depth of 76 m and 64 m below the ground during production. From an adit at level -64 m in the Parallel vein, another shaft was constructed down to -96 m depth below surface. Further mining was carried out along minor adits and stopes on several levels. Their entrances are now closed by concrete and steel covers and they are thus not accessible for inspection.

The macroscopic ore consists of aggregates and thin lenses and bands of chalcopyrite and pyrite (Figure 22). Magnetite and haematite are also commonly found in the calcite-dominated veins, together with lensoidal inclusions and enclaves of the wall-rock (Figure 21 and Figure 22). Sphalerite is found as accessory mineral. The major gangue mineral is calcite, and in minor amounts quartz, plagioclase, amphibole and chlorite. Locally, tourmaline is also abundant. Geochemical analyses of representative ore samples collected in the past by NGU indicate around 1-5 % Cu (NGU; Ore database). Two samples (out of a total of 18) yielded also 1-1,5 g/t Au. No other elements of economic interest were recorded.

*Figure 21: Typical appearance of the copper-mineralised Parallel calcite vein. The central part is strongly foliated and sheared, whereas the vein texture becomes almost completely structureless and massive at the edges. Undeformed to poorly deformed host rock enclaves are visible on the left hand side of the picture (bottle-green irregular lenses). Their strongly sheared equivalent is seen in the pervasively foliated vein core (extremely stretched bottle-green stringers).*

The exploited veins are hosted by the generally weakly deformed to massive greenstones of the Svartfjell Formation of the Nussir Group, just 2 km northeast of the Caledonian Nappe Front. Well-preserved pillow lavas and other primary structures occur in the greenstones between the veins. Greenstones are generally altered at the contact to the mineralised veins and the details of this alteration were studied in the easternmost part of the Parallel vein (site A in Figure 26). The alteration zones are a few cm to a few dm thick and are characterised by

bleaching and localised reddening of the host rock. Minor chalcopyrite-bearing calcite veinlets commonly occur in these zones.

Thin section analysis of the unaltered greenstone (sample JS07-32) reveals fine-grained, ‘dusty’ amphibole-rich mafic matrix with randomly orientated laths of plagioclase (0,3-0,6 mm). Disseminated, fine-grained, euhedral magnetite (0,3-0,5 mm) with inclusions of silicates is common. The greenstone is crosscut by a fine-grained quartz-epidote veinlet. Sample JS07-33, a weakly altered greenstone, contains less mafic minerals and some randomly orientated plagioclase laths, as in the fresh greenstone. Fine-grained, green biotite and chlorite (0,1-0,2 mm) occur around the opaque minerals, mainly euhedral magnetite. A few, partly cracked pyrite grains contain inclusions of chalcopyrite. The most strongly altered greenstone (sample JS07-34), that is in contact with the copper-mineralised carbonate vein, is a fine-grained (0,1-0,2 mm), more chlorite-rich greenstone, when compared to the other samples. Some coarse-grained (10-15 mm), recrystallised laths of plagioclase are found in part of the thin section, whereas the fine-grained plagioclase laths were replaced by alteration minerals. Disseminated grains of carbonate are found. Opaque minerals mainly comprise chalcopyrite and a few pyrite grains, but no magnetite.

XRF-analyses were conducted on samples from both the altered and the “fresh” greenstones (Table 1). Analyses show enrichment in the content of K, Na, Ba and Rb but depleted of Al, Ca and Sr contents, likely due to the alteration of the greenstone. An enrichment of Cu and Co is also obvious. The solutions that precipitated the carbonate veins could therefore have been partially generated in situ by leaching of Ca and Sr from the greenstone host rock.

In summary, out observations suggest that chloritisation, carbonatisation and albitisation are the alteration processes that affected the greenstone in association with the copper mineralisation at the Porsa mine.

Table 1: XRF-analysis of unaltered and altered greenstone at Porsa mine

| | | Unaltered greenstone | Weakly altered greenstone | Altered greenstone |
|---|---|---|---|---|
| | | **JS07-32** | **JS07-33** | **JS07-34** |
| $SiO_2$ | % | 50,40 | 48,30 | 55,20 |
| $Al_2O_3$ | % | 14,00 | 13,70 | 12,40 |
| $Fe_2O_3$ | % | 12,30 | 18,10 | 12,90 |
| $TiO_2$ | % | 1,24 | 1,31 | 0,80 |
| MgO | % | 6,35 | 5,38 | 5,20 |
| CaO | % | 8,20 | 2,82 | 4,98 |
| $Na_2O$ | % | 4,32 | 5,08 | 6,06 |
| $K_2O$ | % | 0,44 | 2,59 | 1,04 |
| MnO | % | 0,15 | 0,11 | 0,12 |
| $P_2O_5$ | % | 0,11 | 0,11 | 0,05 |
| LOI | % | 1,48 | 1,00 | 0,86 |
| Sum | % | 99,10 | 98,60 | 99,60 |
| | | | | |
| S | % | <0,02 | 0,045 | 0,089 |
| As | ppm | <10 | <10 | <10 |
| Ba | ppm | 67 | 208 | 127 |
| Co | ppm | 30,2 | 59,2 | 70,6 |
| Cr | ppm | 93,8 | 103 | 68,4 |
| Cu | ppm | 33,1 | 464 | 1270 |
| Ni | ppm | 67,6 | 100 | 78,7 |
| Pb | ppm | 14,7 | 15,9 | 15,1 |
| Rb | ppm | 8,8 | 80,7 | 22,5 |
| Sr | ppm | 153 | 19,9 | 29,2 |
| V | ppm | 257 | 302 | 191 |
| Y | ppm | 22,8 | 25,3 | 20,4 |
| Zn | ppm | 50,9 | 61,8 | 37 |
| Zr | ppm | 101 | 108 | 64,2 |
| Mn* | ppm | 1020 | 854 | 907 |

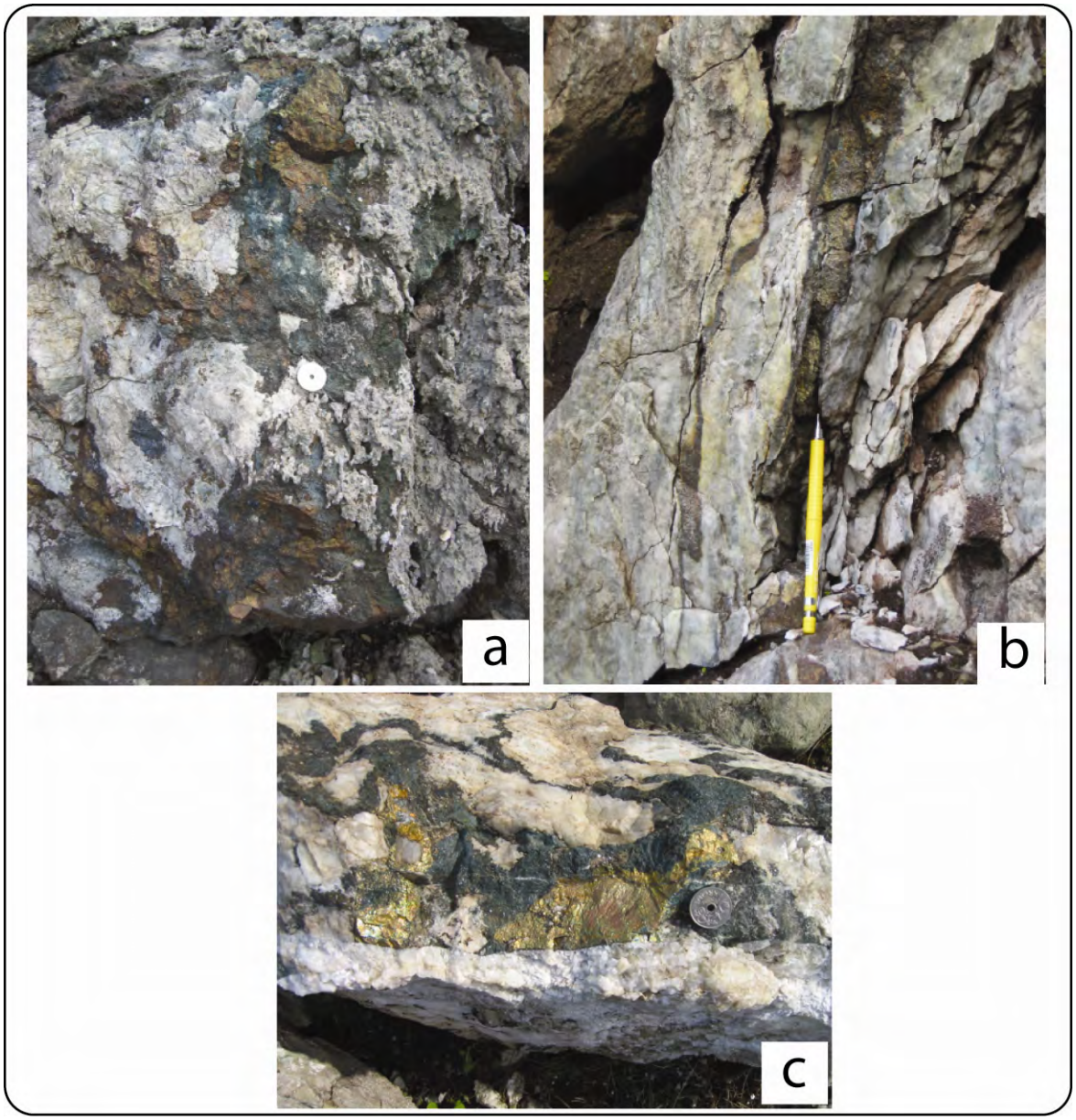


*Figure 22: a): Typical Cu mineralisations at Porsa mine). b): Chalcopyrite aggregates and greenstone xenoliths in structureless, coarse-grained calcite-vein, Parallel vein. c): Chalcopyrite band in foliated calcite-vein, Greville vein. In the lowermost part of the photo is a copper minerals barren and undeformed calcite-vein that crosscuts chalcopyrite aggregates associated with greenstone xenoliths (relationships observed in a loose boulder from Parallel vein).*

The main ore minerals observed in samples collected during our fieldwork are chalcopyrite, pyrite and magnetite. The sequence of formation of the various minerals within the copper mineralised carbonate vein is best illustrated by a sample from site F in the Parallel vein (Figure 26). Aggregates of coarse-grained, bladed magnetite (~10 mm, pseudomorph of haematite) in the carbonate vein are transacted by medium- to coarse-grained chalcopyrite (up to 5 mm), both across and along the texture of the magnetite.

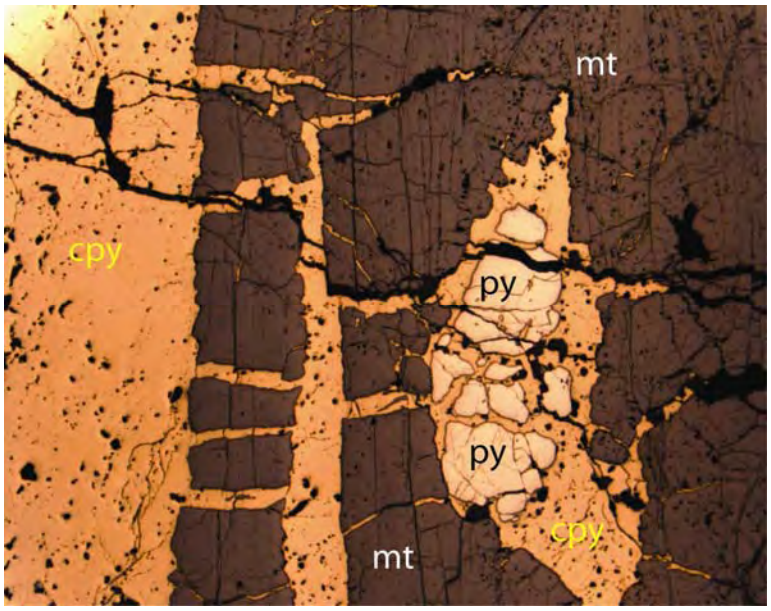


*Figure 23: Microphotograph of chalcopyrite (cpy) that transect magnetite blades (mt) and contains inclusions of pyrite (py) in Parallel vein (reflected light, FOV 4,36x5,40 mm; sample JS07-12).*

Pyrite inclusions in magnetite are partly cracked and infilled by chalcopyrite. All sulphide minerals are crosscut by later thin (0,5-1,5mm) veinlets of anhedral carbonate and minor, very fine-grained quartz (Figure 24). In samples from the Greville mine pyrite is observed both as inclusions and filling micro-cracks in chalcopyrite. Covelline occurs occasionally as alteration rim around chalcopyrite. Common silicates within the copper mineralised carbonate vein studied are albite, quartz, actinolite and chlorite. A few grains of scheelite were identified by use of an UV-lamp. Actinolite commonly comprises long, prismatic needles. Both actinolite and albite indicate partly open-space filling during the formation of the veins. Fragments of greenstone are also common, and often they exhibit subrounded shapes (Figure 25).

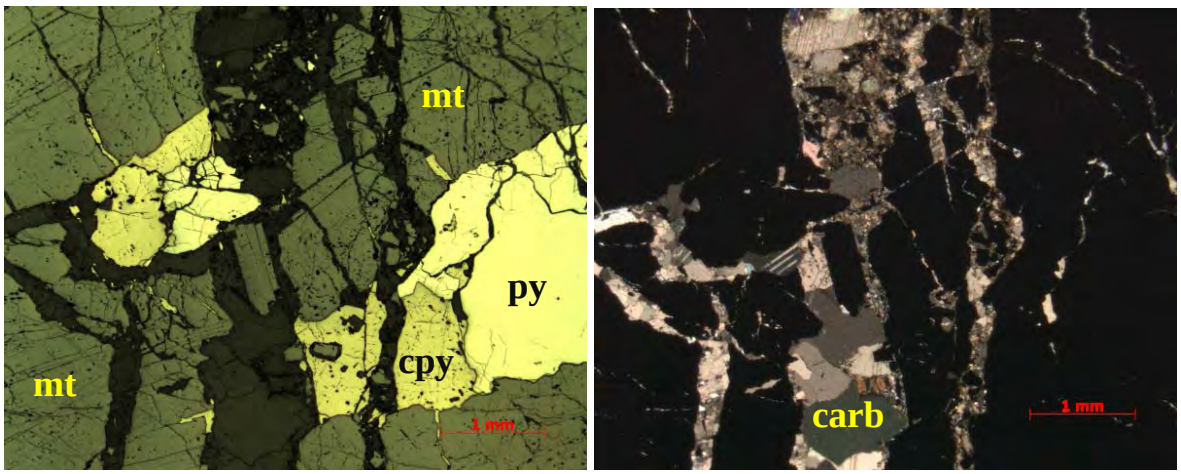

*Figure 24: Microphotograph of a chalcopyrite (cpy)-pyrite (py) veinlet that crosscuts haematite transformed into magnetite (mt) and is cut by later thin carbonate (carb) veins (left: reflected light, right: transmitted, polarized light; FOV 4,36x5, 40mm; sample JS07-12).*

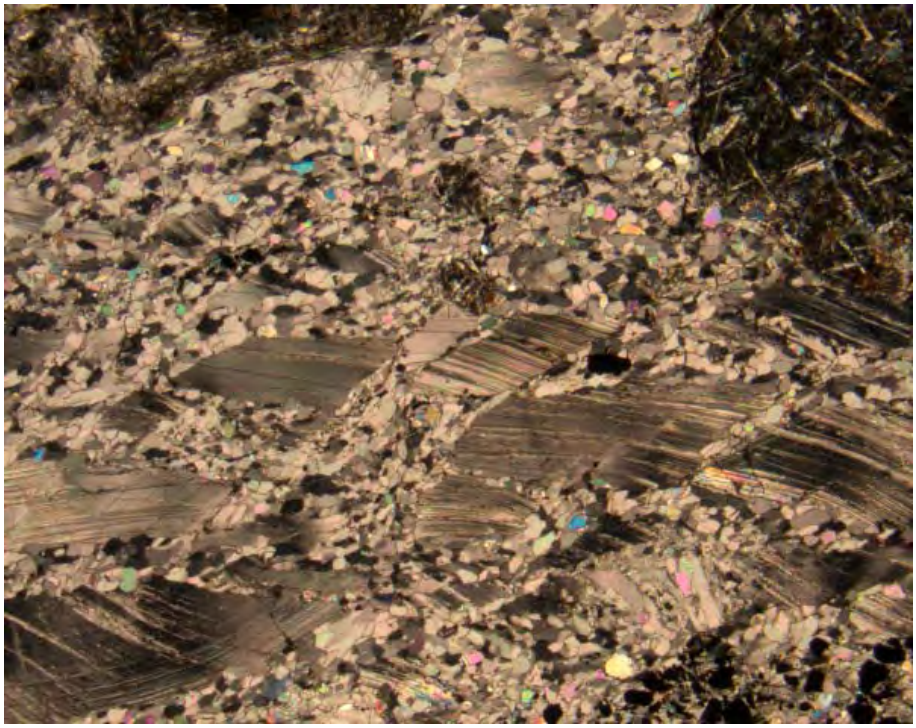

*Figure 25: Microphotograph of sheared, coarse grained calcite in fine grained calcite vein at site III in Greville. Subrounded inclusion of fine grained greenstone in the upper right corner (polarized light, FOV 4,36x5,40 mm; sample JS07-30).*

### 4.1.3 Structural features of Porsa mine

Structural observations were made in a few trenches and minor pits distributed over the entire exposed length of the Parallel vein and in three small open pits along the Greville vein. In addition, crucial information for the model proposed in this report was gathered at outcrop X along the northwestern coastline of Gruvvatnet (Figure 26).

The exploited veins are about 100 metres long and their thickness varies between 3 and 10 m and they seem to taper off at depth (NGU; Ore database). Their spatial distribution and geometric arrangement, together with the distribution of some other minor veins reported in old technical reports, show that the veins are possibly distributed in an echelon fashion and that they display sinistral stepping, with a major overlapping between contiguous segments (Figure 26). For example, the Parallel vein strikes approximately 90°-100° in its eastern part and dips subvertically over a length of 50 m. From locality C (Figure 26) a shallow trench was dug westward to verify the potential continuation of the vein, but only greenstone was

exposed. A similarly oriented segment of the Parallel vein can instead be found and followed for another 20 m slightly offset to the south by a lateral step (Figure 26).

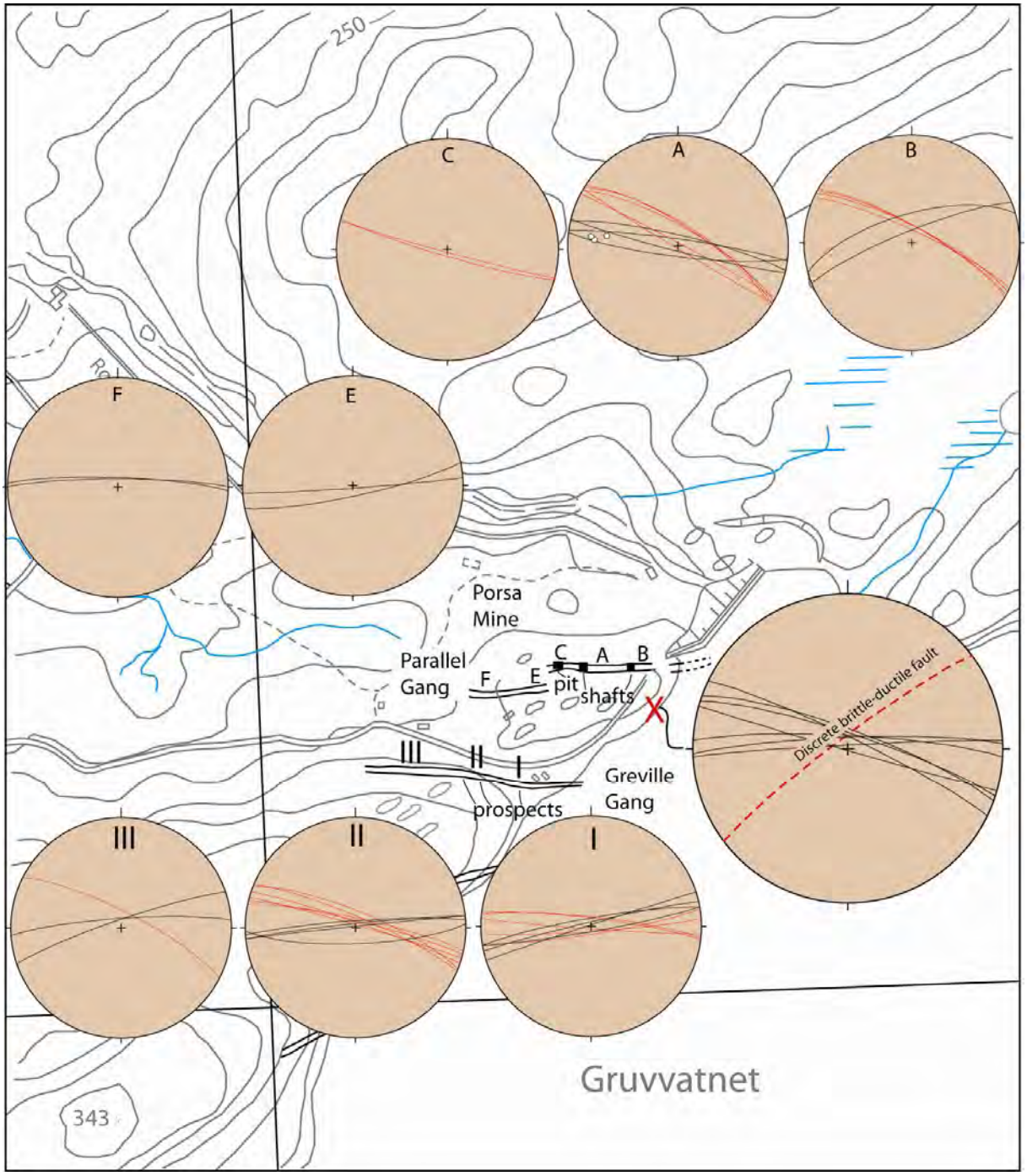


*Figure 26: Detailed map of the Porsa ore-bearing Parallel and Greville veins. Stereonets plot the orientation of the pervasive mylonitic foliation within the central part of the veins (referred to as "Si" in the text and plotted by the red great circles) and the orientation of the geometrically discordant external foliation of the vein (Se) as observed away from the high-strain core.*

Structural analysis of the individual veins shows that they contain a very pervasively sheared central core (Figure 21 and Figure 27). In it the foliation is very penetrative and is defined by

sheared calcite and strongly sheared and stretched inclusion trains of the greenstone host rock (Figure 27). The edges of the veins are, on the other side, generally much less deformed, display more massive, structureless textures and often contain only poorly deformed blocks of greenstone ripped off by dilation from the host rock. Despite the lack of such a penetrative planar fabric, however, the external portions of the veins also contain an easily recognizable weak foliation.

Ore minerals occur as irregular aggregates and lenses in the outer part of the calcite vein and as deformed stringers and bands in the foliated part (Figure 27). Several phases of precipitation of calcite and sulphides are found.

Key to the structural model proposed in this report was the observation that there exists a systematic and consistent geometric relationship between the orientation of the foliation in the central part of the vein (from now on referred to as “internal foliation, Si”) and in the external portions (referred to as “external foliation, Se”).

*Figure 27: Detail of the subvertical, strongly sheared inner part of the Parallel vein (Si). Note the presence of undeformed blocks of the host rock to the left and their significant shearing/stretching in the core of the ductile shear zone. View to the east.*

The stereonets of Figure 26 show two systematic sets of planar orientations, for example at site A, B and C of the Parallel vein and I, II and III of the Greville vein. Red great circles plot foliation planes typical for Si, whereas black great circles plot Se. Field relationships are

shown in Figure 28, where one example from the Parallel vein and one from the Greville vein illustrate a consistent geometric pattern, whereby Se is asymptotically bent into Si. This geometric relationship suggests a component of simple shear along Si, which led to the formation of the pervasive foliated vein cores and to the passive dragging and rotation of Se into the shear direction. A few subhorizontal stretching lineations (e.g. site A in Figure 26) suggest strike-slip shearing and the geometry of the sigmoidal asymptotic bending of Se into Si indicates consistently a dextral sense of shear.

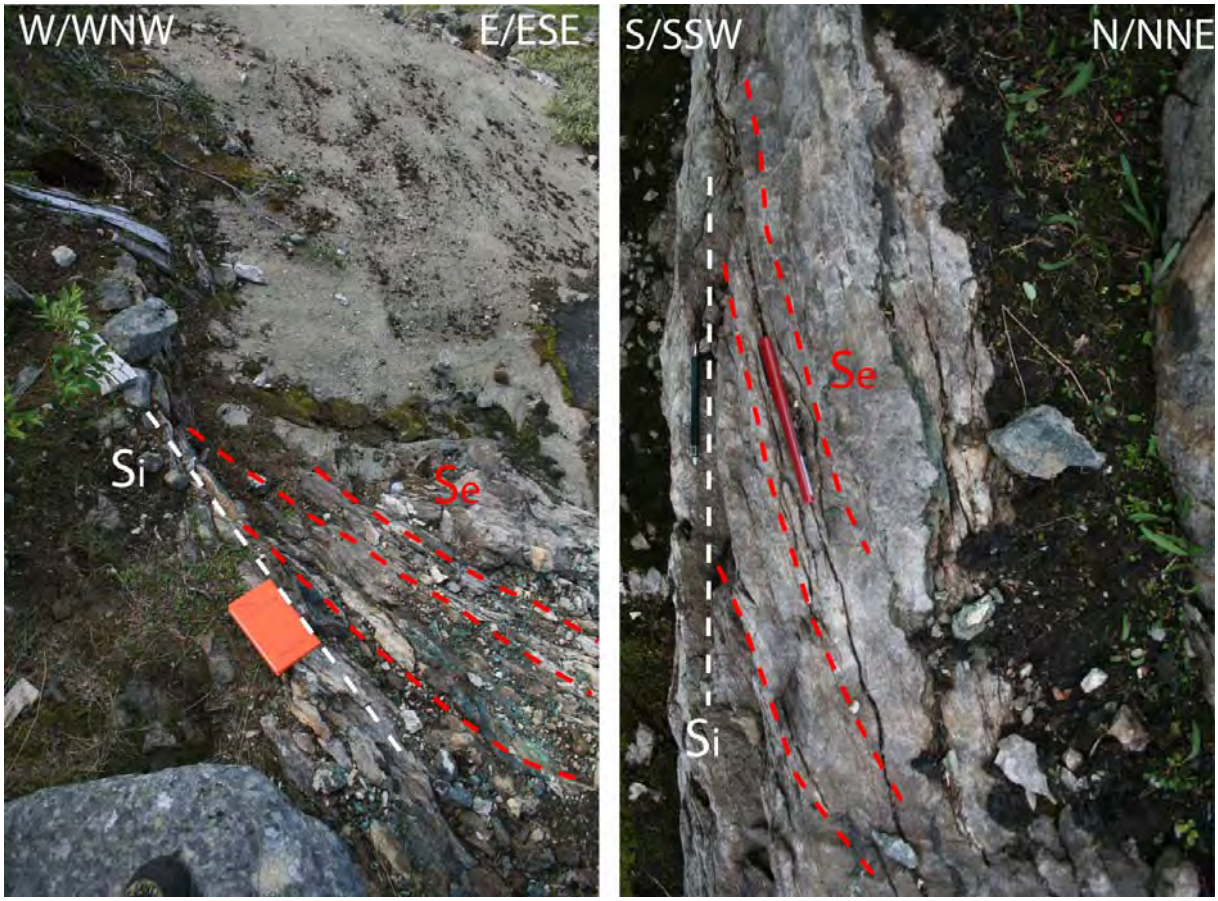


*Figure 28: Geometric relationship between Si and Se observed at locality B of the Parallel vein and I of the Greville vein (see Figure 26 for their location). Both photos are taken looking down on a subhorizontal slab.*

Dextral kinematics is confirmed by several other indicators found within the veins. Figure 29, for example, shows a dextral shear band offsetting a thin calcite vein observed at site I in the Greville vein.

Figure 30 shows a schematic model for the development of the veins and their subsequent mineralisation. The coexistence of structural features that can be ascribed to different rheological domains (plastic/brittle vs. viscous/ductile) requires a complex kinematic/dynamic model for the Porsa mineralisation. According to our interpretation, the subvertical veins are

shear dilational fractures that occupy the central part of a ductile dextral shear corridor, which strikes about northeast-southwest and has a subvertical dip. These shear dilational fractures formed in the central part of the shear zone, oriented perpendicularly or at least at high angle to the synkinematic greatest instantaneous extension direction.

There is plenty of evidence supporting dilation within and in the immediate vicinity of the mineralised veins, such as dense networks of hydrofractures and large blocks of greenstone ripped off the walls of the country rock hosting the veins. Viscous deformation overprinted the fabrics of this early pressure-dependent plastic behaviour (brittle deformation; e.g. Figure 27).

*Figure 29: Dextral shear band offsetting a thin calcite vein in Greville. Note the malachite staining. Photograph taken looking down.*

Studies of natural “ductile shear zones” have established that there is a clear tendency for fluid to flow into and along shear zones. Pressure-dependent initial fracturing and microcracking, highly enhanced in zones of high strain rate or overpressured fluid phases, can result in a pressure-dependent viscoplastic rheology of the shear zone still under bulk viscous conditions, without any or only very limited overall loss of cohesion. This is probably the case at Porsa, where initial plastic deformation and opening of dilatant fissures could be due to overpressured fluids. These fluids circulated in the dilatant rock volumes, caused copper mineralisation and localised later ductile deformation.

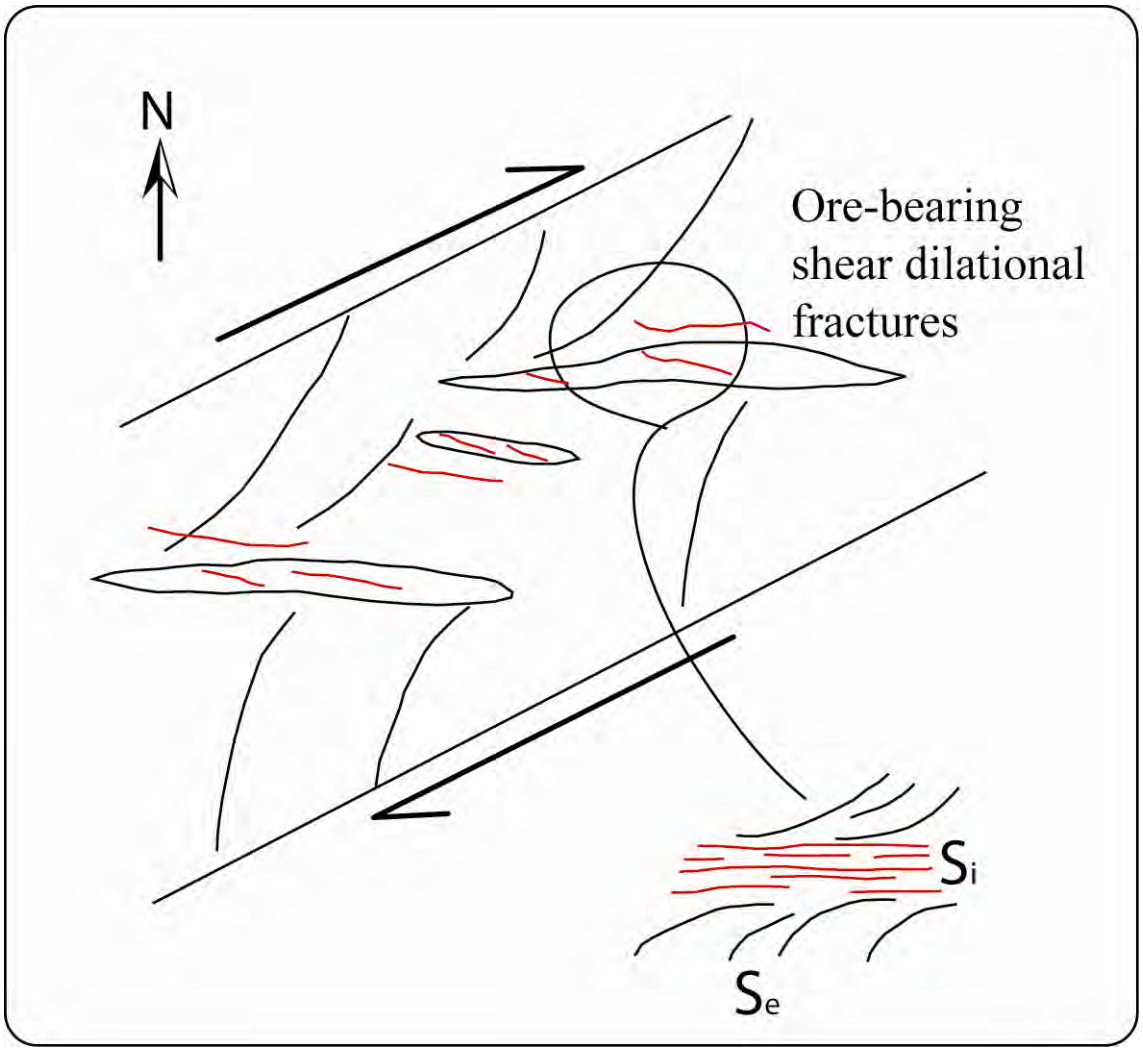


*Figure 30: Schematic model of vein generation and subsequent shearing. Initial pressure-dependent plastic (brittle) deformation generated dilational fractures, led to fluid flow and copper mineralisations and finally also localised later viscous (ductile) strain.*

Strong arguments in favour of this model were derived from outcrop "x" on Figure 26. A polished rock surface on the shore of Gruvvatnet (Figure 31a) contains a well-exposed NE-ENE/SW/WSW-striking brittle-ductile shear zone. Its orientation, shown in Figure 26, is indeed similar to the orientation of the dextral shear corridor necessary for the model of Figure 30.

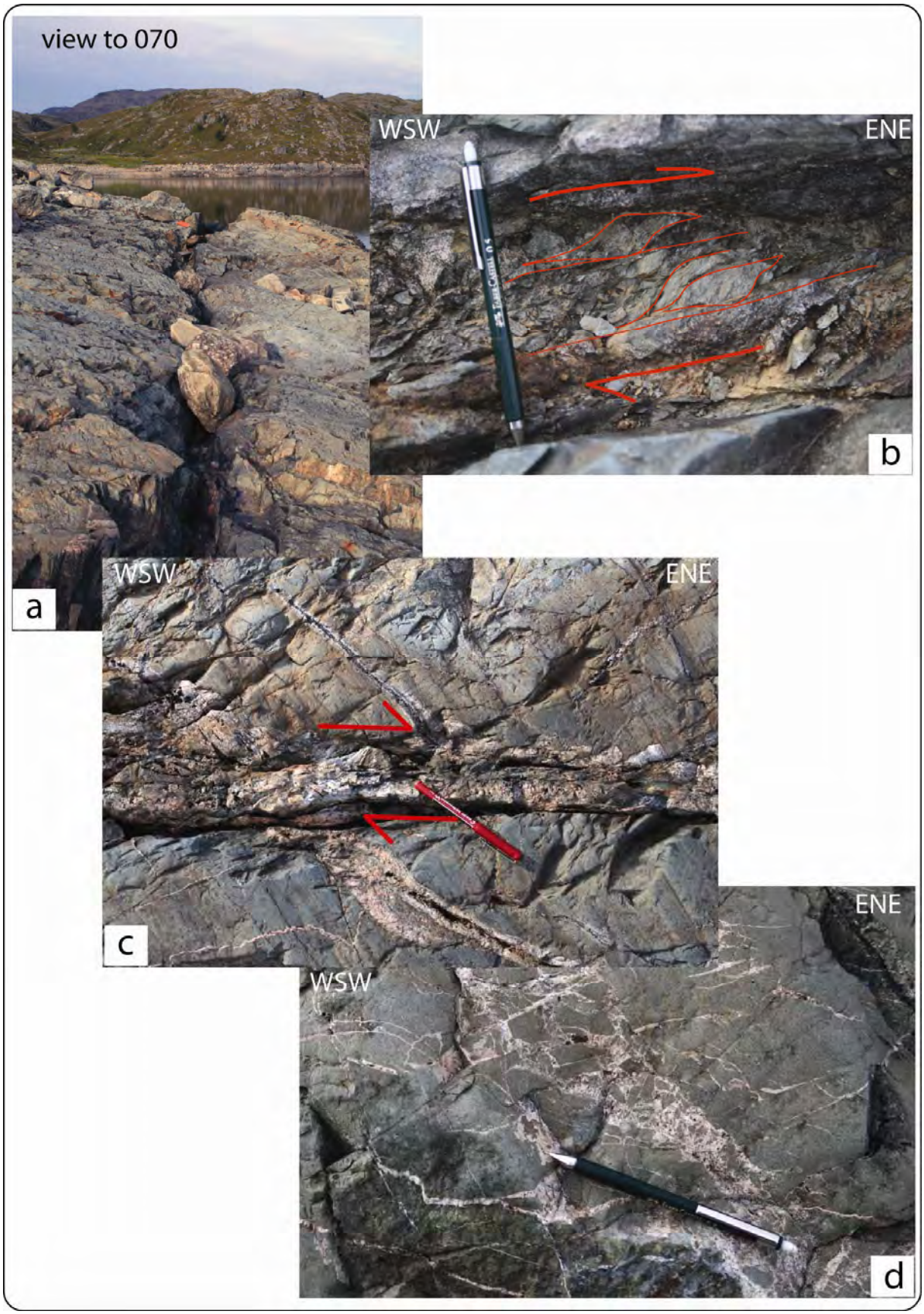


*Figure 31: a): View of the discrete brittle-ductile shear zone on the northwestern coast of Gruvevatnet (red cross on Figure 26). b): Detail of the fault zone core, with foliated cataclasites and protomylonites. Asymmetric clasts and foliation boudins indicate dextral kinematics. c): Dextral offset of a joint across the shear zone. d): Dense network of calcite*

*filled hydrofractures in the greenstones immediately to the south of the shear zone. Photographs b, c and d are taken looking down on a subhorizontal slab.*

The fault zone is about 1 m wide, is slightly undulating and is characterized by a core defined by foliated cataclasites and phyllonites. Dilational fractures and joints are associated with the shear zone and represent Riedel type shears. These define a very pervasive, yet localised, fracture cleavage. Fractures strike from E/W to W-WNW/E-ESE, thus identical in orientation to the mineralised Porsa and Greville veins and to Si and Se.

Asymmetries within the core as well as the distribution of Riedel shears indicate a dextral sense of shear parallel to subhorizontal stretching lineations (Figure 31b and c). Figure 31c shows a dilatant fracture, infilled by stretched calcite fibres, which is offset dextrally by the main fault. This observation supports the model proposed for the development of the copper mineralisation exploited at Porsa, whereby early dilation was overprinted by dextral ductile shearing (Figure 30). Also, Figure 31d shows hydrofractures associated with the brittle-ductile shear zone, demonstrating the importance of an overpressured fluid phase in the evolution of these structures. These similarities are used to make the shear zone a small-scale analogue for the shear corridor within which the Porsa mineralisation was formed.

Study of a thin section from one of the veins in Figure 31c shows a very fine-grained, dark and ‘dusty’, magnetite-rich greenstone that is gradually bleached towards a fine- to medium-grained (0,3-0,6 mm) albite vein, which is up to 6 mm wide. Minor magnetite and pyrite occur within the vein, and a significant enrichment of euhedral to sub-euhedral magnetite and partly pyrite along the rim of the vein is found (Figure 32). The albite vein is obliquely crosscut by very thin quartz-albite veinlets.

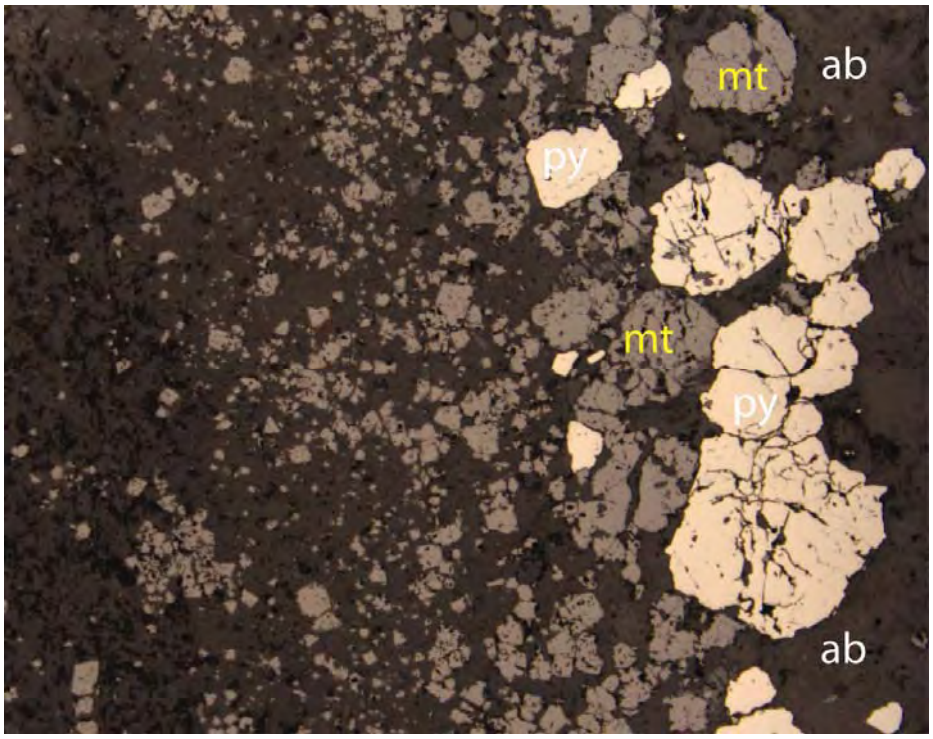


*Figure 32: Microphotograph showing enrichment of magnetite (mt, grey colour) and pyrite (py, light grey/pinkish colour) along the outer rim of an albite (ab) vein (reflected light, FOV 4,36x5,40 mm; sample JS07-31).*

### 4.2 Bachke mine

The main mining activity in the Vesterdalen area took place at the beginning of the 19$^{th}$ century, with main focus on Bachke mine.

Bachke mine is located around 400 m a.s.l., 200 m northeast of the Ivtasvarri peak and around 2 km southwest of the top of mountain Middagstinden, in between the Vesterdalen and Kvalsunddalen valleys (UTM 34N 602062 7813435; Figure 20). The Bachke deposit was discovered in the autumn of 1900 and mining was carried out by various companies, but mainly by Vesterdalens Kobbergruber A/S. The main part of the extracted ore, about 3000-4000 t, was sold to Kåfjord Kobbergruber in Alta. Further exploration, including drilling, was commenced in 1926 and mining of additional 8000 t was achieved in the period 1929-1931.

Mining exploited four parallel quartz-carbonate veins. The veins are hosted by greenstones of the Nussir Group and are orientated northwest-southeast, with variable but generally steep dips. Mining was carried out predominantly along the 100 m long Bachke vein (Bachke shaft) and later along Lund and Puntervold veins through the Kvalsund adit. The depth of the mine is about 50 m below ground level.

Unfortunately, the ore can be studied only in boulders from the tailings due to the lack of easily accessible mineralised rocks in the mine. The main sulphide minerals are chalcopyrite

and pyrite. Magnetite and haematite occur in subordinate amounts. Krause (1980) described uraninite as an accessory mineral on crosscutting veinlets. The vein matrix is composed of quartz, calcite, albite, chlorite and fragments of wall-rock (Figure 33). Just minor chloritization of the greenstone is observed. The thickness of the veins is 1-1,5 m. Sulphides occur as veinlets, lenses and aggregates in the quartz-carbonate vein. Their appearance was suitable for hand-cobbing of high-grade copper ore in the past. Geochemical analyses of representative ore samples previously collected by NGU yield between 1-7,5 % Cu (NGU; Ore database).

*Figure 33: Chalcopyrite in quartz-chlorite vein at Bachke mine.*

*Figure 34: Pillow lava with cherty lenses at Bachke mine. View to the southeast.*

The greenstone is dark green and commonly magnetite-bearing. Pillow lava textures are well preserved in the area close to the main shaft and indicate way-up towards the southeast (Figure 34).

Both chalcopyrite- and haematite-dominated veinlets are found in the quartz veins in the greenstone, which is generally fine grained and rich in plagioclase. It contains randomly oriented plagioclase laths (0,1-0,3 mm) and short prismatic grains of biotite (0,1-0,2 mm) and amphibole. A typical example of the copper mineralisation is shown in Figure 35. Chalcopyrite with a few inclusions of pyrite is intergrown with lath-shaped haematite. Molybdenite occurs as minor inclusions (10-100 µm) in chalcopyrite and albite.

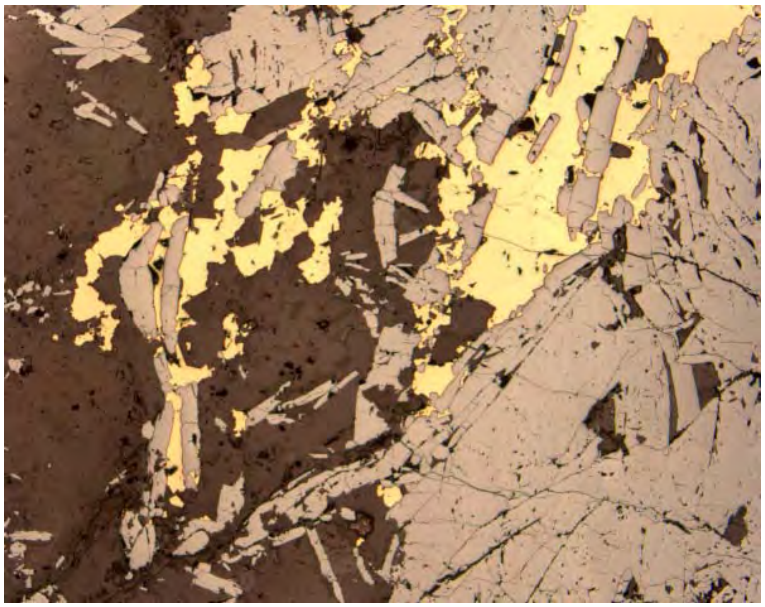

*Figure 35: Microphotograph of chalcopyrite (yellow) and haematite (grey) mineralisation in quartz vein at Bachke mine (reflected light, FOV 2,36x2,98 mm; sample JS07-25).*

Due to the lack of exposure, it was not possible to gather sufficient information to elaborate a consistent structural model for the mineralisation at Bachke. Nonetheless, some interesting observations were made (Figure 36).

A northeast-southwest striking, subvertical shear zone was observed in the Nussir Group greenstones hosting the mineralisations (red great circles of Figure 36d). The shear zone, c. one meter wide, is fully ductile at the scale of the outcrop and, based on subhorizontal stretching lineations and the asymmetric deflection pattern of the external fabric into the shear plane (Figure 36c), is interpreted as a dextral strike-slip shear zone.

At the now partially closed entrance of the Kvalsund adit, there is a 1 m thick, steep shear zone (SW-dipping black great circle in the stereonet of Figure 36d and Figure 36a). No obvious kinematic indicators were observed, although the weak deflection of the external fabric in the shear zone suggests a normal top-to-the-N/NNE kinematics. A similar sense of displacement was observed on a striated surface immediately above the adit entrance (Figure 36b), with a top-to-the-NNW normal sense of shear along a moderately NNE-dipping plane (Figure 36b and d).

Given the paucity of observations it is difficult to integrate the gathered information in a consistent structural evolutionary scheme. We limit ourselves in here to the observation that there exist geometric and kinematic similarities between the dextral ductile shear zone at Bachke and the dextral shear corridor at Porsa, possibly suggesting a genetic relationship between the two.

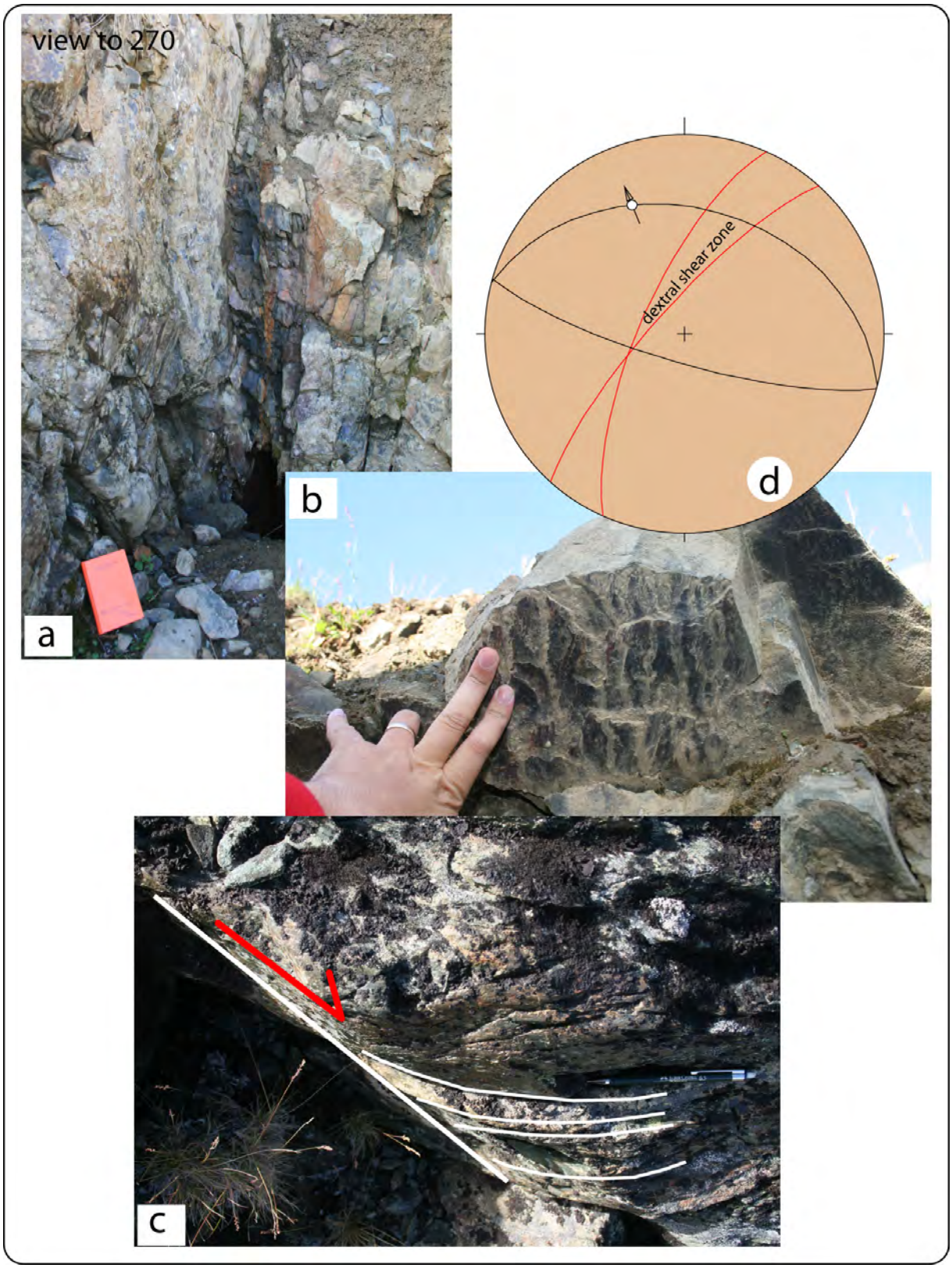


*Figure 36: Structural features at Bachke mine. a): Discrete steep shear zone at the entrance of Kvalsund adit. The shear zone is plotted in Figure 36d by the steep, S-dipping black great circle. No obvious stretching lineation or kinematic indicators were observed, although the general impression is of a top-to-the-N normal displacement. b): Striated plane above the entrance of the adit, defining a moderately-dipping top-to-the-NNW normal fault (Figure 36d). c): Ductile shear zone deforming Nussir greenstones in the Bachke Mine area. The asymmetric bending of the external fabric into the shear plane indicates dextral kinematics.*

*The shear plane dips subvertically to the NW (red great circles of Figure 36d) and contains subhorizontal stretching lineations. d): Stereonet summarising the structural features observed at Bachke.*

### 4.3 Hans prospect

The Hans prospect is located southeast of the Vesterdalen river, about 240 m east of the Vesterdalen prospect (UTM 34N, 601973 7814224; Figure 20). An adit that is 1,2 m wide and 1,5 m high can be followed for c. 20 m towards the south (long axis oriented 170°). The prospect dump contains about 50 $m^3$ of rock boulders spread down the slope. Geochemical analyses of two representative ore samples previously collected by NGU yielded 1,74 and 1,92 % Cu (NGU; Ore database).

Copper mineralisations are seen in a 10 cm thick carbonate vein that is hosted by the greenstone. The vein displays a sharp contact to the wall-rock and contains numerous lensoidal inclusions of it. Chalcopyrite forms aggregates in the vein but is also found in veinlets parallel to the contact to the wall-rock. The greenstone is fine-grained, dark green and magnetite-bearing.

### 4.4 Hallingstad prospect

The Hallingstad prospect is located south of the Vesterdalen river and c. 120 m east of Hans prospect, at the same altitude (UTM 34N, 602095 7814245; Figure 20). A 15 m long, 3 m wide and up to 6-7 m high open stope was excavated in dark green, magnetite-bearing greenstones as in the Hans deposit. At the southern end of the trench there is a minor, irregular underground stope, not accessible for inspection. Chalcopyrite is found in carbonate veinlets that apparently belong to two different sets:

1) Subparallel, c. north-south oriented, steeply dipping carbonate veins that are 1-10 cm thick. There is no extensive alteration of the greenstone along the veins. Very little evidence of these veins is now preserved and it was not possible to establish geometric or kinematic constraints on their genesis. The stope was dug parallel to their direction and it is assumed that they contained they highest copper grade.
2) Subhorizontal carbonate veins (Figure 37) genetically associated to an intraformational thrust fault visible in the western wall of the stope. A discrete glide surface dips moderately to the westsouthwest and foliation planes in the greenstone above and below it are asymptotically bent in the shear plane (Figure 37). Their asymmetry indicates reverse kinematics. The lack of clear stretching lineations on the

shear plane prevents the determination of the accurate transport direction, although approximately top-to-the-E, NE is inferred on the basis of the outcrop-scale geometry.


*Figure 37: Discrete thrust in the west wall of the Hallingstad prospect. Subhorizontal carbonate veins containing chalcopyrite are associated with the shear zone and are genetically linked to it, as predicted by the orientation of the instantaneous tensional vector shown in the inset.*

It is proposed that these veins represent the product of dilational strain genetically linked to the thrust. The stress field associated with the shear plane shown in Figure 37 generated a subvertical tensional stress (at the current orientation), thus perpendicular to the vein walls (inset in Figure 37). In the carbonate veins chalcopyrite is present predominantly as aggregates, but is also found as disseminated grains (Figure 37). The Vesterdalen area is structurally characterised by the presence of numerous thrusts with a general top-to-the-SE transport direction (see section 3.3), thus in good agreement with these meso-scale structural observations.

## 4.5 **Ingebrigtsen prospect**

The Ingebrigtsen prospect is located along the northwestern slope of the Vesterdalen valley, around 400 m north of the Vesterdalen prospect (UTM 34N, 0601736, 7814631; Figure 20). It is an approximately 5-6 m deep, inclined shaft and a small trench (Figure 38). A second, minor and now covered shaft is found about 25 m farther down the hillside, and the dump consists of approximately 60 $m^3$ of debris.

A coarse-grained quartz-carbonate vein hosted by greenstone of the Nussir Group is exposed in both the shaft and the trench. The contact between the vein and the greenstone is very irregular, and the vein contains fragments of the wall-rock. The vein is c. 2-4 m thick and composed of calcite and ankerite as well as subordinate quartz. Chalcopyrite constitutes aggregates and veinlets in the quartz-carbonate vein, commonly deposited along the margin of greenstone inclusions. Analyses of a representative sample of the ore give 0,9 % Cu.

*Figure 38: Ingebrigtsen copper occurrence. The photo shows the prospect inclined shaft within an irregular quartz-carbonate vein hosted by the greenstones.*

### 4.6 Vesterdalen prospect

The Vesterdalen prospect is located near the bottom of the valley Vesterdalen (Figure 20). An old mining track, which used to connect Neverfjord with Bachke mine, can be used to reach the prospect. Several prospecting trenches are located close to this track. Exposures are very scarce and of poor quality, thus complicating the analysis of the outcropping lithologies and of the local structural framework.

This copper occurrence was first discovered in the early 1900s. Christiania Spigerverk investigated further the mineralisation in the 1960s by a trenching and sampling program. Due to the relative low copper values recorded at that time, the exploration program was ended. Prospektering AS mapped and sampled the area in 1990 and elevated gold values were detected. NGU confirmed independently the high Au values in 1991 as part of a regional sampling programme in Finnmark. Two samples, collected from one of the dumps, yielded 3 and 10 g/t Au with 5,0 and > 10 % Cu, respectively (NGU; Ore database). Terra Control AS acquired the rights to the area in 2004.

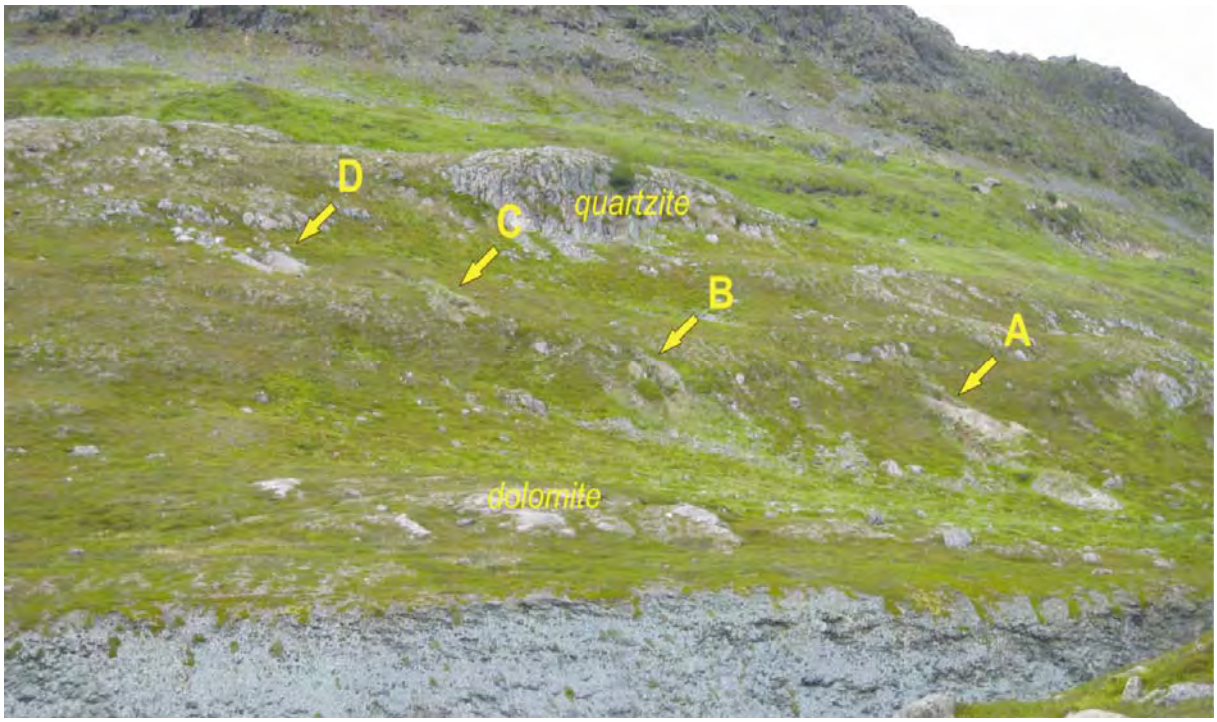


*Figure 39: View of the trenches of the Vesterdalen prospect, looking towards north-northwest. The length between trench A and D is approximately 160 m.*

Four trenches can be accessed. The major trench is the easternmost, A in Figure 39, where fine- to medium-grained, reddish-grey dolomites with local minor lenses of malachite are exposed (Figure 40). Dolomite is interbedded with thin layers of red schists, whose foliation strikes about 215° and dips 50° northwest. A major dump with copper-mineralised rock debris is located beside this trench and contains abundant malachite-stained boulders of dominantly impure dolomite. Malachite is the dominant copper mineral, but bornite and chalcosite are also identified in fresh cuts. Sulphides comprise aggregates and thin veinlets. Copper mineralisations are also found in boulders of dolomite containing irregular quartz lenses and in the red schist.

*Figure 40: Lens of malachite in dolomite in trench A in the Vesterdalen prospect.*

Unmineralised dolomites with irregular intercalations of dark schists and/or greenstones occur in trench B, whereas schist boulders are found in trench C. Trench D contains only boulders of impure quartzites, derived from an outcrop immediately above the trench. The copper-mineralised zone thus seems to be restricted to the rocks found in trench A. It is not found in other outcrops in the area nearby, and no outcrops were observed along the assumed strike extension. It is thus difficult to determine in the field the shape and size of the mineralisation without the aid of geophysical surveys and/or drilling.

The dark rocks in the upper part of Figure 39 are the greenstones hosting the Ingebrigtsen occurrence (section 4.5). This photo thus illustrates that the greenstone form the ridges in the area and the metasediments the valleys.

Seven samples of the Vesterdalen Cu-mineralisation were collected from the dump beside trench A and were analysed by ICP-ES (Table 2). Five of them represent various dolomite rocks, one sample is a copper-mineralised red siltstone and one is a mafic rock. The analysed samples yielded values in the range 0,64-9,76 % Cu and 0,2-16,4 g/t Au. There is no clear correlation between the contents of copper and gold. Silver occurs with values in the range < 2 - 45 g/t. Elevated molybdenum contents were found in a few of the dolomite samples, with 0,9 % Mo as maximum value.

*Table 2: Analysis of ore samples by ICP-ES after aqua-regia digestion for 23 elements and fire assay for the precious metals (Au, Pt and Pd). Analysis made by ACME Analytical Laboratories, Vancouver, Canada.*

| Sample no. | Locality | UTM WGS84 | | | Rock description | Mo | Cu | Pb | Zn | Ag | Ni | Co | Mn | Fe | As | Sr | Cd |
|---|---|---|---|---|---|---|---|---|---|---|---|---|---|---|---|---|---|
| | | Zone | East | North | | % | % | % | % | ppm | % | % | % | % | % | % | % |
| JS07-05 | N 07/14 | 35 | 388433 | 7820514 | Pyrite+chalcopyrite aggregates in coarse grained quartz-carbonate veins | 0,001 | 0,281 | <,01 | 0,02 | <2 | 0,013 | 0,003 | 0,06 | 7,92 | <,01 | 0,001 | <,001 |
| JS07-10 | Porsa | 34 | 601802 | 7810513 | Chalcopyrite+bornite aggregates in greenstone | <,001 | 7,642 | <,01 | <,01 | 4 | 0,017 | 0,012 | 0,05 | 14,67 | <,01 | 0,001 | <,001 |
| JS07-11 | Porsa | 34 | 601718 | 7810517 | Chalcopyrite-pyrite disseminations along greenstone in banded carbonate vein | <,001 | 1,142 | <,01 | <,01 | <2 | 0,004 | 0,004 | 0,24 | 4,35 | <,01 | 0,006 | <,001 |
| JS07-12 | Porsa | 34 | 601703 | 7810516 | Chalcopyrite aggregates in coarse grained carbonate vein | <,001 | 3,427 | <,01 | <,01 | 4 | 0,011 | 0,011 | 0,25 | 8,36 | <,01 | 0,006 | <,001 |
| JS07-23 | Vesterdalen | 34 | 601741 | 7814246 | Carbonate-bearing siltstone with lenses of chalcosite | 0,042 | 3,435 | <,01 | <,01 | 31 | 0,001 | 0,004 | 0,43 | 0,91 | <,01 | 0,028 | <,001 |
| JS07-24 | Ingebrigtsen | 34 | 601733 | 7814624 | Chalcopyrite, veinlets and aggregates in carbonate-quartz vein | <,001 | 0,875 | <,01 | <,01 | <2 | 0,004 | 0,008 | 0,71 | 4,83 | <,01 | 0,009 | <,001 |
| LPN07-01 | Vesterdalen | 34 | 601741 | 7814246 | Copper mineralisation in coarse grained carbonate | 0,005 | 9,756 | <,01 | <,01 | 6 | <,001 | 0,002 | 0,24 | 0,34 | <,01 | 0,018 | <,001 |
| LPN07-02 | Vesterdalen | 34 | 601741 | 7814246 | Copper mineralisation in coarse grained carbonate | 0,001 | 0,637 | <,01 | <,01 | <2 | 0,001 | 0,002 | 0,18 | 0,37 | <,01 | 0,012 | <,001 |
| LPN07-03 | Vesterdalen | 34 | 601741 | 7814246 | Copper mineralisation in fine grained carbonate rock | 0,039 | 6,371 | <,01 | <,01 | 15 | 0,002 | 0,004 | 0,26 | 0,47 | <,01 | 0,019 | <,001 |
| LPN07-04 | Vesterdalen | 34 | 601741 | 7814246 | Copper veinlets in banded carbonate rock | 0,233 | 6,683 | <,01 | <,01 | 18 | 0,003 | 0,006 | 0,38 | 0,47 | <,01 | 0,024 | <,001 |
| LPN07-05 | Vesterdalen | 34 | 601741 | 7814246 | Copper mineralisation in carbonate-quartz rock | 0,899 | 6,974 | <,01 | <,01 | 45 | 0,002 | 0,004 | 0,38 | 0,74 | <,01 | 0,022 | <,001 |
| LPN07-06 | Vesterdalen | 34 | 601741 | 7814246 | Copper mineralisation in mafic rock | 0,006 | 0,217 | <,01 | <,01 | <2 | 0,006 | 0,010 | 0,02 | 17,32 | <,01 | 0,001 | <,001 |

| Sample no. | Locality | UTM WGS84 | | | Rock description | Sb | Bi | Ca | P | Cr | Mg | Al | Na | K | W | Hg | Au** | Pt** | Pd** |
|---|---|---|---|---|---|---|---|---|---|---|---|---|---|---|---|---|---|---|---|
| | | Zone | East | North | | % | % | % | % | % | % | % | % | % | % | % | ppm | ppm | ppm |
| JS07-05 | N 07/14 | 35 | 388433 | 7820514 | Pyrite+chalcopyrite aggregates in coarse grained quartz-carbonate veins | <,001 | <,01 | 0,58 | 0,004 | <,001 | 0,27 | 0,12 | 0,02 | 0,01 | <,001 | <,001 | <,01 | <,01 | <,01 |
| JS07-10 | Porsa | 34 | 601802 | 7810513 | Chalcopyrite+bornite aggregates in greenstone | <,001 | <,01 | 1,93 | 0,021 | <,001 | 0,32 | 0,23 | 0,01 | 0,04 | 0,002 | <,001 | 0,14 | <,01 | <,01 |
| JS07-11 | Porsa | 34 | 601718 | 7810517 | Chalcopyrite-pyrite disseminations along greenstone in banded carbonate vein | <,001 | <,01 | 25,84 | 0,009 | <,001 | 0,19 | 0,15 | 0,01 | 0,04 | <,001 | <,001 | 0,30 | <,01 | <,01 |
| JS07-12 | Porsa | 34 | 601703 | 7810516 | Chalcopyrite aggregates in coarse grained carbonate vein | <,001 | <,01 | 24,60 | 0,002 | <,001 | 0,18 | 0,10 | 0,01 | 0,01 | 0,001 | <,001 | 0,74 | <,01 | 0,01 |
| JS07-23 | Vesterdalen | 34 | 601741 | 7814246 | Carbonate-bearing siltstone with lenses of chalcosite | <,001 | <,01 | 19,42 | 0,010 | 0,001 | 6,88 | 0,13 | 0,02 | 0,07 | 0,001 | <,001 | 4,87 | 0,02 | <,01 |
| JS07-24 | Ingebrigtsen | 34 | 601733 | 7814624 | Chalcopyrite, veinlets and aggregates in carbonate-quartz vein | <,001 | <,01 | 16,79 | 0,014 | 0,013 | 7,23 | 0,36 | 0,05 | 0,02 | <,001 | <,001 | 0,01 | 0,01 | <,01 |
| LPN07-01 | Vesterdalen | 34 | 601741 | 7814246 | Copper mineralisation in coarse grained carbonate | <,001 | <,01 | 16,11 | 0,009 | <,001 | 9,27 | 0,05 | 0,03 | 0,02 | 0,003 | <,001 | 0,19 | <,01 | <,01 |
| LPN07-02 | Vesterdalen | 34 | 601741 | 7814246 | Copper mineralisation in coarse grained carbonate | 0,001 | <,01 | 8,51 | 0,022 | <,001 | 4,70 | 0,16 | 0,05 | 0,05 | <,001 | <,001 | 0,31 | 0,02 | <,01 |
| LPN07-03 | Vesterdalen | 34 | 601741 | 7814246 | Copper mineralisation in fine grained carbonate rock | 0,001 | <,01 | 13,56 | 0,011 | 0,001 | 7,93 | 0,20 | 0,02 | 0,06 | 0,002 | 0,001 | 16,44 | <,01 | <,01 |
| LPN07-04 | Vesterdalen | 34 | 601741 | 7814246 | Copper veinlets in banded carbonate rock | 0,001 | <,01 | 15,05 | 0,012 | 0,001 | 8,46 | 0,19 | 0,02 | 0,06 | 0,002 | <,001 | 6,79 | 0,02 | <,01 |
| LPN07-05 | Vesterdalen | 34 | 601741 | 7814246 | Copper mineralisation in carbonate-quartz rock | <,001 | <,01 | 15,95 | 0,019 | 0,001 | 8,64 | 0,17 | 0,03 | 0,03 | 0,003 | <,001 | 3,96 | <,01 | <,01 |
| LPN07-06 | Vesterdalen | 34 | 601741 | 7814246 | Copper mineralisation in mafic rock | 0,001 | <,01 | 0,36 | 0,059 | 0,003 | 4,78 | 2,90 | 0,01 | 0,01 | <,001 | <,001 | 0,06 | 0,02 | 0,01 |

Microscopic examination of thin sections of the dolomitic rock shows that the dolomite is heterogeneous with respect to grain size, mineral content and texture. It is basically structureless and is crosscut by veinlets of various compositions. Both samples of coarse grained (2-10 mm) and more fine to medium grained (≤ 0,1-1 mm) dolomite were collected. Quartz, plagioclase, K-feldspar, chlorite and muscovite occur in various proportions and grain sizes. Chlorite most commonly comprises foliated bands in association with quartz and opaque minerals. Chlorite is colourless to pale green in transmitted, parallel light. Accessory minerals include monazite and sphene.

The copper mineralogy is very complex. Digenite seems to dominate, but bornite, chalcosite, covelline and malachite also occur. Primary copper-minerals are bornite and digenite. They occur both as cement (Figure 41), but also as veinlets (Figure 44) in the dolomitic rock. Chalcosite is found as tiny exsolution lamellaes in the digenite. Bornite and digenite are replaced by covelline and malachite in various proportions. Covelline commonly replaces digenite along cleavage planes (Figure 41). Se-bearing covelline is also found, commonly as minor ruler-formed inclusions (Figure 42 and Figure 43). Malachite occurs as rims or complete replacements of other copper minerals (Figure 42 and Figure 43), and is also found as inclusions and along cracks in carbonate and powellite.

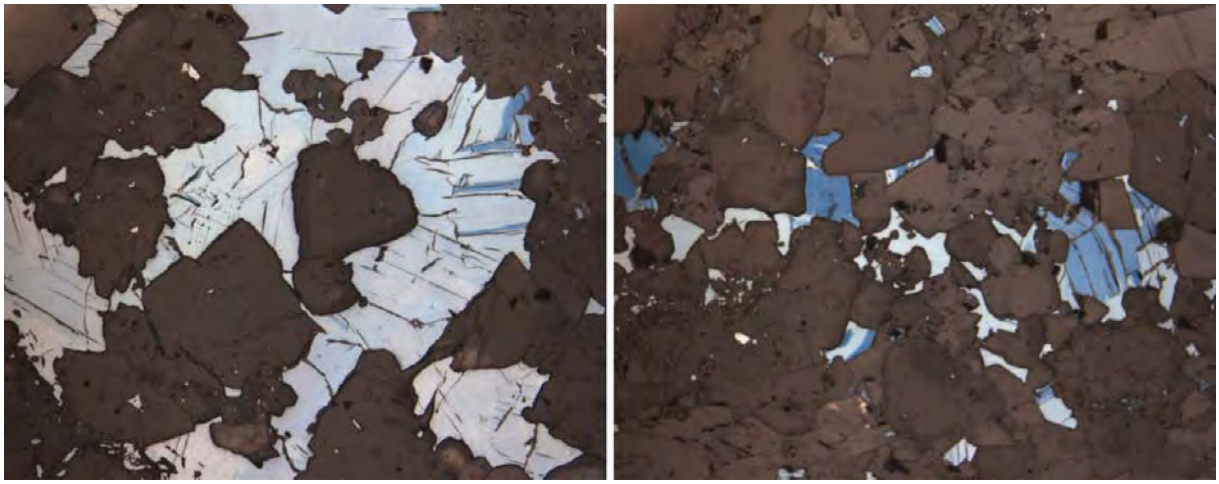

*Figure 41: Microphotograph of digenite (pale blue) replaced by covelline in various proportions in dolomitic rock (reflected light. FOV 1,18x1,49 mm; sample LPN07-03)*

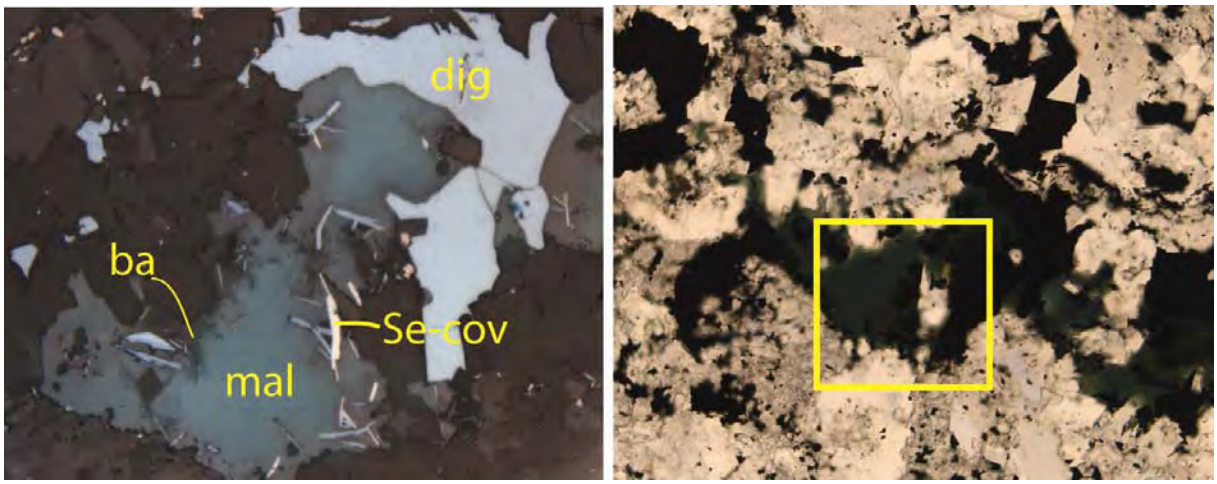


*Figure 42: Microphotograph of digenite (dig), malachite (mal) with barite (ba, darker grey than malachite) rim and inclusions of Se-covelline rulers (Se-cov) comprise an aggregate in carbonate-feldspar rock. Left: reflected light (FOV 0,58x0,73 mm). Right: transmitted, parallel light. The yellow frame shows the location of Figure 43 (FOV 1,18x0,1,49 mm; sample LPN07-04).*

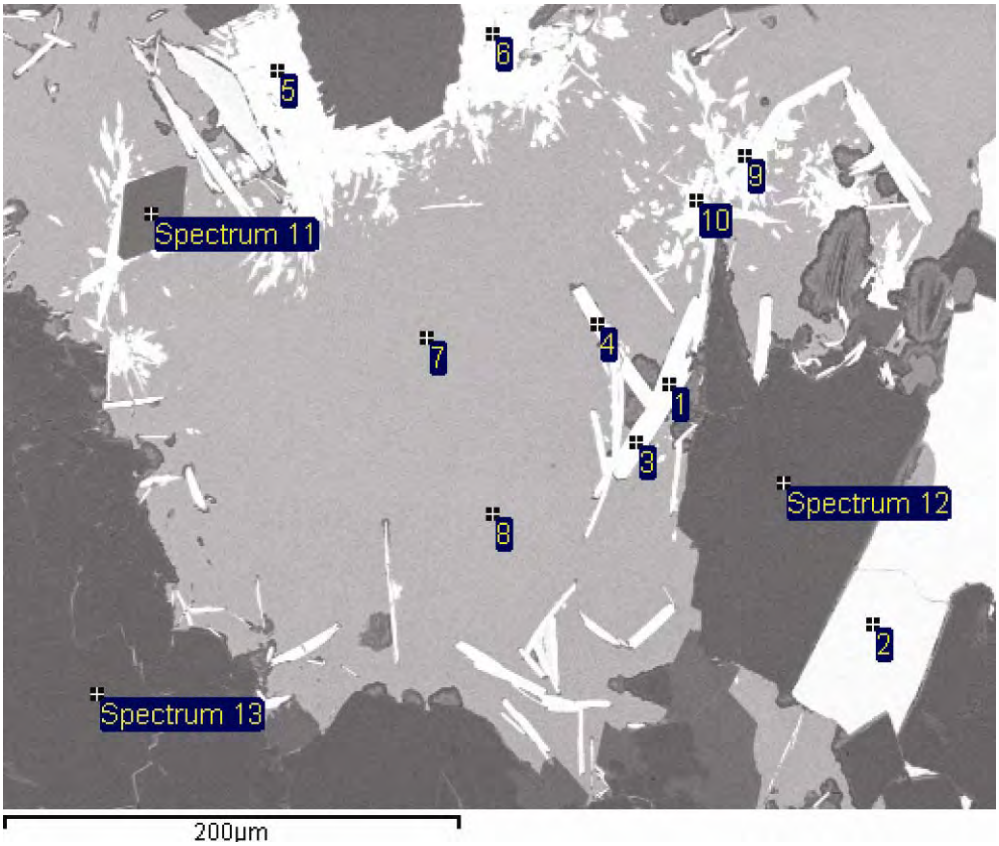


*Figure 43: Detailed BSE-image of Figure 42. Se-covelline (sites 1,3,4,9), digenite (site 2), barite (sites 5,6,10), malachite (sites 7,8), K-feldspar (site 11) and Na-feldspar (sites 12,13; sample LPN07-04).*

The elevated molybdenum content in parts of the copper-mineralised dolomite samples is due to the presence of powellite, a calcium molybdate ($CaMoO_4$). No molybdenite has been identified so far in the polished thin sections. Powellite occurs both as well developed crystals

(0,5-1,5 mm) and grains with more irregular crystal boundaries (Figure 44). Powellite grains with irregular boundaries commonly have a core of digenite (Figure 45). Several well developed crystals of powellite occur in a 1-2 mm thin veinlet. These crystals are locally crosscut by grains of digenite (Figure 44). Powellite is also found as inclusions in coarse-grained digenite in the same veinlet (Figure 46), and indicates that the formation of powellite is probably contemporaneous with the deposition of digenite. Powellite is probable formed under conditions of high oxygen fugacity ($fO_2$) and/or low sulphur fugacity ($fS_2$) as indicated by the Cu-rich copper minerals.

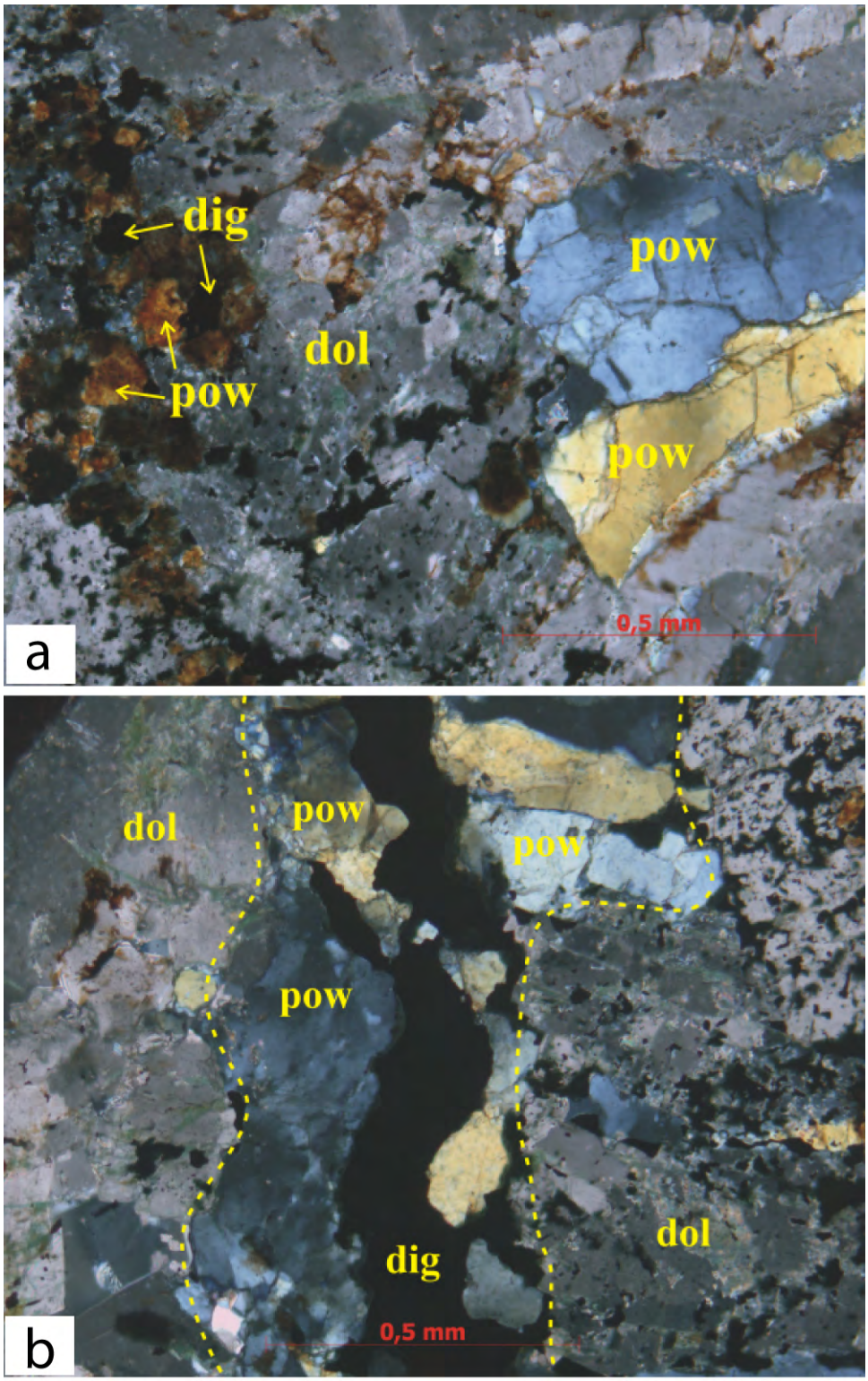


*Figure 44: a): Microphotograph of powellite (pow) with well developed crystals (to the right) and with irregular boundaries (to the left) in dolomite (dol) rock. b): powellite with well developed crystals and digenite (dig) in a veinlet in dolomite rock (polarised light, sample LPN07-05).*

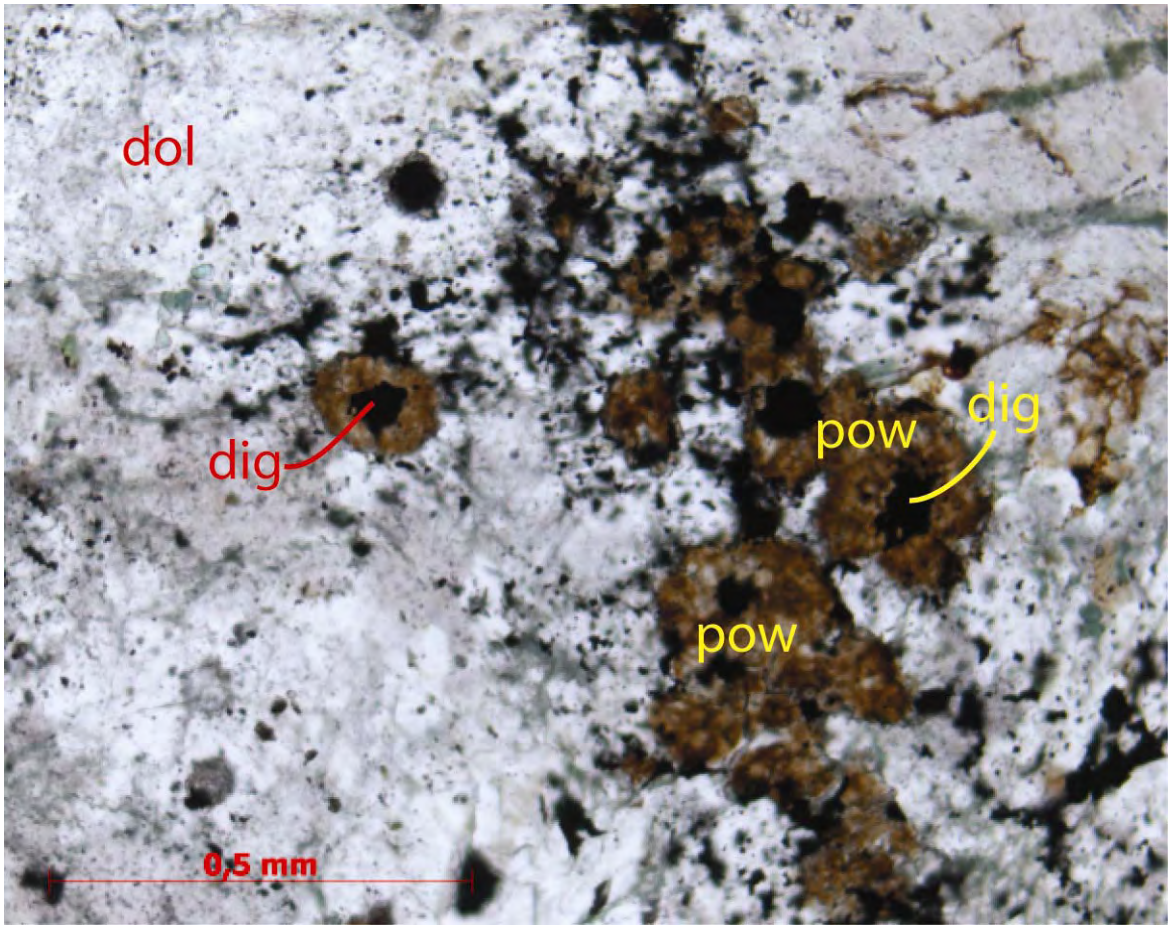


*Figure 45: Microphotograph of powellite (pow) with irregular boundaries and common cores of digenite (dig )in a dolomite-dominated (dol) rock (parallel light, sample LPN07-05).*

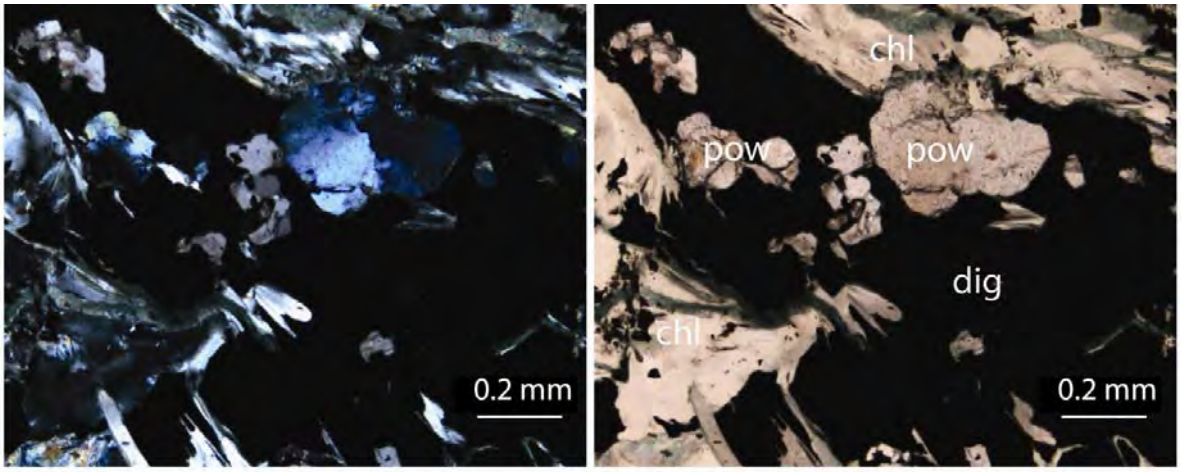


*Figure 46: Microphotograph of powellite (pow) inclusions in digenite (dig) enveloped by chlorite (chl) and feldspar (left: polarized light, right: parallel light; sample LPN07-05).*

High $fO_2$ during the formation of the Vesterdalen mineralisation is also suggested by the deposition of barite and uranium minerals. Barite is found as cement in the dolomitic rock, inclusions in dolomite, rims/replacement of malachite (Figure 43) as well as along cracks in

powellite and dolomite. Accessory U-minerals include brannerite, orthobrannerite and uraninite. Most commonly they were observed as tiny (2-5µm) inclusions in digenite.

The red siltstone is a very fine-grained rock with a weakly-developed foliation. Some elongated, 1-1,5 mm long clastic aggregates of quartz-carbonate-plagioclase, subhedral dolomite grains and accessory muscovite rulers can be identified. The rock is less fine-grained around lenses or bands of more medium-grained dolomite (up to 0,5 mm) and opaque minerals (up to 2 mm). Opaque minerals are predominantly bornite, locally replaced by digenite and covelline in various amounts, especially along crystal cleavage planes (Figure 47). Very fine-grained (5-20 µm) inclusions of a Bi-telluride (+Se?) occur in the Cu-minerals (Figure 47), and a few tiny uraninite (2-5µm) grains were observed as inclusions in dolomite. Barite occurs as cement, and along cracks and as inclusions in dolomite. Powellite also occurs locally as disseminations in the red siltstone.

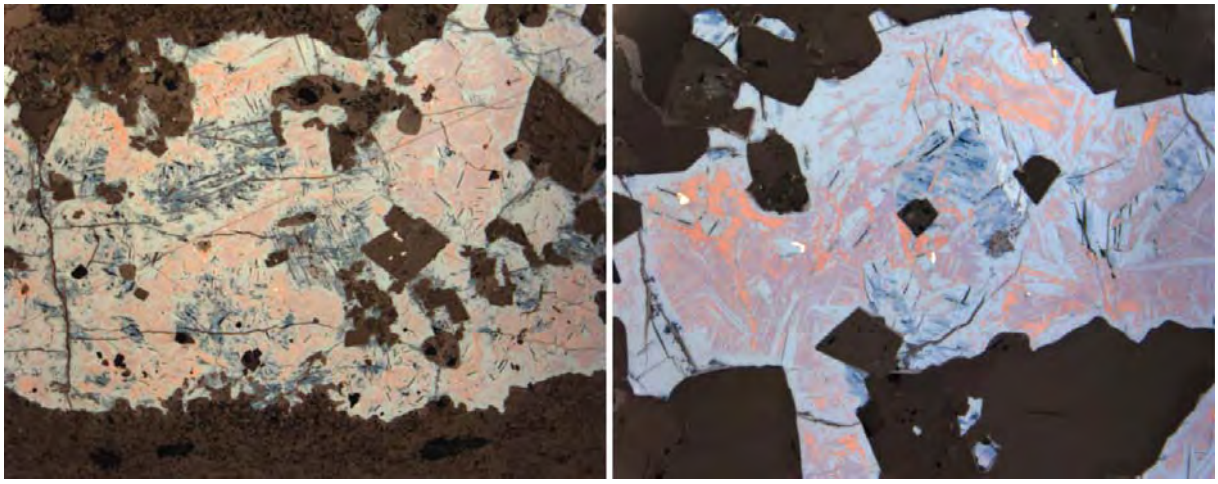

*Figure 47: Left: Microphotograph of bornite (reddish brown), digenite (pale blue) and covelline (dark blue) lens in siltstone (FOV 2,36x2,98 mm, reflected light). Right: microphotograph of bornite, digenite and covelline with very fine grained inclusions of Bi-telluride (high reflectance; FOV 0,58x0,73 mm, reflected light; sample JS07-23).*

# 5. Qualitative interpretation of the new airborne geophysical survey with regard to the structural framework of the area

## 5.1 Introduction

We utilize here modern airborne geophysical data (magnetic, frequency-domain EM and gamma ray spectrometry) flown and processed in 2007 by NGU on a contract basis for Nussir AS. Helicopter-borne geophysical measurements were carried out in the area shown by Figure 48. Acquisition, system calibration and processing details of the helicopter borne geophysical survey are described by Heincke et al. (2008). Thus we provide here only a brief summary of the most relevant acquisition parameters.

Data collection was carried out with a narrow line spacing of ~100 m and a low average flying altitude of 65 m (resulting in an average bird height of 35 m). During the survey, the radiometric crystal was fixed on the bottom side of the helicopter, whereas the magnetometer and the EM system were placed in a bird hanging 30 m below the helicopter.

Because data coverage is significantly denser along inline directions (interval of ~2 m for magnetic and electromagnetic and of ~ 20 m for radiometry dataset), flight lines were directed northeast-southwest, thus at high angle to the regional structural grain.

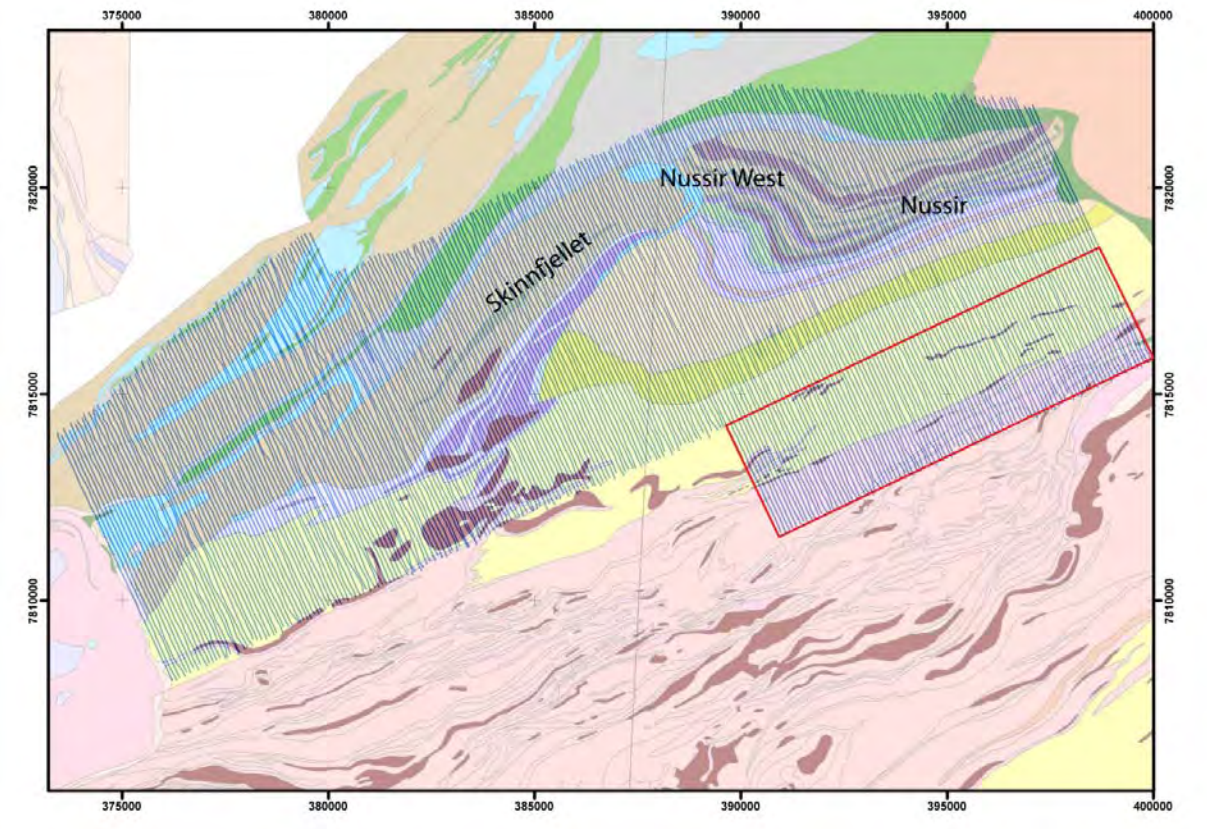

*Figure 48: Areal extent of NGU geophysical survey. Blue lines indicate the flight lines of the helicopter survey. The area enclosed by the red rectangle was surveyed for a different client and is not discussed in detail in this report.*

The caesium magnetometer measured the absolute value of the magnetic field (total magnetic field). During the interpretation phase, however, we relied mostly on the vertical derivatives of the magnetic total field, because the vertical gradient is less influenced by the regional field and emphasizes more local anomalies and structural grain. The magnetic data provide information on the geometries of magnetic susceptibility contrasts in the near surface and deep geology of the area. Many of the magnetic anomalies in the study area are caused by susceptibility contrasts at the surface or at shallow depths. Therefore the magnetic data contribute enormously to our understanding of the positions of rock bodies at the surface as well as their continuations at depth, helping constrain geological cross-sections.

The scintillation detector recorded the gamma ray spectra. By processing the gamma ray spectra, the near-surface concentrations of the isotopes $^{232}$ Th, $^{238}$U and $^{40}$K could be determined. Ground concentrations variations from potassium, uranium and potassium look very similar (Figure 50). This is caused by a direct correlation between thorium and uranium concentrations in many rock types and the attenuation effect of moisture in the ground/soil on gamma radiation from all three radioelements. The radiometric data provide the radioelement signature of the upper 50 cm of the ground. This may be the signature of the exposed bedrock or of overburden. If the overburden is dry and locally derived, its signature reflects the bedrock geology beneath. Large-scale banding and compositional variations are also discernible in the radiometric data, which can therefore contribute information on geologic structure.

The electromagnetic frequency-domain system comprised 5 coil pairs that were arranged both horizontal coplanar and coaxial. The emitted frequencies ranged from 880 to 34133 Hz. Helicopter EM measurements provide estimates of apparent resistivities in the shallow ground by inverting inphase and quadrature data of the different frequencies. Processing showed that inphase data are strongly influenced by the bedrock magnetic susceptibility and that the associated apparent resistivities are not representative for the resistivity distributions (Heincke et al., 2008). Accordingly, apparent resistivities anomalies from quadrature data are used to identify highly conductive structures.

It was assumed that only the EM method has the potential to detect the thin Nussir I copper-bearing horizon. Pilot 2-D geoelectrical and IP (induced polarisation) field measurements along and across the Nussir I deposit yielded resistivities values from 50-200 and 1000-10000 Ωm for the mineralisation and the surrounding rocks, respectively. EM modelling (Rønning et

al., 2007) showed that the highest frequency (34133 Hz) should be able to detect this rather weak conductivity contrast.

Figure 49 through to Figure 52 show images of selected results of the geophysical survey over the study area, as per Heincke et al. (2008). Our interpretation of the geophysical dataset is largely qualitative, because it is based on visual inspection of the geophysical images, integrated by field observations and geological data held within a GIS system. Figure 53, for instance, shows three examples of the images used within the GIS system to enhance our understanding of the local geology and to implement the information extracted from the analysis of the geophysics into a comprehensive, “ground-thruthed” geological model.

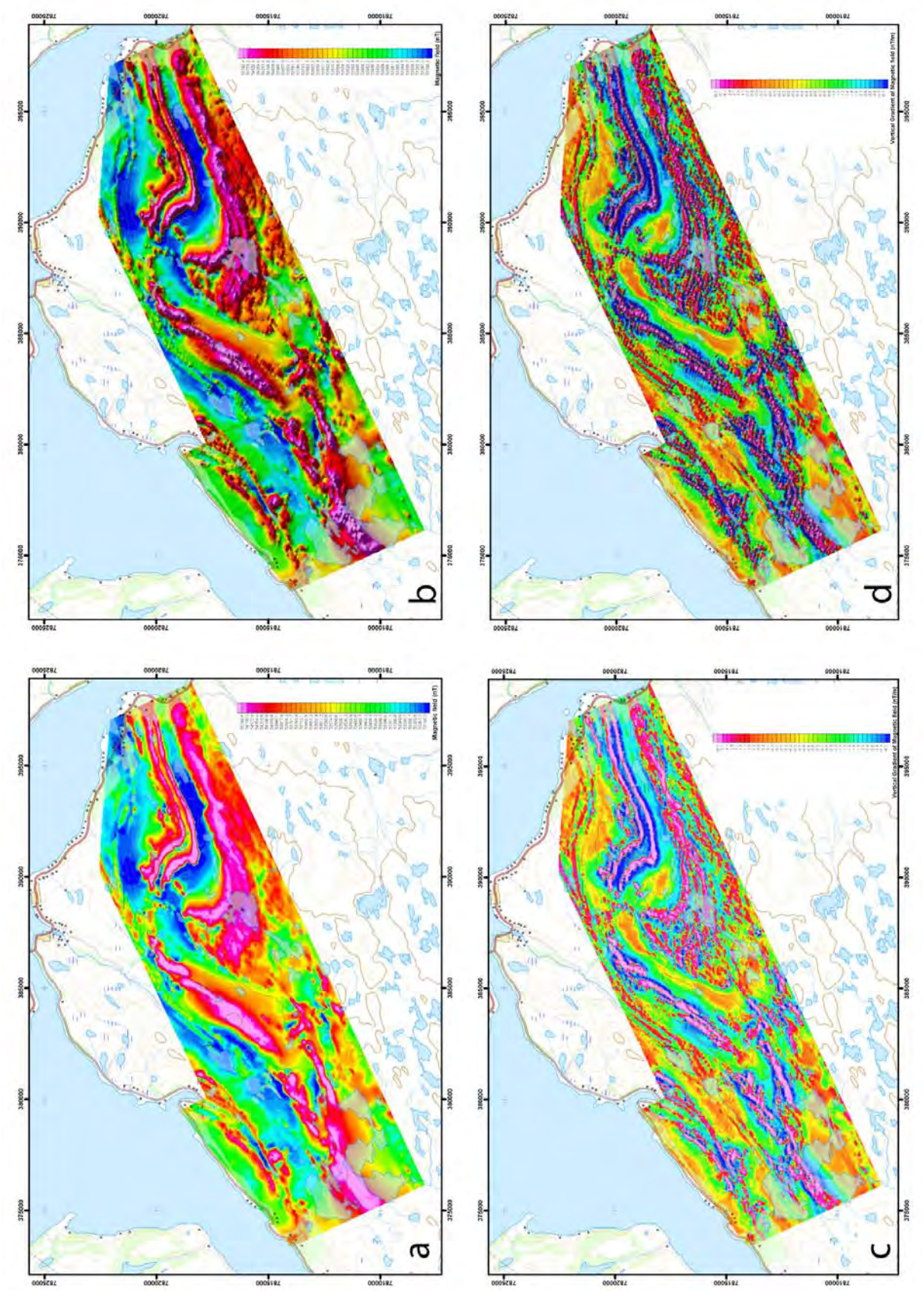


*Figure 49: a): Magnetic total field. b): Colour shaded relief presentation of the total field with a virtual light source in the NE. c): Vertical gradient of the total field. d): Colour shaded relief presentation of the vertical gradient with a virtual light source in the NE. Due to the high latitude it can be reasonably assumed that the maxima of the total magnetic field and its derivatives are located immediately above their associated sources/structures.*

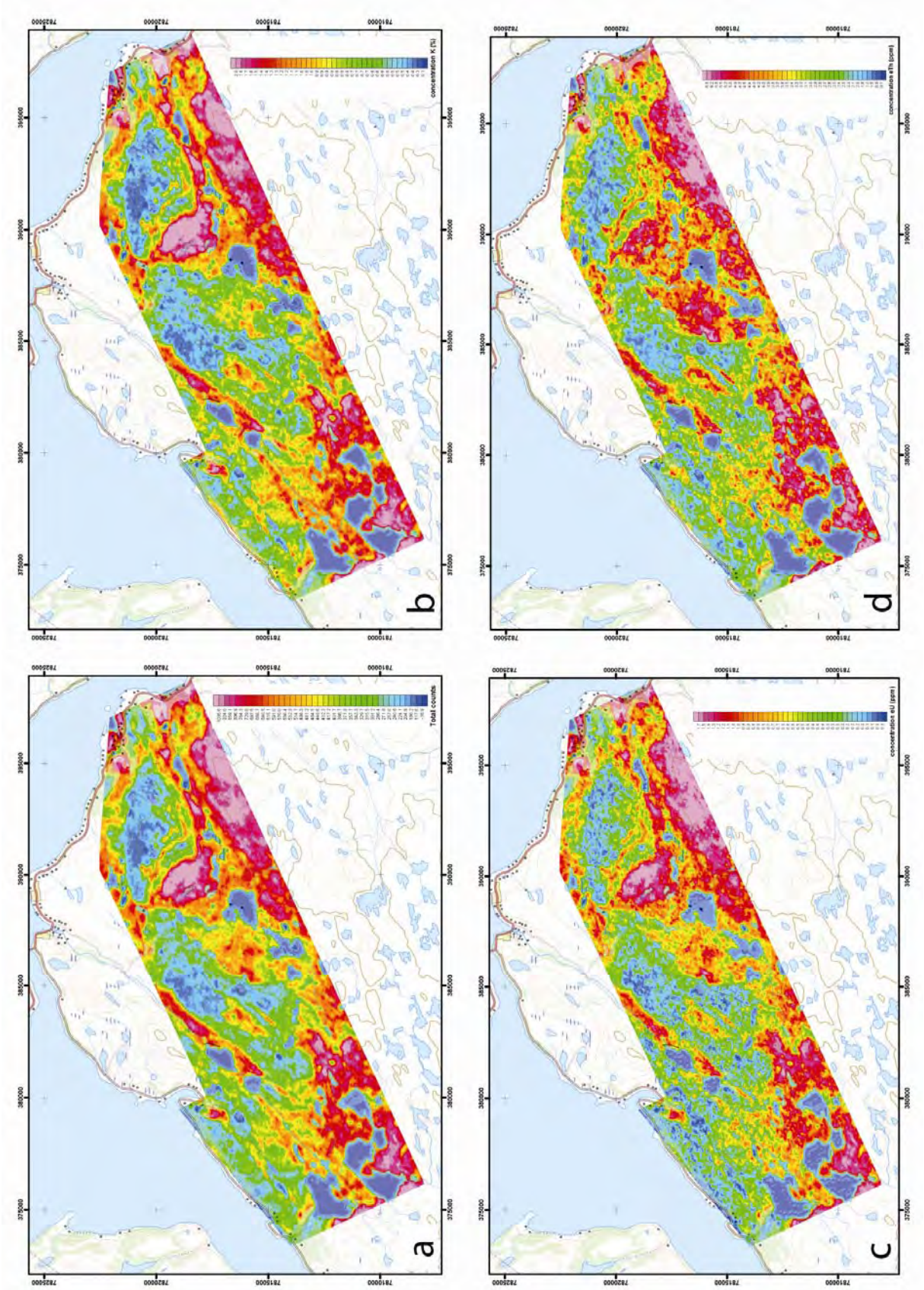


*Figure 50: a): Total count radiometric data. b): Potassium radiometric concentration. c): Equivalent uranium radiometric concentration. d) Equivalent thorium radiometric concentration.*

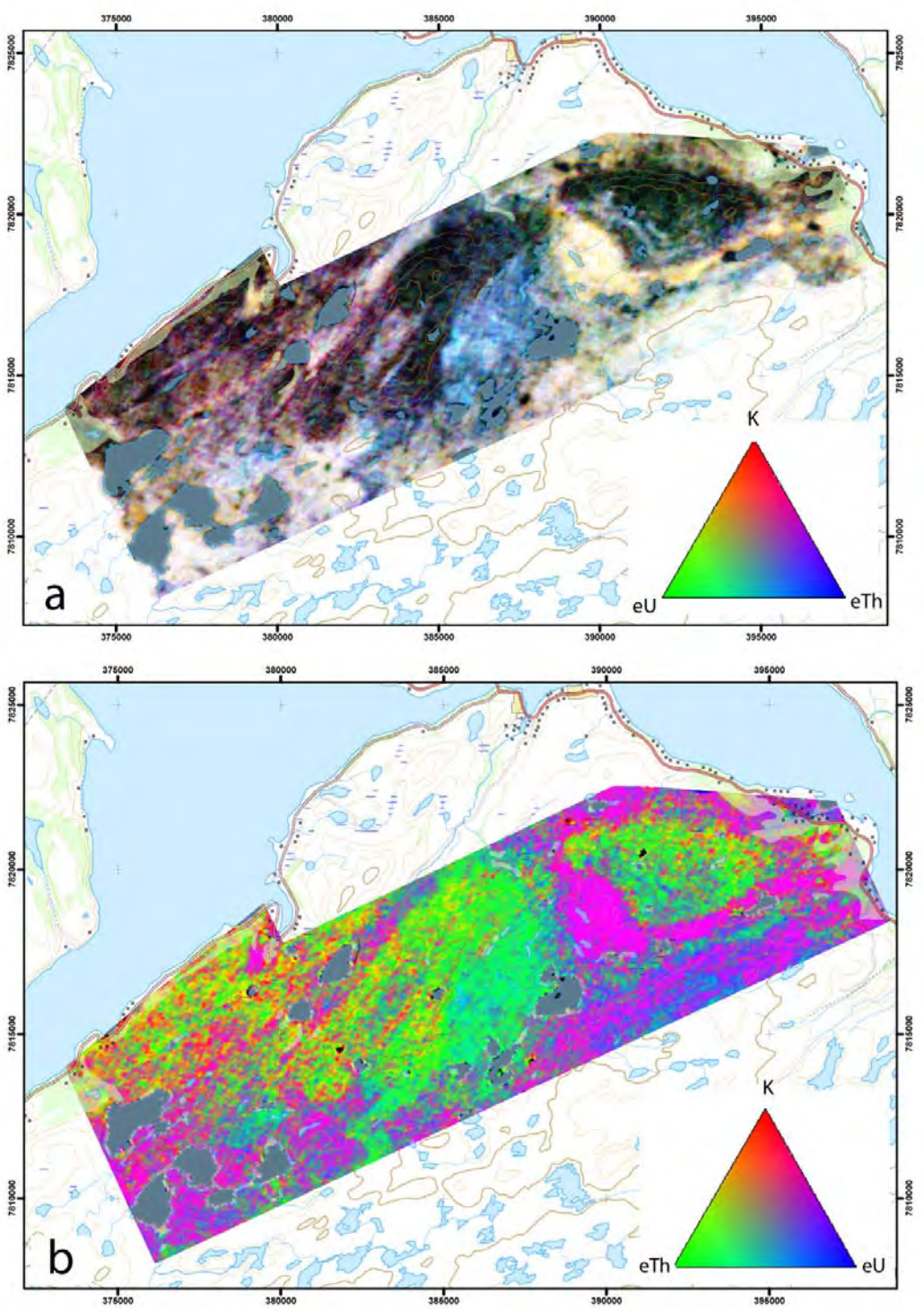


*Figure 51: Ternary plots of the radiometric data. RGB colour coding is used and colour scales are histogram equalized. In contrast to a), concentrations are normalized to the accumulated concentrations of all three radio nuclides in b).*

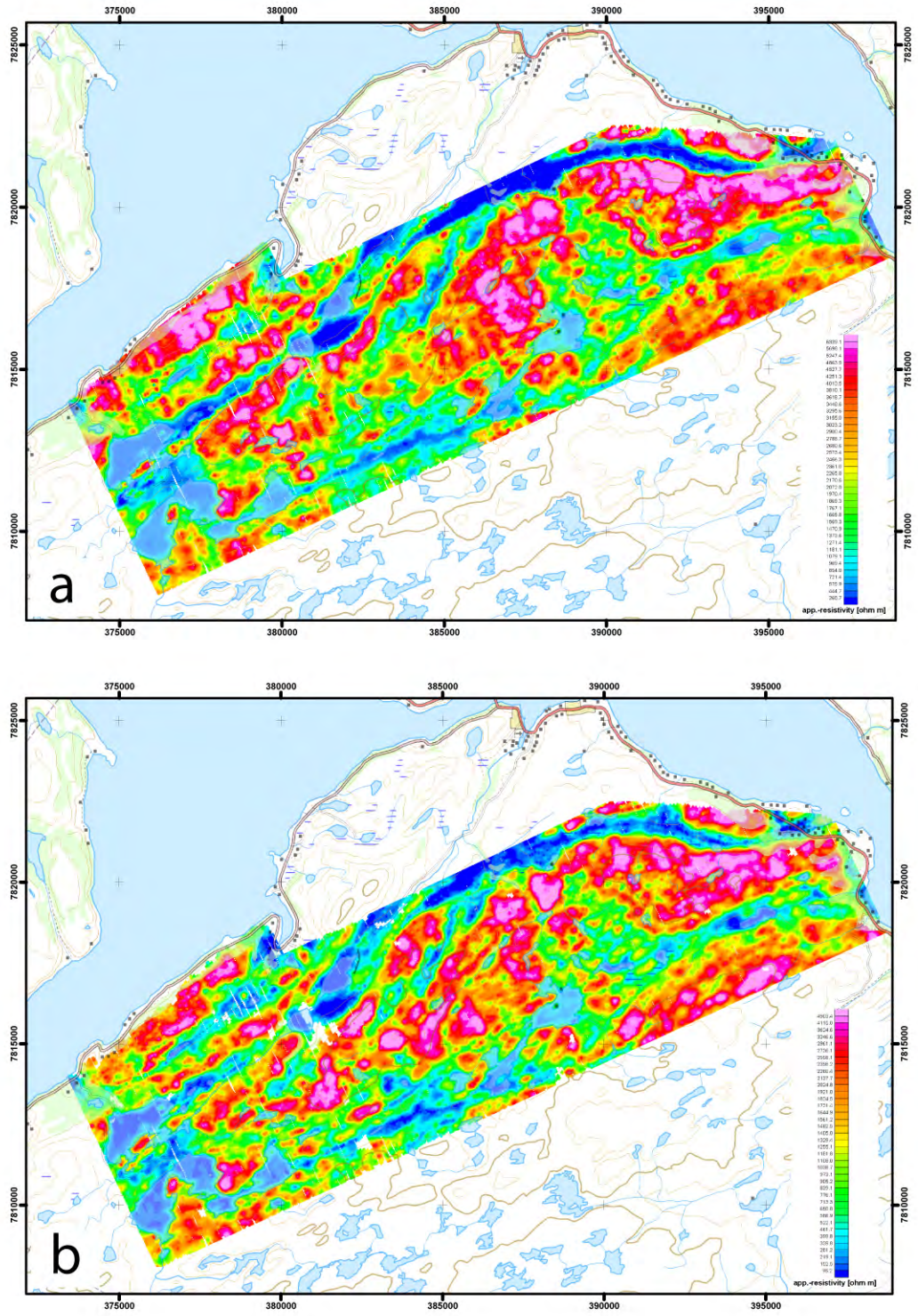


*Figure 52: a): EM resistivity obtained from 7001 Hz (coaxial) quadrature data. b): EM resistivity obtained from 34133 Hz (horizontal coplanar) quadrature data.*

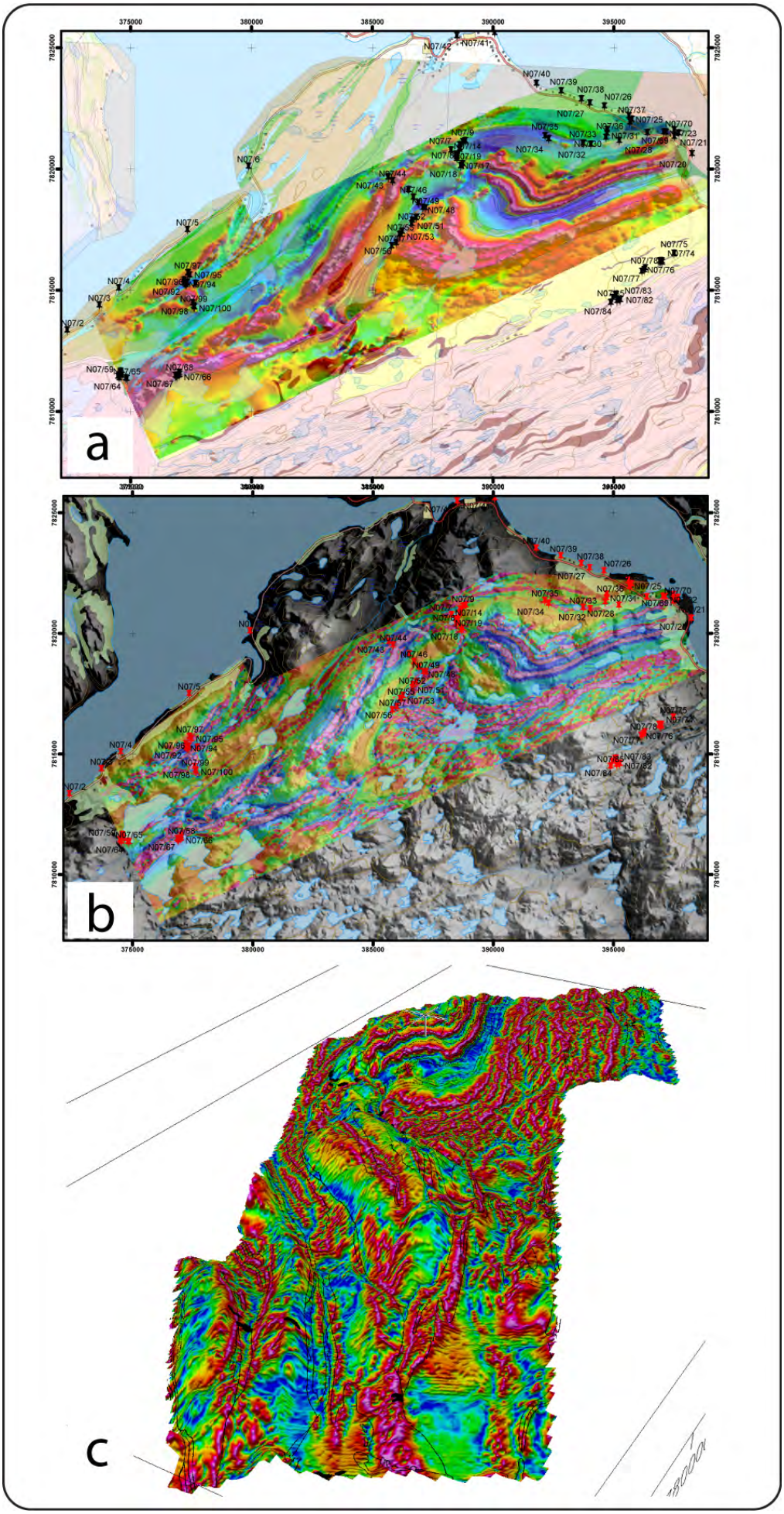
375000
380000
385000
390000
395000
7825000
7820000
7815000
7810000
a
b
c

*Figure 53: Examples of some of the images generated during this study and used to interpret the new geophysical dataset. a): Colour shaded relief presentation of the magnetic total field with a virtual light source in the NE overlain with the geological map and location of our field observation points. b): Black and white shaded digital elevation model, with magnetic total field and observation localities analysed during the study. c): 3D view of the area, with tilt derivative and geological contacts draped on the digital elevation model. View to the northeast from the Porsa mine area.*

## 5.2 Results

Figure 54 shows a first, coarse interpretation of the vertical gradient of the total magnetic field, where black lines are drawn along the most prominent anomalies. This simple interpretation, which at this stage still neglects the existing geological information, helps nonetheless to define the first-order structural grain of the area and allows the identification of crucial targets for further, detailed inspection and analysis. The white line, which corresponds to a continuous magnetic anomaly in Figure 54 and is very obvious also in the EM resistivity data of Figure 52, separates a southern domain, characterised by intense folding and thrusting, from a northern block, which is predominantly shaped by the severe shortening and stratigraphic repetition due to the Porsa thrusts (section 3.5).

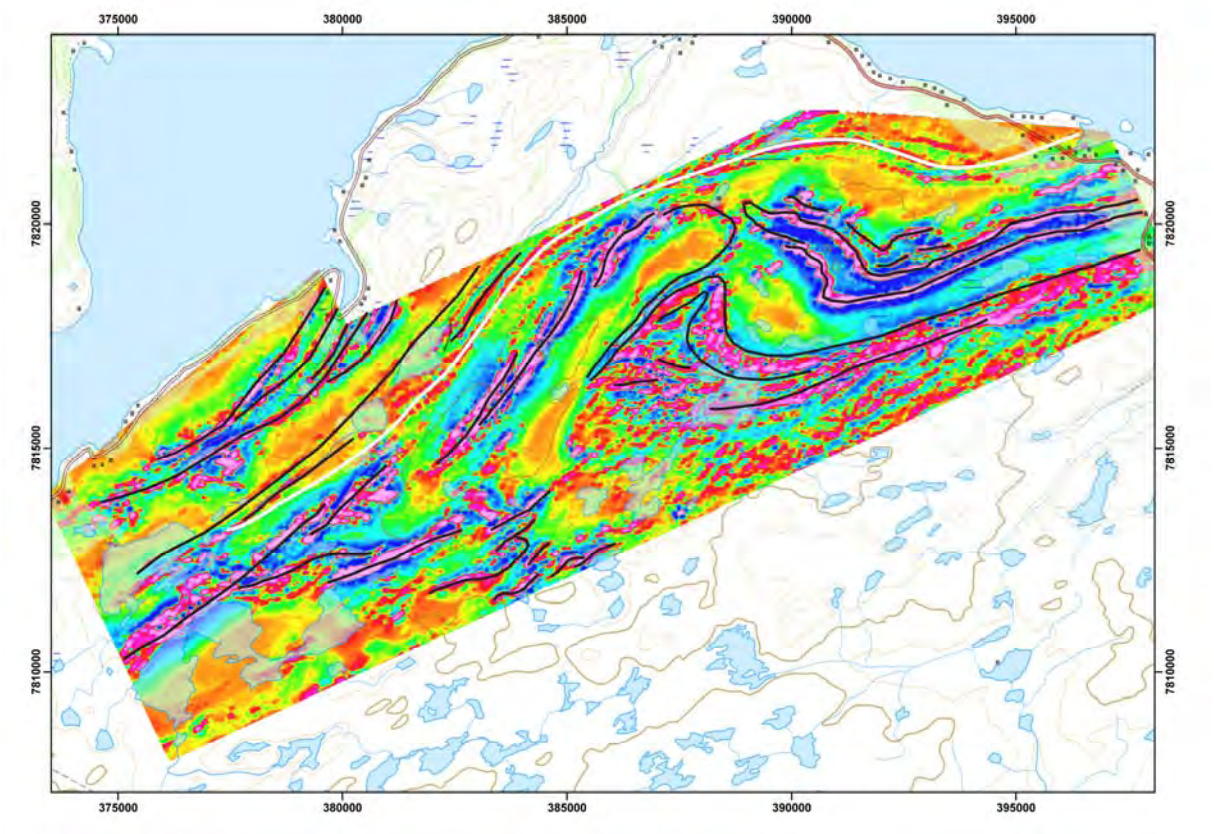


*Figure 54: Major anomalies traced on the vertical gradient of the total magnetic field.*

Key to the understanding of the Nussir I mineralised body and to the establishment of its potential Nussir II continuation, is the analysis of Nussir West area, where detailed field observations were made. Figure 55 shows its magnetic and radiometric signatures, with a red line highlighting the thrust discontinuity proposed by Pharaoh et al. (1983). The vertical derivative of the total magnetic field (Figure 55a) shows that the Nussir greenstones to the east of the red line are characterised by two very prominent, parallel high anomalies. A third, weaker and less continuous anomaly parallels these two anomalies farther to the north. These features are the most prominent elements of the magnetic signature in the greenstones of Nussir Mountain. They are folded about a NE-SW trending axis and can be readily traced eastward, where they strike ENE-WSW. The same fold geometry is shown by the anomalies generated by the Saltvatn Group lithologies, south of the yellow line. The Nussir I ore body is itself folded by this structure, which generated local thickening and duplication of the deposit. It is obvious from the visual inspection of the figure that these high anomalies do not continue simply to the west of the red line, where a single, yet extremely irregular and laterally stepped magnetic anomaly is instead observed. The radiometric dataset is less conclusive with regard to the detailed internal architecture of the greenstone bodies exposed to the east and west of the discontinuity, but, on the other hand, highlights significant compositional similarities between the two greenstone bodies, expressed by a similar total count signature (Figure 55b) and, above all, the ternary radiometric information of Figure 55c. It needs to be mentioned that only the radioactive concentrations of the uppermost 1-2 m are detected by gamma ray spectrometry and therefore the radiometric signature reflects only the surface geology.

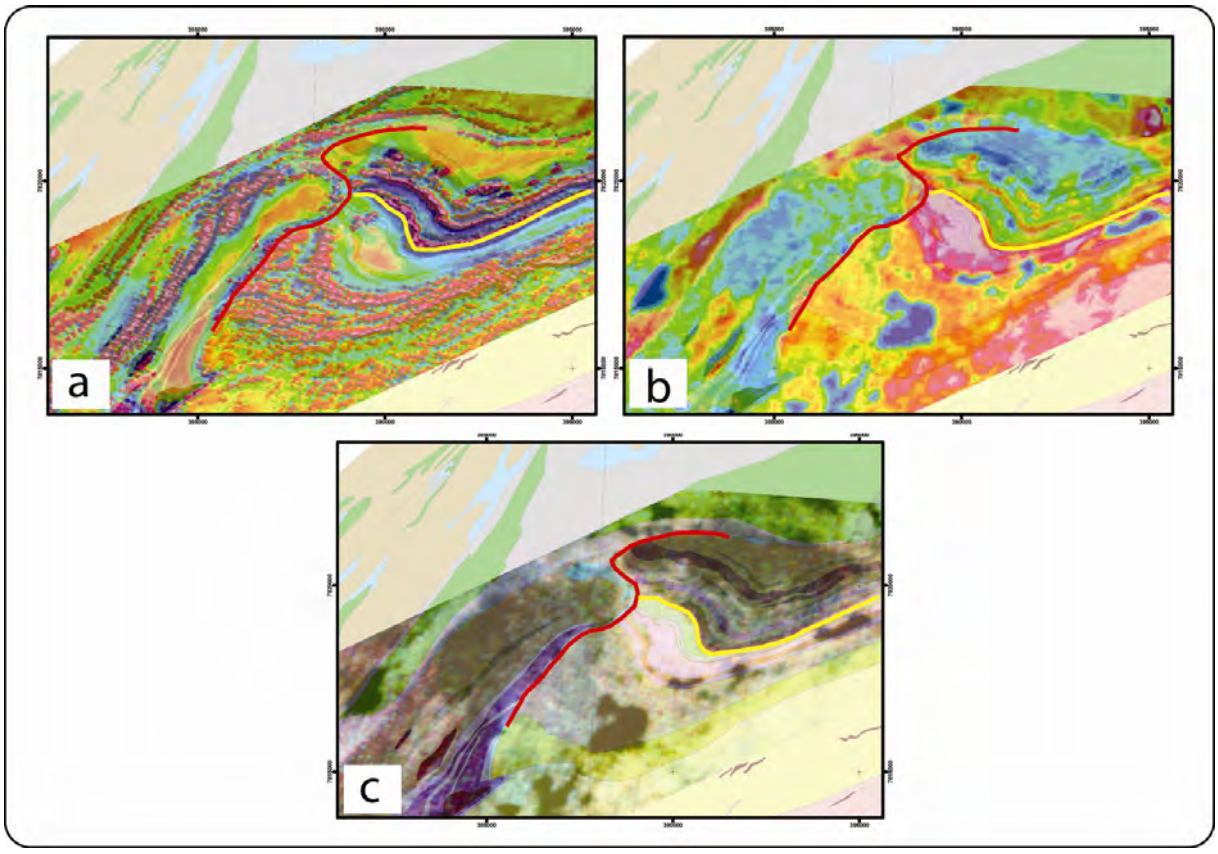


*Figure 55: Geophysical signature of the Nussir west area, with geological information drawn on top of the vertical gradient of the magnetic total field (a), the radiometric total count (b) and the ternary radiometry (c). The red line traces the location of the thrust discontinuity of Pharaoh et al. (1983). The yellow line shows the boundary between the Nussir (to the north) and Saltvatn Groups (to the south).*

Our preferred interpretation of the local structural framework is shown in Figure 56. White lines are used to trace the main anomalies within the greenstones. Supported by the results discussed in section 3.2, the Skinnfjellet greenstone body is interpreted as being folded by a Fn+1 antiform, with an undulating axial trace trending generally SW-NE. The northeasternmost termination of the antiform is covered by the dolomites described in section 3.1. We trace the fold nose, however, not by following the curved map pattern of the dolomites, but instead by joining the high magnetic anomalies of the underlying greenstones, which are the likely source of the magnetic signature from underneath a presumably very thin dolomite occurrence. The southeastern limb of the antiform is easily identified and corresponds to the top-to-the-NW sheared contact between dolomites and greenstones and the Dypelv conglomerates (section 3.2). The conglomerates contain also early Fn folds, which are the oldest structural feature recognised by us within the Repparfjord Window (see Sandstad et al., 2007).

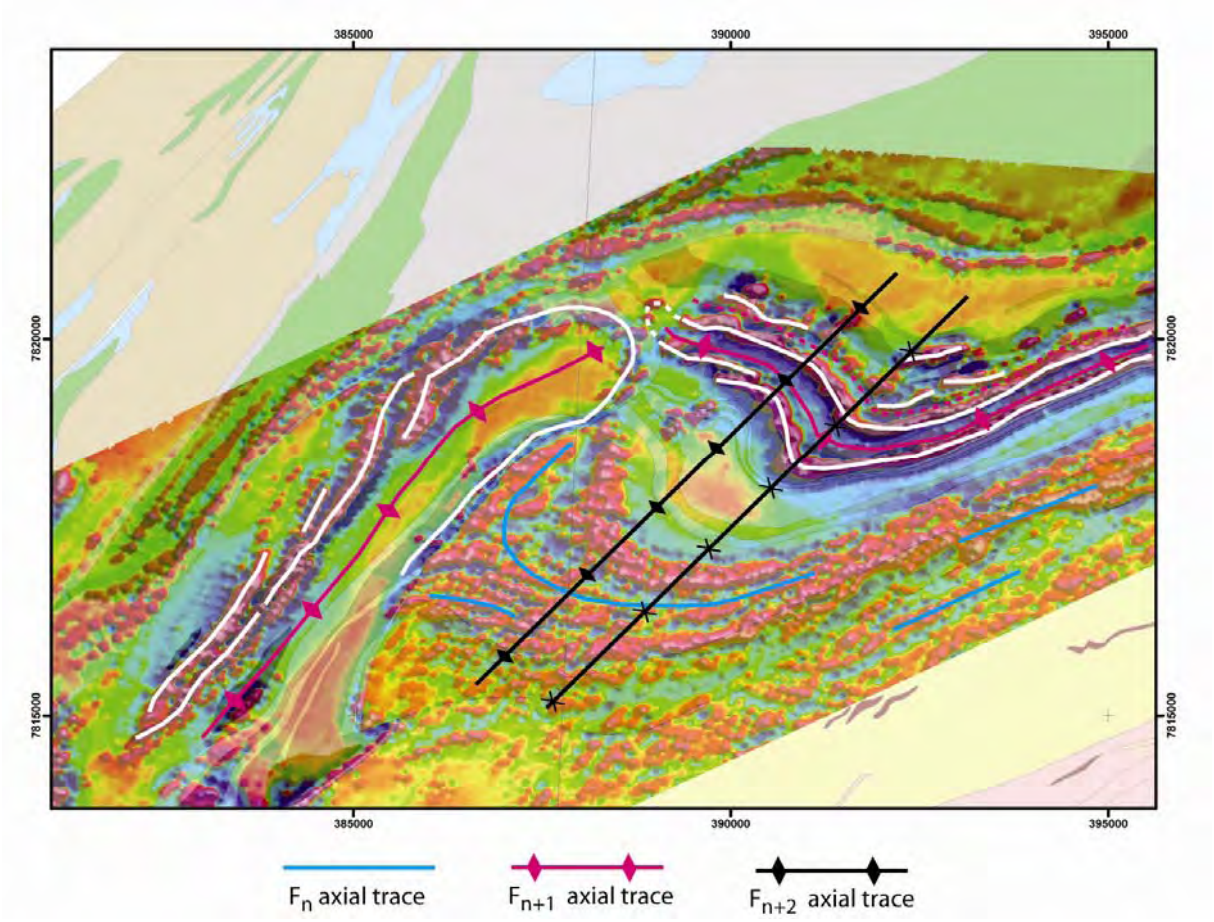


*Figure 56: Structural elements (as per definition derived from field observations) interpreted for the Nussir West area and traced on the vertical gradient of the total magnetic field.*

Later Fn+2 shortening generated the prominent folds that refold Fn+1 and Fn folds. Fn+2 are the folds that caused the current folded pattern of the Nussir and Saltvatn Group lithologies in the Nussir West area.

The main implication of our interpretation is that, although with a different geometry, we continue the Fn+1 axial trace from Skinnfjellet to Nussirt, thus across the trace of Pharaoh et al.'s (1983) discontinuity. The two to three obvious and strong anomalies within the Nussir greenstones are in our opinion the result of tight folding, and not a primary feature of the tectonostratigraphy of the Nussir Group. Also, we suggest that it is the same greenstone body that extends east and west of the discontinuity suggested by Pharaoh et al. (1983), as indicated by the striking similarities in the radiometric ternary plot of Figure 57. Minor lithological differences may be due to the plunge of the Fn+1 fold that affects the Nussir group, which results in different structural levels exposed at the surface. In addition, the low magnetic signature that characterises the uppermost part of the Saltvatn Group seems to continue undisturbed beneath the southeasternmost part of the Skinnfjellet antiform, thus in disagreement with the presence of the major thrust discontinuity of Pharaoh et al. (1983).

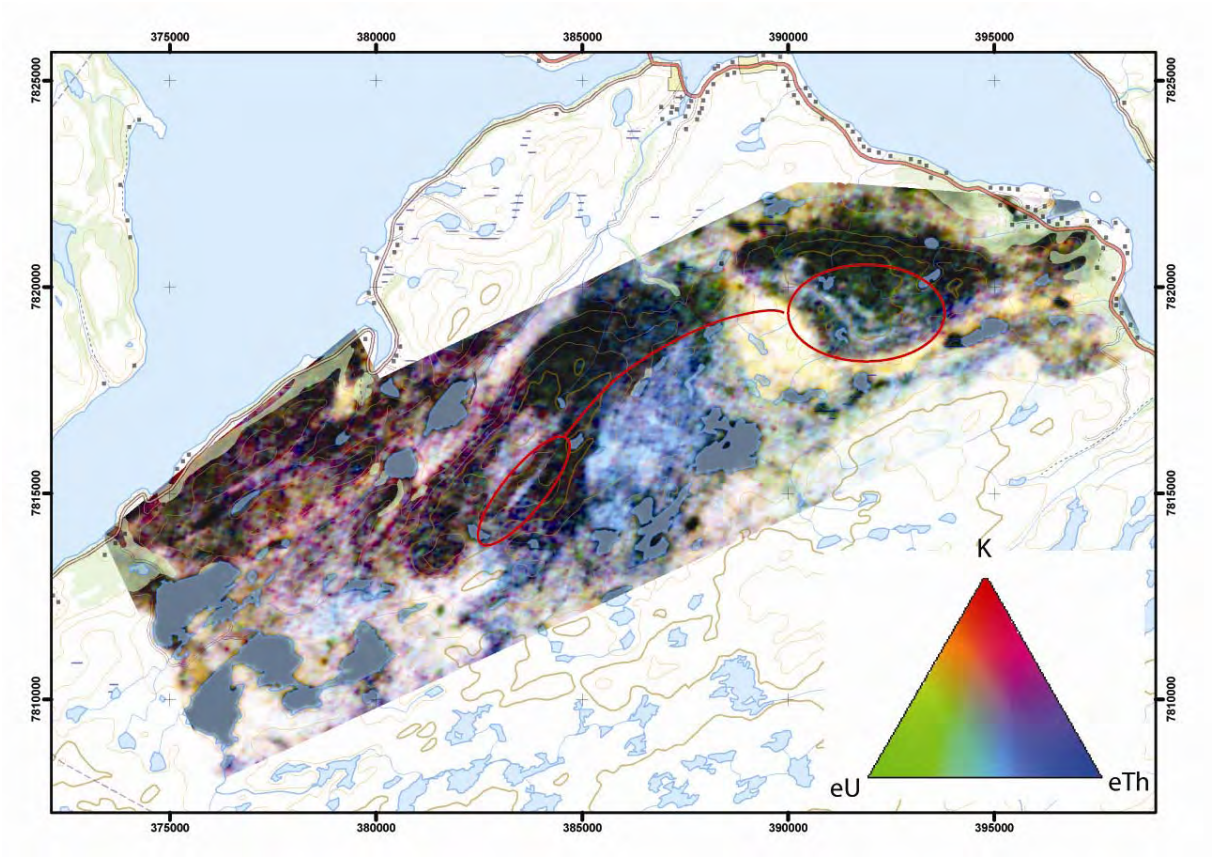


*Figure 57: RGB ternary plot showing significant compositional similarities between the greenstones of Skinnfjellet and Nussir. Red circles highlight the identical signature of a mafic tuff layer.*

This interpretation is expanded further in the next chapter where, after integration with the geological background and the rest of the information gathered with this study, we propose a model for the overall structural development of the area.

The Porsa area is in our opinion another key in the unravelling of the complex structural framework of this part of the Repparfjord Window. Our interpretation benefited greatly from the analysis of the regional digital elevation model, with the vertical derivative of the total magnetic field and the geological contact shape files draped onto it. Figure 58 shows the 3D image together with several interpretative lines drawn on it. The northwestern region is clearly controlled by densely spaced Porsa thrusts, which duplicate the stratigraphy and likely accommodated significant shortening. Structural analysis of the Porsa and Bachke mines area indicated the existence of a mineralised dextral transpressional shear corridor in the area, developed under ductile conditions. We rely on these observations to draw the thrust that runs immediately to the southeast of Porsa Mine and on the existing geological map to trace it along strike to the northeast. We propose that this transpressive structure forms the basal

detachment below the large Skinnfjellet greenstone antiform, possibly emerging on its southeastern limb, although in that position we document top-to-the-NW kinematics (see also Pharaoh et al., 1983). At this stage we have no control on the dip of the thrust plane. As mentioned earlier, though, we propose top-to-the-NW thrusting to be a local effect due to flexural slip folding mechanism at the time of Fn+1 folding of the greenstones. This thrust cuts obliquely a strong E/ENE-trending magnetic anomaly, which corresponds to metamorphosed mafic and ultramafic (serpentinitic) tuffs. Both composition and magnetic signatures are very similar to those of the serpentinitic tuffs exposed in the Nussir Mountain area, indicating a likely correlation between them. We interpret this anomaly as folded to the southeast by a train of tight upright folds. Folding disrupted the continuity of the anomaly in the core region and the overall geometry can thus only be guessed from the geophysical pattern analysis. Detailed field mapping (Nilsen and Nilsson, 1996), however, confirms the existence of a complex train of ENE/WSW-trending folds, cored by gabbros belonging to the lowermost Holmvatn Group. We suggest that the gabbros are exposed in proximity to the hinge zone of these folds, which enhanced geometrically their relative exhumation to the present erosional surface. As shown in Figure 58, the easiest interpretation is to assign these folds to the Fn+2 folding phase that so dramatically shaped the Nussir West area.

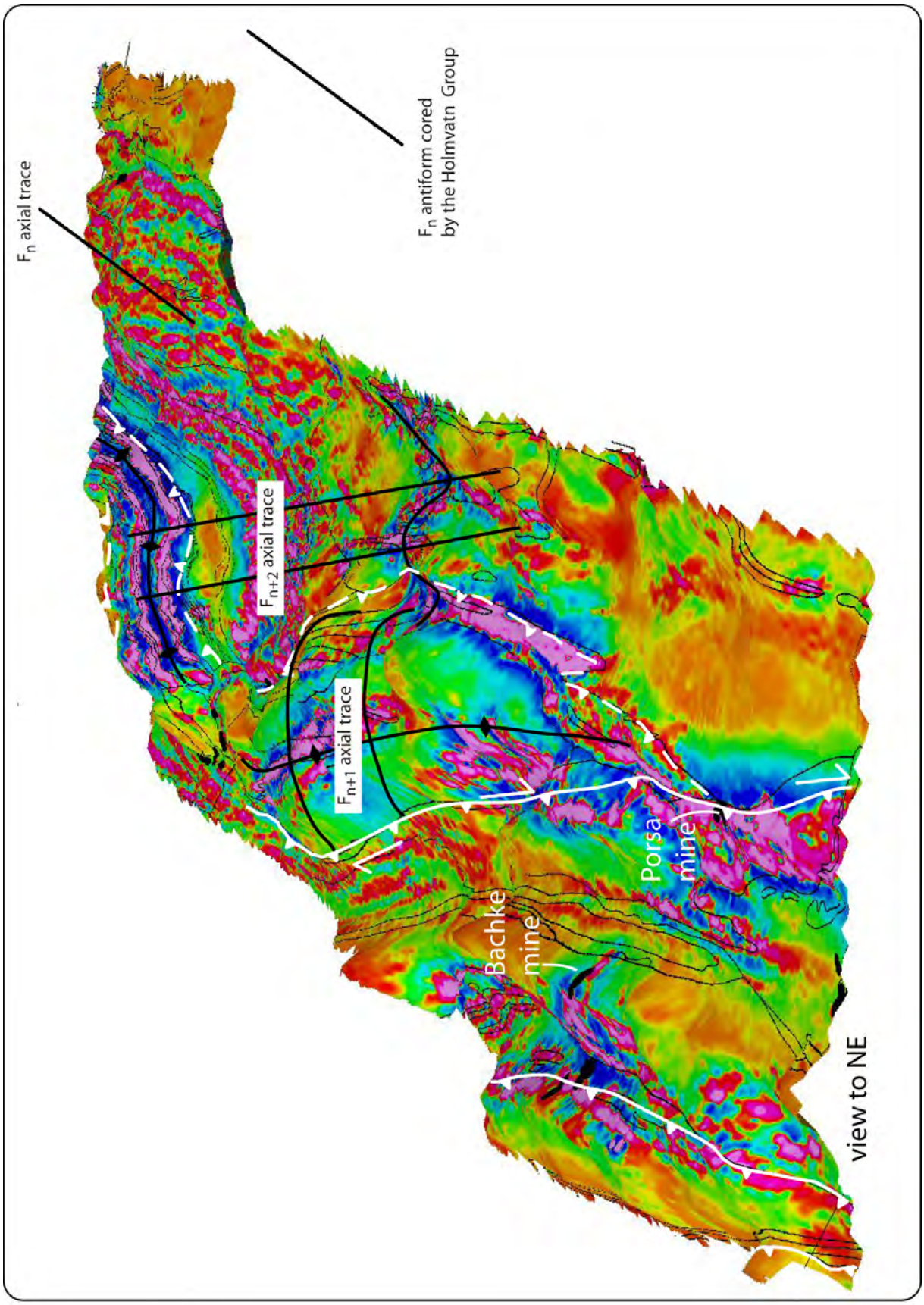


*Figure 58: 3D view of the geophysical survey obtained by draping the vertical gradient of the total magnetic field onto the digital elevation model of the area. White lines trace thrust trends, whereas black lines are axial traces and outline of selected folds.*

Without further investigations, however, it cannot be excluded that these folds are actually slightly misaligned Fn folds, which would belong to the first-order E/ENE-W/WSW folding of the Repparfjord Window.

## 6. Discussion

The results of the field work component of this study can be used, in conjunction with the interpretation of the new, high-resolution geophysical survey, to critically discuss and refine models and ideas on the geology of the northern sector of the Repparfjord Window and to offer robust alternatives regarding the structural framework of the area and its links to the studied mineralisations.

Existing ideas on the geology of the area are predominantly based upon, and incorporate significant elements of, the work of Pharaoh et al. (1983), who significantly modified some of the earlier interpretations of Reitan (1963; see Figure 2). The map presented in Figure 4 still reflects to a large extent the tectonostratigraphy defined by these authors.

As mentioned in the introduction, Reitan (1963) correlated the Nussir greenstone lavas with those of the Holmvatn Group to the south and, in addition, he also considered the contact between the Nussir greenstones and the Saltvatn Group as being tectonic, with a thrust along the southern flank of Nussir Mountain. On the other hand, Pharaoh et al. (1983) suggested that there exist significant differences between the Nussir and Holmvatn greenstones and that they should not be correlated. Moreover, and more importantly to this discussion, Pharaoh et al. (op. cit.) concluded that there is "little" evidence for a tectonic contact along the southern flank of Nussir, (although, admittedly, not well exposed) and that actually there appears to be a normal stratigraphic boundary with a conformable passage between the Saltvatn Group (which includes the Nussir I ore dolomite) and the Nussir Group. This relationship is crucial in Pharaoh et al.'s (op. cit.) model because it directly constrains the location of the major discontinuity (a Svecokarelian thrust in their model), which bounds to the west both the Nussir and Saltvatn Groups. Several aspects of this "thrust" model, however, remain unclear, including the thrust intriguing "bend" in its middle part, its lateral continuation and the fact that Nussir greenstones form the footwall to the thrust to the southwest of the bend, but the hanging wall to the east. No satisfactory explanations were proposed.

As mentioned earlier in the report, our observations do not suggest the existence of this structural discontinuity and the interpretation of the new geophysics corroborates this idea. We actually believe that there is physical continuity between lithologies and structures to the west and east of Pharaoh et al.'s (1983) discontinuity. The Skinnfjellet greenstones are interpreted as correlating directly with the Nussir greenstones. We suggest that the large Fn+1 Skinnfjellet antiform can be traced into the Nussir greenstones. Folding style, however, changes along strike of the fold axial trace.

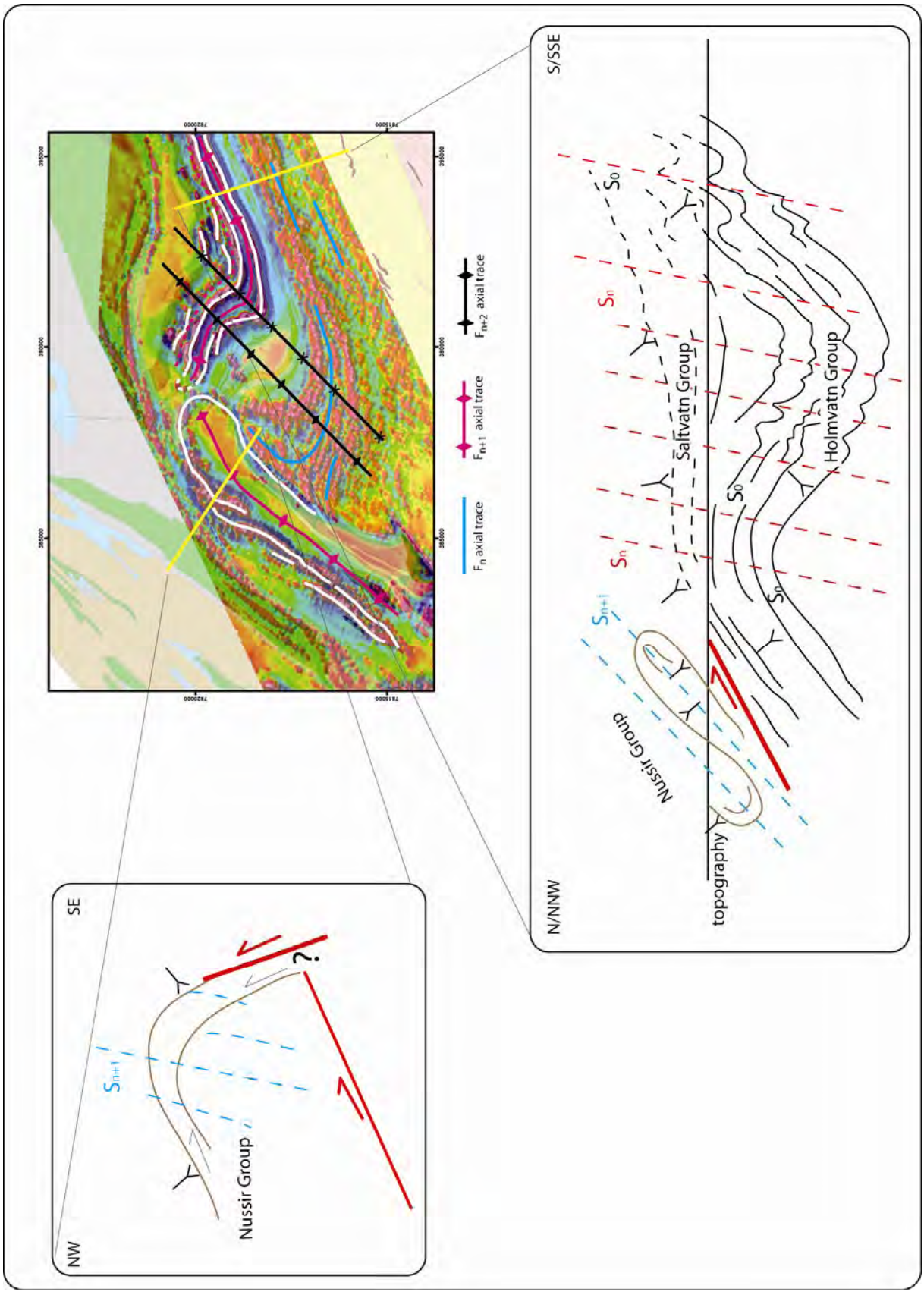


*Figure 59: Schematic cross sections across Fn+1 folds. The wavelength of the fold decreases to the east and the antiform evolves from open to isoclinal. The axial plane changes its attitude in space from upright in the Skinnfjellet antiform to inclined in the Nussir Mountain area.*

Figure 59 shows the change in style and geometry along the axial trace from west to east along the same Fn+1 fold (thus across the discontinuity of Pharaoh et al., 1983). Due to the paucity of detailed observations, the Skinnfjellet cross-section is an extremely simplified sketch, which does not account for the presence of second-order folds and thrust faults.

The different magnetic anomaly pattern between the eastern and western sectors of Nussir West area remains puzzling and is not readily explained. We suggest, however, that later structural reworking of the Skinnfjellet antiform may have disrupted the initial magnetic signature of the greenstones, which was likely identical to that preserved in the Nussir Mountain area.

Younging directions along the easternmost profile of Figure 59 are constrained from our own observations within the Ulveryggen Formation of the Saltvatn Group (Figure 60; Sandstad et al., 2007), but are taken from the map of Pharaoh et al. (1983) farther to the north. The geometry of our cross-section accounts for the observed vergence, younging direction and bedding/cleavage relationships. However, south-verging younging directions are reported throughout Nussir greenstones in the Nussir West area, whereas the presence of the postulated, isoclinal fold system would require localised inversion of the younging direction (Figure 59). Establishing younging directions in massive greenstones is not easy and localised changes might have been overlooked.

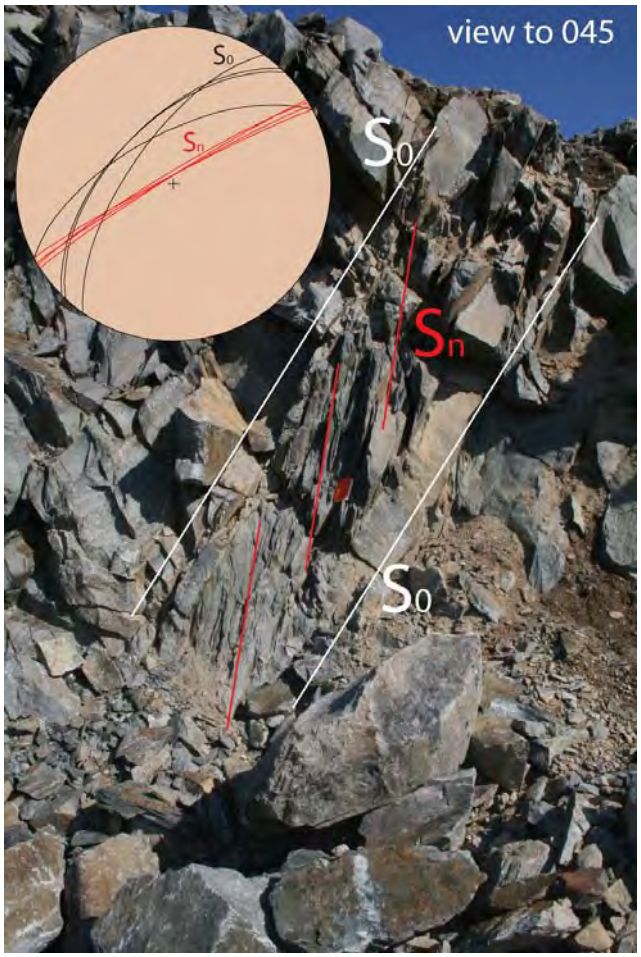


*Figure 60: Bedding ($S_0$)-cleavage ($S_n$) relationships observed at locality N 07/71 (UTM 35N, 396996 7816109) and suggesting antiform to the south. The cleavage is developed in a more shaly bed of the Ulveryggen Formation metasedimentary sequence.*

The sketch cross-sections also point out another important element of our model. We introduce a thrust fault at the base of all greenstones, thus in line with the early scheme of Reitan (1963). Analysis and interpretation of the geophysics suggest that the greenstones of the study area belong all to the Nussir Group and that they rest discordantly on a tectonic contact. Thus, the Nussir Group is separated by a fault contact from the Saltvatn Group in the Nussir West Area. Thrusts with top-to-the-SE transport direction are indeed common in the region and we propose that the large greenstone bodies form part of their hanging wall stratigraphy. In this model, Fn+1 folds belong to the hanging wall to the thrusts and were transported passively toward the foreland. Folding (Fn+1) and thrust faulting might be the expression of the same shortening episode, with early folding followed by later, discrete thrusting. According to this model, the Saltvatn Group is in the footwall to one of these thrusts. If the existence of a thrust separating Saltvatn and Nussir Groups is confirmed by more field observations and possibly high-resolution seismic profiling, the genesis of the

Nussir I ore deposit should be re-evaluated in the possible perspective of synkinematic fluid circulation at the toe of an advancing nappe and thrust edifice.

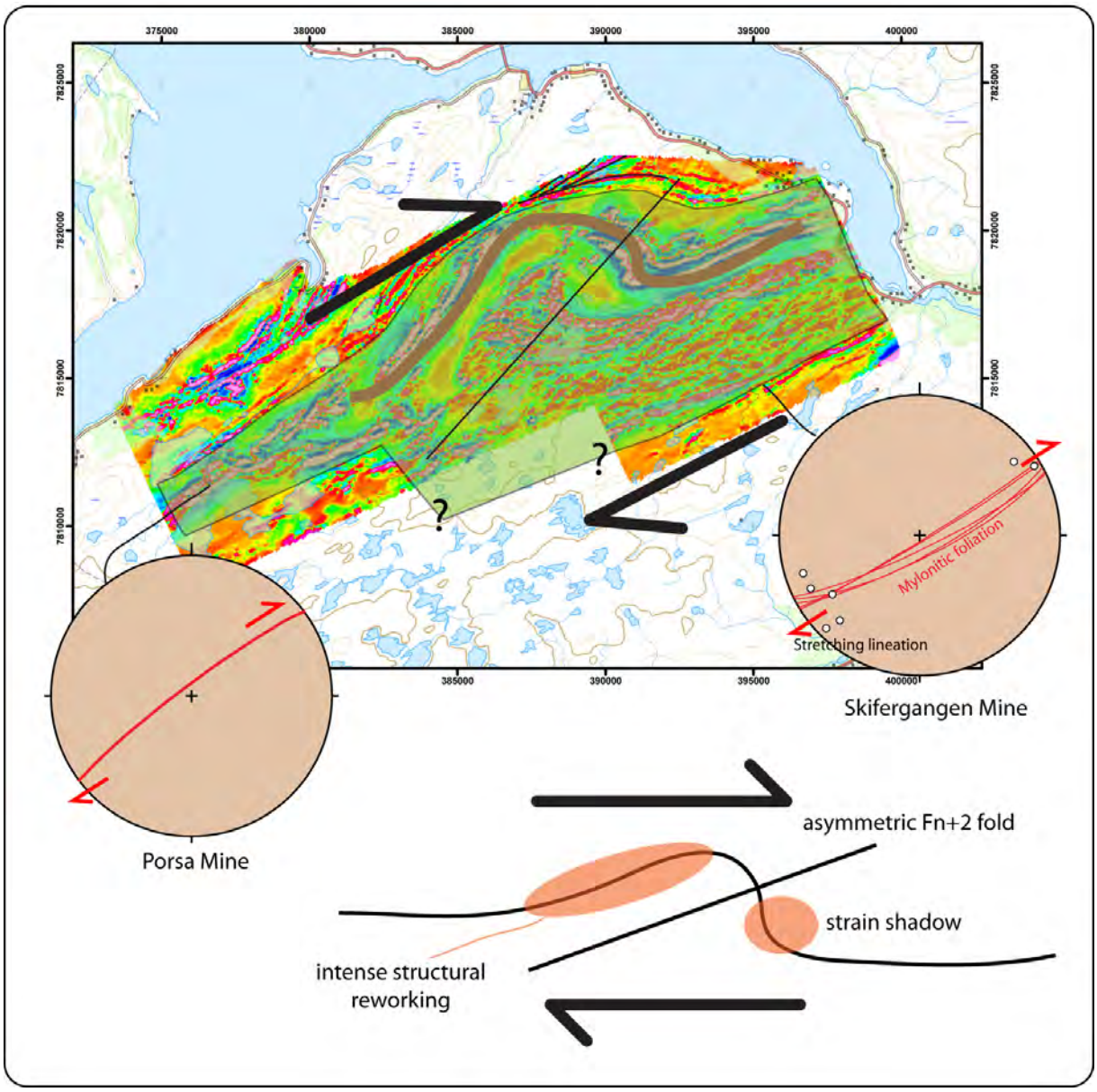


*Figure 61: Asymmetric dextral Fn+2 folds are explained by the documented presence of a ductile dextral shear corridor.*

Field investigations in the Porsa and Bachke mines area (sections 4.1and 4.2) showed the existence of a dextral, ductile shear corridor that trends about northeast-southwest. The mineralisation at Porsa was shown to be syn-genetic with this dextral shearing. Structural analysis at Skifergangen (not discussed in this report) demonstrates an identically oriented, dextral ductile shear zone not far from the contact between the Saltvatn and Holmvatn Groups. Figure 61 plots the orientation of mylonitic foliation at Skifergangen, where subhorizontal stretching lineations constrain strike-slip dextral kinematics. When this

information is integrated into the overall geological picture established by this study, it is apparent that the study area forms a large-scale asymmetric dextral “clast”, bound to the north and south by these dextral corridors, In this model, Fn+2 folds become asymmetric, dextral and northeast-vergent folds, intrafolial within the overall regional structural grain. The sketch of Figure 61 illustrates the details of this model. Dextral flow generates an asymmetric Fn+2 fold, whose vergence is entirely consistent with the independently-established kinematics of the bounding shear zones. Given the asymmetry of the fold with respect to the background flow, the long back limb undergoes intense structural reworking during shearing and folding. The front limb, on the other hand, remains “sheltered” in a strain shadow, which results in relatively little structural overprint. The back limb corresponds to the greenstones exposed in the Skinnfjellet antiform. Here, as mentioned earlier, there is a strong magnetic anomaly. It is, however, far from being a simple, straight anomaly (like, for example, those found in the Nussir Mountain area). It is instead very irregular, often laterally stepped and composite of several individual linear anomalies (Figure 62).

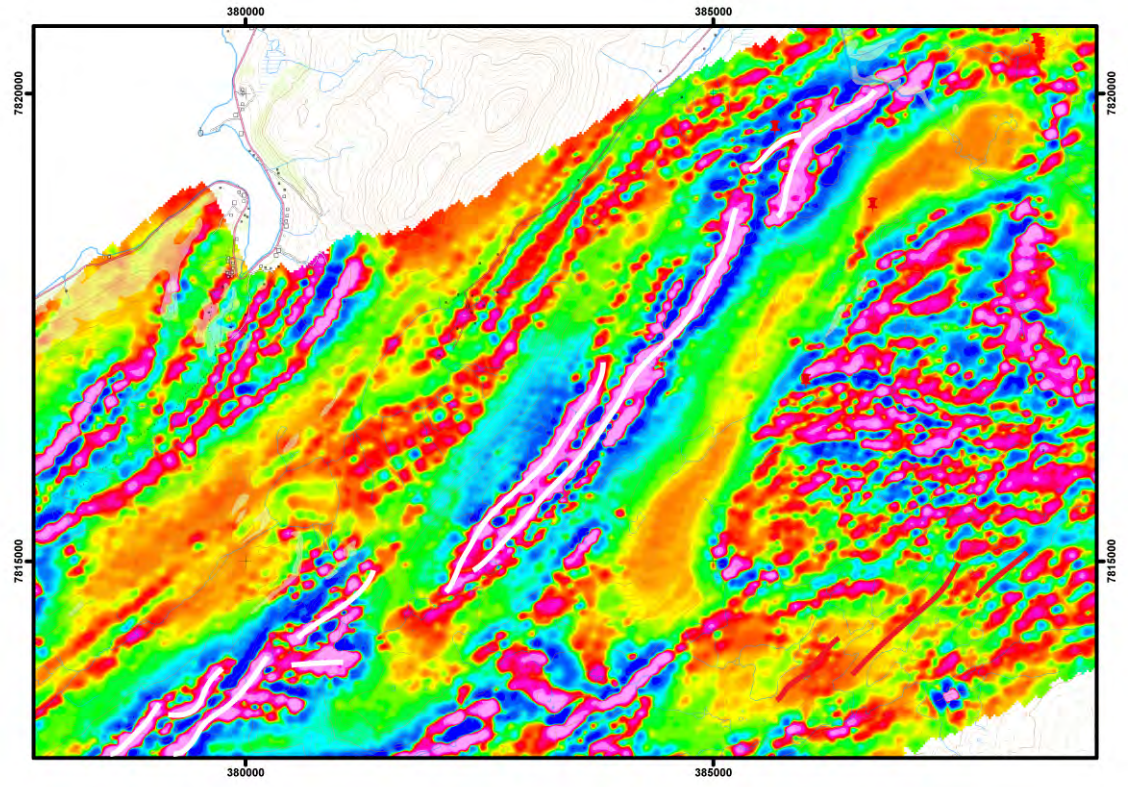


*Figure 62: Irregular and laterally stepped magnetic anomaly on the northwestern limb of the Skinnfjellet antiform.*

It is suggested that this sector was strongly overprinted and disrupted structurally during the dextral shearing episode and the development of the Fn+2 folds. Prior to this deformational event, it can be argued that the overall structural grain of the greenstones (hence their

geophysical signature) matched that still preserved on the front limb of the Fn+2 fold, protected from severe overprinting by its position within a pressure shadow.
The significance of this dextral shear corridor is not understood yet, and more work is needed to correlate it with the larger-scale structural framework. It could be a separate, late event that postdates the top-to-the-SE thrusts or, more probably, it represents the result of strain partitioning during the transpressional thrusting episode, whereby oblique shearing was partitioned into a top-to-the-SE thrusting and a dextral strike-slip component.

Fieldwork and structural observations in several parts of the Repparfjord Window, integrated by the new, high-resolution geophysical survey, produced a revised, comprehensive picture of the regional structural framework of the window, of its tectonostratigraphy and of the main deformational phases that have affected the basement rocks. A few problematic issues remain, however, especially with regard to the age of deformation. We were able to reconstruct a relative geochronology for the deformational events (based on overprinting, geometrical and kinematic relationships), but we still lack direct time constraints on the fabrics and structures described. This becomes particularly relevant given the difficulties encountered with the identification of the Lomvatn Formation, a Neoproterozoic series that is described as a correlative of the Dividal Group and that potentially represents a useful time marker. Highly deformed and isoclinally folded schists were observed at several localities, sharply truncated by the overriding Caledonian nappe system. These rocks are deformed coherently with the remaining Paleoproterozoic sequence exposed in the window, thus requiring a common deformation history. Pharaoh et al. (1983), however, described those rocks as belonging to the Lomvatn Formation, which instead should be formed by only very gently cleaved metasediments resting unconformably upon the Paleoproterozoic sequence. No sign of this unconformity was observed during our work. This in turn has major implications on the age of deformation as seen in the area. If what we have observed is in fact Lomvatn Formation lithologies, then all the deformation observed in the area is post-Neoproterozoic. On the other hand, if the Lomvatn Formation is simply not exposed in the localities we have investigated (thus in stark contrast to the map of Pharaoh et al., 1983), deformation can still be of Svecokarelian age and can predate the emplacement of the Caledonian system. This is our favourite interpretation at the moment.
Given the intimate relationship that was demonstrated between some of the mineralisations investigated by this study and the surrounding structures, it is therefore difficult to assign ore formation to specific orogenic events.

## 7. Conclusions and suggestions for future work

Our results are based on the critical analysis of previous studies of the area, our own fieldwork and on the qualitative structural interpretation of the recently acquired, helicopter-borne geophysical survey. Although fieldwork was very limited, some conclusions can be drawn and recommendations for future work given. Alternative suggestions are put forward when it is not possible to be conclusive.

- *Nussir I and the possible continuation into Nussir II*

Key to the understanding of a possible existence of a southwestward continuation of Nussir I into the postulated Nussir II is the geological and structural evolution in the Nussir West area. Our preferred interpretation, i.e. the Nussir Group greenstones occupying the hanging wall of a thrust with top-to-the-SE transport direction, calls for a possible continuation of Nussir I below this thrust plane on the southeastern side of Skinnfjellet. The dip of the thrust plane is, however, an important factor. Although we lack direct field constraints on the geometry of the structure, it can be argued that the dip of this thrust is probably steep, as indicated by the abrupt termination of the magnetic anomalies of the highly magnetic Djupelv Formation conglomerate. If the conglomerate continued at shallow depth beneath the greenstones of Steinfjellet, then the magnetic signature of this formation should be encountered as deeply seated magnetic anomalies, which is not the case, thus suggesting a sharp truncation by the thrust plane. Detailed modelling of the geophysical data along selected profiles could shed more light on this structural issue, and in turn on the possible extension of Nussir I. Alternatively, the sharp termination of the stratigraphy of the Djupelv and Stangvatn Formation against the discontinuity on the southeastern side of Skinnfjellet calls for the existence of a primary discontinuity developed prior to the shortening and folding history. This could be a steep top-to-the E (present orientation) normal fault that bounded a small, asymmetric graben to the east, where the sedimentary sequence containing Nussir I was initially deposited. It is crucial to understand the exact nature of this discontinuity, because depending on its presence or lack thereof, Nussir I may or may not continue to the west into Nussir II.

Hence, if Nussir II exists and the mineralisation is syngenetic and stratabound, it should either be located at deep levels beneath the Skinnfjellet greenstones (provided the thrust is shallow), or might not extend any farther than the present extension of the Stangvatn Group. Drilling in the continuation of the mapped Nussir I mineralisation after ground geophysics (IP) is highly recommended and remains the ultimate test to the existence of Nussir II.

- *The Nussir I mineralisation*

The proposed structural model is also relevant to an alternative interpretation of the formation of the Nussir I mineralisation. Several of the copper mineralisations that were investigated in the area have been shown to be genetically linked to ductile shearing along dextral shear zones. These shear zones are likely linked to transpressional thrusts with top-to-the-SE transport direction (Porsa thrusts). The formation of the Nussir mineralisation could itself be due to synkinematic fluids at the toe of one of these thrusts. Whether the precipitation of the mineralising fluids was due to a chemical trap or to the presence of impermeable layers in the footwall has to be further investigated.

Textures of the Nussir I mineralisation observed in drill cores in fact suggest that this mode of formation might be a valid alternative to the existing syngenetic model. Preliminary drill core logging indicates that copper minerals occur mainly in fractures and veinlets and are thus linked to a deformational episode. The mineralisation is assumed to be post-diagenetic and is most probably postdating the formation of the penetrative planar fabrics. Copper-mineralised veinlets that crosscut the foliation that becomes texturally obliterated in alteration zones have been observed in several drill cores (Ihlen & Sandstad, NGU internal note 24.01.08).

Recommendations:

- ✓ Detailed investigations of existing drill cores to better characterize the nature of the mineralisation, addressing the syngenetic vs. epigenetic issue.
- ✓ Structural mapping along the Nussir I mineralisation with the goal of verifying the geometry proposed in Figure 59.
- ✓ Identification of favourable target areas for copper mineralisations in front of thrusts with top-to-the-SE transport direction, both in geophysical data and in the field

- *Vesterdalen prospect*

The areal extent of the copper-gold mineralisation found so far in the Vesterdalen prospect is limited, but very interesting values of copper and gold have been recorded in rock samples, and the area warrants further investigations.

Recommendations:

- ✓ Geophysical ground measurements (EM and IP) should be performed, and the structural model presented in this report should be kept in mind when interpreting the results. This will assist delineate follow-up drilling targets.

- ✓ Examination of the Beritsjord prospect, with a similar geological setting (NGU, Ore database).

- *Revision of the regional map*

The study has shown that several aspects of the regional map need significant revision. More detailed interpretations of the air-borne geophysical data in conjunction with mapping in the field should be performed. Critical aspects of our new structural interpretation should be tested on the ground. Most critical for the understanding and evolution of the Nussir mineralisation are:

- ✓ Detailed mapping along profiles across the upper part of the Stangvatn Group and the greenstones exposed in the Nussir mountain. The existence of the suggested thrust at the base of the greenstones and the folding within the greenstones should be verified.
- ✓ The existence of a Neoproterozoic Lomvatn Formation should be investigated at several localities. As direct age dating (see below) of the various deformational events is hard to perform, indirect dating of the main tectonic events, i.e. whether they are Svecokarelian or Caledonian, can be constrained by the positive identification of Neoproterozoic sequences.

- *Geochronology*

Existing ages are scarce in the Repparfjord Window. More ages from structurally-constrained sites and fabrics are necessary in order to fully unravel the geological and structural history of the area, including the formation of the copper (-gold) mineralisations. The following is suggested:

- ✓ Re-Os molibdenite dating of the copper mineralisations. Very fine-grained molybdenite was documented in accessory amounts in the Bachke mine and slight enrichment of Mo (~120 ppm) has been found in drill cores from the Nussir mineralisation. Alternatively, other sulphides can also be dated.
- ✓ U-Pb isotopes of synkinematic titanite in shear zones.
- ✓ C- and Sr-isotopes of carbonates of the Porsa Group. Both Paleproterozoic and Neoproterozoic ages have been suggested for the rocks of the Porsa Group. Dating of these will put further constraints on the tectonic history.
- ✓ U-Pb zircon dating of various igneous rocks, although it may be difficult to identify suitable targets in the Nussir Group. A provenance study of the Saltvatn Group will only give a minimum age and is not recommended at this early stage.

## 8. References


Heincke, B.H., Koziel, J., Walker, P. & Lynum,R. Helicopter-borne geophysical measurements for mineral exploration at Nussir, Kvalsund commune in Finnmark. NGU report 2008.020. (confidential).

Jensen, P.A. 1996: The Altenes and Repparfjord tectonic windows, Finnmark, northern Norway: Remnants of a Palaeoproterozoic Andean-type plate margin at the rim of the Baltic Shield. Unpubl. Dr. Thesis, Univ. of Tromsø.

Krause, M. 1981: Some uranium mineralisations in the Raipas Suite of the Komagfjord tectonic window, Finnmark, Norway. Nor. geol. unders. 355, 49-52.

Nilsen, K. & Nilsson, L.P. 1996: VARGSUND berggrunnskart 1935 4, M 1: 50 000, foreløpig utgave. Nor. geol. unders.

Pharaoh, T.C. 1985: Volcanic and geochemical stratigraphy of the Nussir Group of Artic Norway - an Early Proterozoic greenstone suite. Jour. Geol. Soc. London, 142, 259-278.

Pharaoh, T.C. & Brewer, T.S. 1990: Spatial and temporal diversity of early Proterozoic volcanic sequences - comparisons between the Baltic and Laurentian shields. Prec. Res. 47, 169-189.

Pharaoh, T.C. & Pearce, J.A. 1984: Geochemical evidence for the geotectonic setting of early Proterozoic metavolcanic sequences in Lapland. Prec. Res. 25, 283-308.

Pharaoh, T.C., Ramsay, D.M. & Jansen, Ø. 1983: Stratigraphy and structureof the northern part of the Repparfjord-Komagfjord window, Finnmark, northern Norway. Nor. geol. unders. 377, 1-45.

Rice, A.H.N. 1998: Stretching lineations and structural evolution of the Kalak Nappe Complex (Middle Allochton) in the Repparfjord-Fægfjord area, Finnmark, northern Norway. Norsk Geolog. Tidsskr. 78, 277-289.

Rønning, J.S., Dalsegg, E. and Walker, P. 2007: Vurdering av helikoptergeofysikk over Nussirforekomsten, Kvalsund kommune i Finnmark. NGU report 2007.060. (confidential).

Sandstad, J.S., Viola, G. & Nilsson, L.P. 2007: Reconnaissance structural geological mapping and field XRF-analyses of the Ulveryggen copper deposit, Finnmark, Norway, NGU report 2007.064, 16pp.

Siedlecka, A., Iversen, E., Krill, A.G., Lieungh, B., Often, M., Sandstad, J.S. & Solli, A. 1983: Lithostratigrahpy and correlation of the Arcaean rocks of Finnmarksvidda and the Sørvaranger district. Nor. geol. unders. 403, 7-36.